Risø-R-411

RISØ

Risø-R-411

Nonlinear Finite Element Analysis of Concrete Structures

Niels Saabye Ottosen

Risø National Laboratory, DK-4000 Roskilde, Denmark
May 1980

The original document from which this microfiche was made was found to contain some imperfection or imperfections that reduce full comprehension of some of the text despite the good technical quality of the microfiche itself. The imperfections may be:

- missing or illegible pages/figures
- wrong pagination
- poor overall printing quality, etc.

We normally refuse to microfiche such a document and request a replacement document (or pages) from the National INIS Centre concerned. However, our experience shows that many months pass before such documents are replaced. Sometimes the Centre is not able to supply a better copy or, in some cases, the pages that were supposed to be missing correspond to a wrong pagination only. We feel that it is better to proceed with distributing the microfiche made of these documents than to withhold them till the imperfections are removed. If the removals are subsequestly made then replacement microfiche can be issued. In line with this approach then, our specific practice for microfiching documents with imperfections is as follows:

1. A microfiche of an imperfect document will be marked with a special symbol (black circle) on the left of the title. This symbol will appear on all masters and copies of the document (1st fiche and trailer fiches) even if the imperfection is on one fiche of the report only.

2. If imperfection is not too general the reason will be specified on a sheet such as this, in the space below.

3. The microfiche will be considered as temporary, but sold at the normal price. Replacements, if they can be issued, will be available for purchase at the regular price.

4. A new document will be requested from the supplying Centre.

5. If the Centre can supply the necessary pages/document a new master fiche will be made to permit production of any replacement microfiche that may be requested.

The original document from which this microfiche has been prepared has these imperfections:

☒ missing pages/~~XXXXXXX~~ numbered: 90 not printed.

☐ wrong pagination

☐ poor overall printing quality

☐ combinations of the above

☐ other

INIS Clearinghouse
IAEA
P. O. Box 100
A-1400, Vienna, Austria

RISØ-R-411

NONLINEAR FINITE ELEMENT ANALYSIS OF CONCRETE STRUCTURES

Niels Saabye Ottosen

Abstract. This report deals with nonlinear finite element analysis of concrete structures loaded in the short-term up until failure. A profound discussion of constitutive modelling on concrete is performed; a model, applicable for general stress states, is described and its predictions are compared with experimental data. This model is implemented in the AXIPLANE-program applicable for axisymmetric and plane structures. The theoretical basis for this program is given. Using the AXIPLANE-program various concrete structures are analysed up until failure and compared with experimental evidence. These analyses include panels pressure vessel, beams failing in shear and finally a specific pull-out test, the Lok-Test, is considered. In these analyses, the influence of different failure criteria, aggregate interlock, dowel action, secondary cracking, magnitude of compressive strength, magnitude of tensile strength and of different post-failure behaviours of the concrete are evaluated.

(Continued on next page)

May 1980
Risø National Laboratory, DK 4000 Roskilde, Denmark

Moreover, it is shown that a suitable analysis of the theoretical data results in a clear insight into the physical behaviour of the considered structures. Finally, it is demonstrated that the AXIPLANE-program for widely different structures exhibiting very delicate structural aspects gives predictions that are in close agreement with experimental evidence.

INIS descriptors: A CODES, CLOSURES, COMPRESSION STRENGTH, CRACKS, DEFORMATION, FAILURES, FINITE ELEMENT METHOD, PRESTRESSED CONCRETE, PRESSURE VESSELS, REINFORCED CONCRETE, SHEAR PROPERTIES, STRAIN HARDENING, STRAIN SOFTENING, STRAINS, STRESS ANALYSIS, STRESSES, STRUCTURAL MODELS, TENSILE PROPERTIES, ULTIMATE STRENGTH.

UDC 539.4 : 624.012.4 : 624.04

ISBN 87-550-0649-3
ISSN 0106-2840

Risø Repro 1981

CONTENTS

PREFACE

This report is submitted to the Technical University of Denmark in partial fulfilment of the requirements for the lic. techn. (Ph.D.) degree.

The study has been supported by Risø National Laboratory. Professor dr. techn. Mogens Peter Nielsen, Structural Research Laboratory, the Technical University of Denmark has supervised the work.

I want to express my gratitude to professor Nielsen for his guidance and to lic. techn. Svend Ib Andersen, Engineering Department, Risø National Laboratory for the opportunity to perform the study.

1. INTRODUCTION

The present report is devoted to nonlinear finite element analysis of axisymmetric and plane concrete structures loaded in the short-term up until failure. Additional to the prerequisites for such analysis, namely constitutive modelling and finite element techniques, emphasis is placed on the applications, where real structures are analysed. It turns out that the finite element analysis offers unique opportunities to investigate and describe in physical terms the structural behaviour of concrete structures.

The finite element analysis is performed using the program AXIPLANE, developed at Risø. The use of this program is given by the writer (1980). The scope of the present report is twofold: (1) to provide an exposition of matters of general interest; this relates to the constitutive modelling of concrete, to the analysis of the considered structures and to some aspects of the finite element modelling; (2) to give the specific theoretical documentation of the AXIPLANE-program. Moreover, a selfcontained exposition is aimed at.

The important section 2 treats constitutive modelling of concrete. Both the strength and the stiffness of concrete under various loadings are discussed and a constitutive model valid for general triaxial stress states and previously proposed by the writer is described and compared with experimental data.

Section 3 deals with the constitutive equations of reinforcement and prestressing. These models are quite trivial and interest is focussed only on a formulation that is computationally convenient in the AXIPLANE-program.

Section 4 describes different finite elements aspects. The AXIPLANE-program uses triangular elements for simulation of the concrete, whereas one- and two-dimensional elements simulate

arbitrarily located reinforcement bars and membranes. Linear displacement fields are used in all elements resulting in perfect bond between concrete and steel. Based on Galerkin's method, the fundamental equations in the finite element displacement method are derived in section 4.1. Readers familiar with the finite element method may dwell only with the important section 4.2.2 dealing with different aspects of consideration to cracking, with the introduction of section 4.3 where reinforcement elements are described, and with the general computational schemes as given in section 4.6.

The very important section 5 contains some examples of analysis of concrete structures. The following structures were analysed up until failure and compared with experimental data:

(1) panels with isotropic and orthogonal reinforcement loaded by tensile forces skewed to the reinforcement. The analysis focuses on aspects of reinforcement bar modelling and in particular on simulation of lateral bar stiffness;
(2) a thick-walled closure for a reactor pressure vessel. It represents a structure, where large triaxial compressive stresses as well as cracking are present. The influence of different failure criteria and post-failure behaviours is investigated;
(3) beams failing in shear. Both beams with and without shear reinforcement are considered, and of special interest are aggregate interlock, secondary cracks, influence of the magnitude of tensile strength, and dowel action;
(4) the Lok-Test which is a pull-out test. The influence of the uniaxial compressive strength, the ratio of tensile strength to compressive strength, different failure criteria and post-failure behaviours are investigated and special interest is given to the failure mode.

Moreover, this section shows that a finite element analysis may offer unique possibilities for gaining insight into the load-carrying mechanism of concrete structures.

Finally section 5 demonstrates that the AXIPLANE-program in

its standard form and using material data obtained by usual uniaxial testing, only, indeed gives predictions that are in close agreement with experimental evidence. This is so, even though the considered structures represent very different and very delicate aspects of structural behaviour. Compared with other finite element programs, this makes the AXIPLANE-program quite unique.

2. CONSTITUTIVE MODELLING OF CONCRETE

The structural behaviour of concrete is complex. Both its strength and stiffness are strongly depending on all stress components and the failure mode may be dominated by cracking, resulting in brittle behaviour, or ductility. Deviations from linearity between stresses and strains become more pronounced when stresses become more compressive and even hydrostatic compressive loadings result in nonlinear behaviour, cf. for instance Green and Swanson (1973). In addition, when stresses are compressive, dilatation occurs close to the failure state. It is the purpose of the present section to outline a constitutive model that copes with all the previously mentioned characteristics of loaded concrete. However, before considering stiffness changes of concrete it is convenient to investigate its strength.

2.1 Failure strength

Ultimate load calculations of concrete structures obviously require knowledge of the ultimate strength of concrete. If a priority list is to be set up for constitutive modelling of concrete with respect to realistic predictions of failure loads of structures an accurate failure criterion would certainly be the major factor; correct stress-strain relations would in general be of only secondary importance. In the following we will consider some proposed failure criteria evaluated against experi-

mental data and we will then concentrate on two criteria implemented in the finite element program. Only short-term failure is treated and no consideration is given to temperature effects and fatigue.

2.1.1. Geometrical preliminaries

Considering proportional loading and a given loading rate, a failure criterion for an initially isotropic and homogeneous material in a homogeneous stress state can be expressed in terms of the three stress invariants. Alternatively, the criterion can be given in the form

$$g(\sigma_1, \sigma_2, \sigma_3) = 0 \qquad (2.1.1)$$

where σ_1, σ_2 and σ_3 are the principal stresses that occur symmetrically. Tensile stresses are considered to be positive. When cyclic loading is excluded, the triaxial test results of Chinn and Zimmerman (1965) support the validity of eq. (1) for nonproportional loading also. From the uniaxial tests of Rüsch (1960) it is known that the influence of loading rate is not important when the loading time ranges from some minutes to hours. The influence of stress gradients on the strength has apparently not been investigated experimentally.

It appears to be convenient to use the following three invariants of the stress tensor σ_{ij}

$$\begin{aligned} I_1 &= \sigma_1 + \sigma_2 + \sigma_3 = \sigma_{ii} \\ J_2 &= \frac{1}{6}\left[(\sigma_1 - \sigma_2)^2 + (\sigma_2 - \sigma_3)^2 + (\sigma_1 - \sigma_3)^2\right] \\ &= \frac{1}{2}\left(s_1^2 + s_2^2 + s_3^2\right) = \frac{1}{2} s_{ij} s_{ij} \\ J &= \frac{3\sqrt{3}}{2} \frac{J_3}{J_2^{3/2}} \end{aligned} \qquad (2.1.2)$$

where J_3 is defined by

$$J_3 = \frac{1}{3} (s_1^3 + s_2^3 + s_3^3) = \frac{1}{3} s_{ij} s_{jk} s_{ki}$$

and s_{ij} is the stress deviator tensor defined by

$$s_{ij} = \sigma_{ij} - \frac{1}{3} \delta_{ij} \sigma_{kk}$$

where the usual tensor notation is employed with indices running from 1 to 3. The principal values of the stress deviator tensor are termed s_1, s_2 and s_3. I_1 is the first invariant of the stress tensor; J_2 and J_3 are the second and third invariants of the stress deviator tensor. The often applied octahedral normal stress σ_o and shear stress τ_o are related to the preceding invariants by $\sigma_o = I_1/3$ and $\tau_o^2 = 2 J_2/3$. The invariants of eq. (2) have a simple geometrical interpretation when eq. (1) is considered as a surface in a Cartesian coordinate system with axes σ_1, σ_2 and σ_3 - the Haigh-Westergaard coordinate system - and the necessary symmetry properties of the failure surface appear explicitly when use is made of these invariants.

For this purpose, any point, $P(\sigma_1, \sigma_2, \sigma_3)$, in the stress space is described by the coordinates (ξ, ρ, θ), in which ξ is the projection on the unit vector $\bar{e} = (1, 1, 1)/\sqrt{3}$ on the hydrostatic axis, and (ρ, θ) are polar coordinates in the deviatoric plane, which is orthogonal to (1, 1, 1), cf. fig. 1. The length

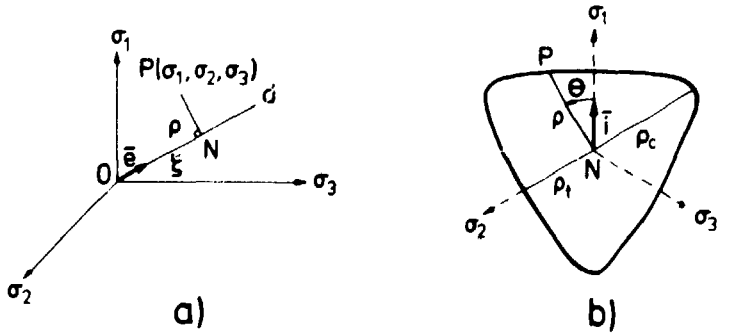

Fig. 2.1.1: (a) Haigh-Westergaard coordinate system;
(b) Deviatoric plane

of $\overline{ON}$ is

$$|\overline{ON}| = \xi = \overline{OP} \cdot \bar{e} = (\sigma_1, \sigma_2, \sigma_3) \frac{1}{\sqrt{3}} \begin{bmatrix} 1 \\ 1 \\ 1 \end{bmatrix} = I_1/\sqrt{3}$$

and $\overline{ON}$ is therefore determined by

$$\overline{ON} = (1, 1, 1)\ I_1/3$$

The component $\overline{NP}$ is given by

$$\overline{NP} = \overline{OP} - \overline{ON} = (\sigma_1, \sigma_2, \sigma_3) - (1, 1, 1)\ I_1/3 = (s_1, s_2, s_3)$$

and the length of $\overline{NP}$ is

$$|\overline{NP}| = \rho = (s_1^2 + s_2^2 + s_3^2)^{1/2} = \sqrt{2J_2}$$

To obtain an interpretation of J, consider the deviatoric plane, fig. 1 b). The unit vector $\bar{i}$, located along the projection of the σ_1-axis on the deviatoric plane is easily shown to be determined by $\bar{i} = (2, -1, -1)/\sqrt{6}$. The angle θ is measured from the unit vector $\bar{i}$ and we have

$$\rho \cos\theta = \overline{NP} \cdot \bar{i}$$

i.e.

$$\cos\theta = \frac{1}{\sqrt{2J_2}}\ (s_1, s_2, s_3) \frac{1}{\sqrt{6}} \begin{bmatrix} 2 \\ -1 \\ -1 \end{bmatrix} = \frac{1}{2\sqrt{3J_2}}\ (2s_1, -s_2, -s_3)$$

Using $s_1 + s_2 + s_3 = 0$ we obtain

$$\cos\theta = \frac{3s_1}{2\sqrt{3J_2}} = \frac{2\sigma_1 - \sigma_2 - \sigma_3}{2\sqrt{3J_2}}$$

As $\sigma_1 \geq \sigma_2 \geq \sigma_3$ is assumed throughout the text, $0 \leq \theta \leq 60^\circ$ holds. Using the identity $\cos 3\theta = 4\cos^3\theta - 3\cos\theta$, the invariant J in eq. (2) is after some algebra found to be given by

$$J = \cos 3\theta \qquad (2.1\text{-}3)$$

The failure criterion eq. (1) can therefore be stated more conveniently using only invariants as

$$f(I_1, J_2, \cos 3\theta) = 0 \qquad (2.1\text{-}4)$$

from which the 60°-symmetry shown in principle in fig. 1 b) appears explicitly. The superiority of this formulation or alternatively $f(I_1, J_2, \theta) = 0$ compared to eq. (1) appears also clearly when expressing mathematically the trace of the failure surface in the deviatoric plane. Generally, only old criteria such as the Mohr criterion, the Columb criterion and the maximum tensile stress criterion use the formulation of eq. (1).

The meridians of the failure surface are the curves on the surface where θ = constant applies. For experimental reasons, as the classical pressure cell is most often applied when loading concrete triaxially, two meridians are of particular importance namely the compressive meridian where $\sigma_1 = \sigma_2 > \sigma_3$ i.e. $\theta = 60^{\circ}$ holds and the tensile meridian where $\sigma_1 > \sigma_2 = \sigma_3$ i.e. $\theta = 0^{\circ}$ applies. This terminology relates to the fact that the stress states $\sigma_1 = \sigma_2 > \sigma_3$ and $\sigma_1 > \sigma_2 = \sigma_3$ correspond to a hydrostatic stress state superposed by a compressive stress in the σ_3-direction or superposed by a tensile stress in the σ_1-direction, respectively.

2.1.2. Evaluation of some failure criteria

Based on the experimental evidence appearing on the following figures and in accordance with earlier findings of for instance Newman and Newman (1971) and the writer (1975, 1977), the form of the failure surface can be summarized as:

1) the meridians are curved, smooth and convex with ρ increasing for decreasing ξ-values;

2) the ratio, ρ_t/ρ_c, in which indices t and c refer to the tensile and compressive meridians respectively, (cf. fig. 1) increases from approx. 0.5 for decreasing ξ- values, but remains less than unity;

3) the trace of the failure surface in the deviatoric plane is smooth and convex for compressive stresses;

4) in accordance with 1), the failure surface opens in the negative direction of the hydrostatic axis.

The tests of Chinn and Zimmerman (1965) along the compressive meridian with a very large mean pressure equal to 26 times the uniaxial compressive strength support the validity of 4) over a very large stress range.

Several important failure criteria have been proposed in the past and some of these have been evaluated by Newman and Newman (1971), Ottosen (1975, 1977), Wastiels (1979) and by Robutti et al. (1979). In addition, Newman and Newman (1971), Hannant (1974) and Hobbs et al. (1977) contain a collection of different experimental failure data. In this report we concentrate on some of the several criteria proposed recently and a classical criterion. The considered criteria are:

- the Reimann-Janda (1965, 1974) criterion originally proposed by Reimann (1965), but here evaluated by using the coefficients proposed by Janda (1974). This criterion can be considered as one of the earliest attempts in modern time to approximate the failure surface of concrete. Some improvements of this criterion were later proposed by Schimmelpfennig (1971).

- the 5-parameter model of William and Warnke (1974) that appears to be the first criterion with a smooth convex trace in the deviatoric plane for all values of ρ_t/ρ_c where $1/2 < \rho_t/\rho_c \leq 1$. Its simplified 3-parameter version with straight meridians has later been adopted by Kotsovos and Newman (1978) and by Wastiels (1979) using different methods for calibration of the parameters.

- the criterion of Chen and Chen (1975) may serve as an example of an octahedral criterion disregarding the influence of the third invariant, $\cos 3\theta$.

- the criterion of Cedolin et al. (1977) corresponds to a failure surface with a concave trace in the deviatoric plane.

- the criterion proposed by the writer (1977). This criterion corresponds to a smooth and convex surface. It will be considered in more details later and it is implemented in the finite element program.

- the classical Coulomb criterion with tension cut-offs. This criterion is also implemented in the finite element program and an evaluation will be postponed until the previously mentioned criteria have been compared mutally and together with some representative experimental results.

As mentioned above we will in the first place disregard the Coulomb criterion with tension cut-offs. The coefficients involved in the criteria considered are calibrated by some distinct strength values, for instance, uniaxial compressive strength σ_c ($\sigma_c > 0$), uniaxial tensile strength σ_t ($\sigma_t > o$), etc. In some proposals such a calibration was already partly carried out leaving only a few strength values to be inserted by the user, while others need more strength values. Noting that all coordinate systems considered here are normalized by σ_c, the applied strength values are shown in the following table.

Table 2.1-1: Strength values used to calibrate coefficients in the failure criteria.

	σ_t/σ_c	σ_{cb}/σ_c	ξ/σ_c	ρ_c/σ_c	ξ/σ_c	ρ_t/σ_c
Reimann-Janda (1965, 1974)						
Willam and Warnke (1974)	0.08	1.15	-3.20	2.87	-3.20	1.80
Chen and Chen (1975)	0.08	1.15				
Cedolin et al. (1977)						
Ottosen (1977)	0.08					

σ_t: uniaxial tensile strength ($\sigma_t > o$), σ_c: uniaxial compressive strength ($\sigma_c > o$), σ_{cb}: biaxial compressive strength ($\sigma_{cb} > o$). The additional strength values applied in the Willam and Warnke criterion are chosen to fit the experimental data of fig. 2.

Fig. 2 shows the comparison of the considered criteria with some experimental results (the attention should also be drawn to the very important international experimental investigation, Gerstle et al. (1978)). The figure shows the compressive and tensile meridians. Except for the proposal of Chen and Chen (1975), a good agreement is obtained for all criteria. The Chen and Chen

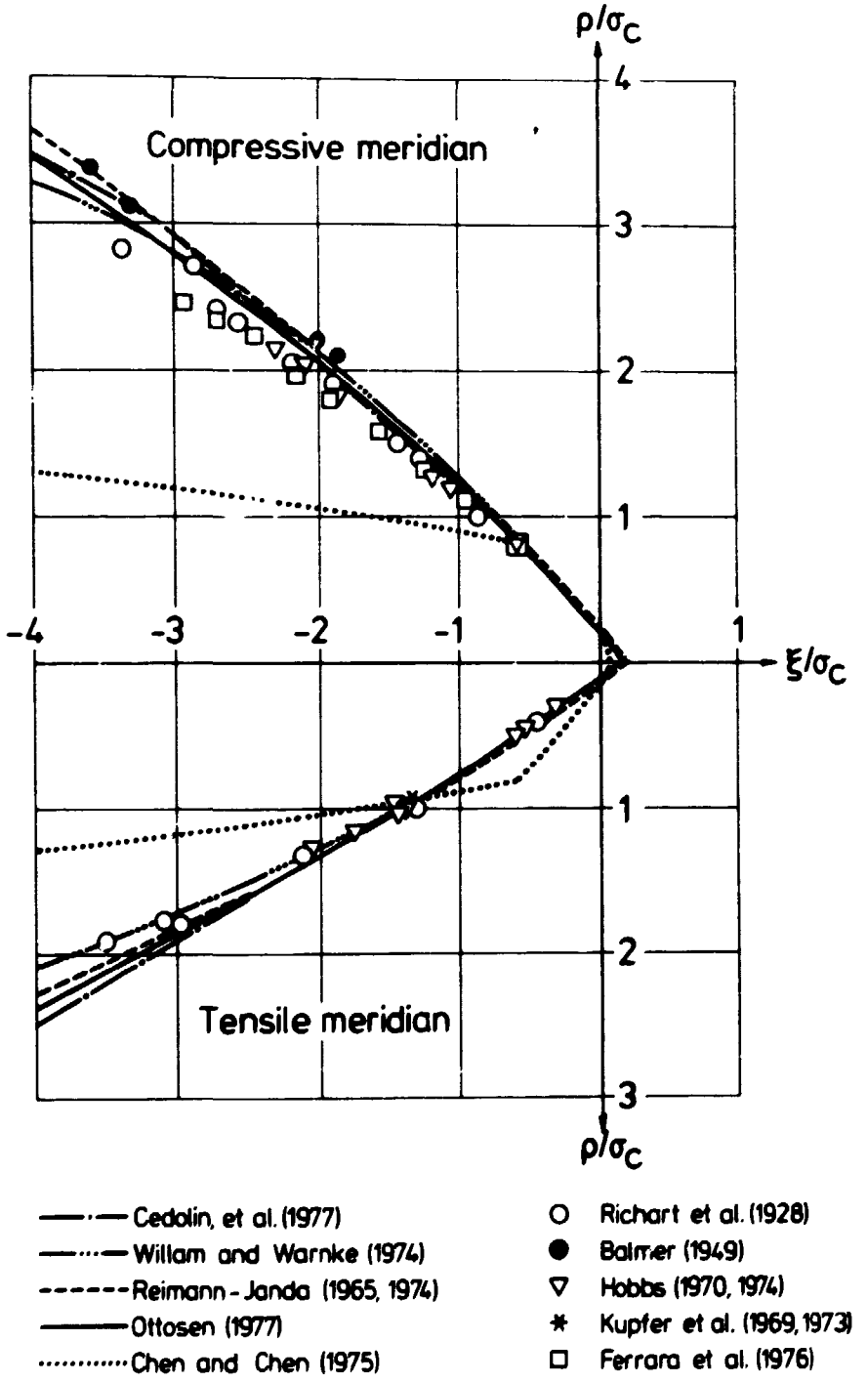

Fig. 2.1-2: Comparison of some failure criteria with some experimental results.

model was used in a strain hardening plasticity theory and to simplify calculations, it neglects the influence of the angle θ leading to a large discrepancy for this model when compared with triaxial experimental results. This will hold for other octahedral criteria as well, for instance that of Drucker and Prager (1952). While the failure surface proposed by Willam and Warnke (1974) intersects the hydrostatic axis for large compressive loading, in the present case when $\xi/\sigma_c \approx -13$, the other surfaces open in the direction of the hydrostatic axis.

The predicted shape in the deviatoric plane for $\xi/\sigma_c = -2$ corresponding to small triaxial compressive loadings, is shown in fig. 3 for the considered criteria. The proposal of Reimann-Janda

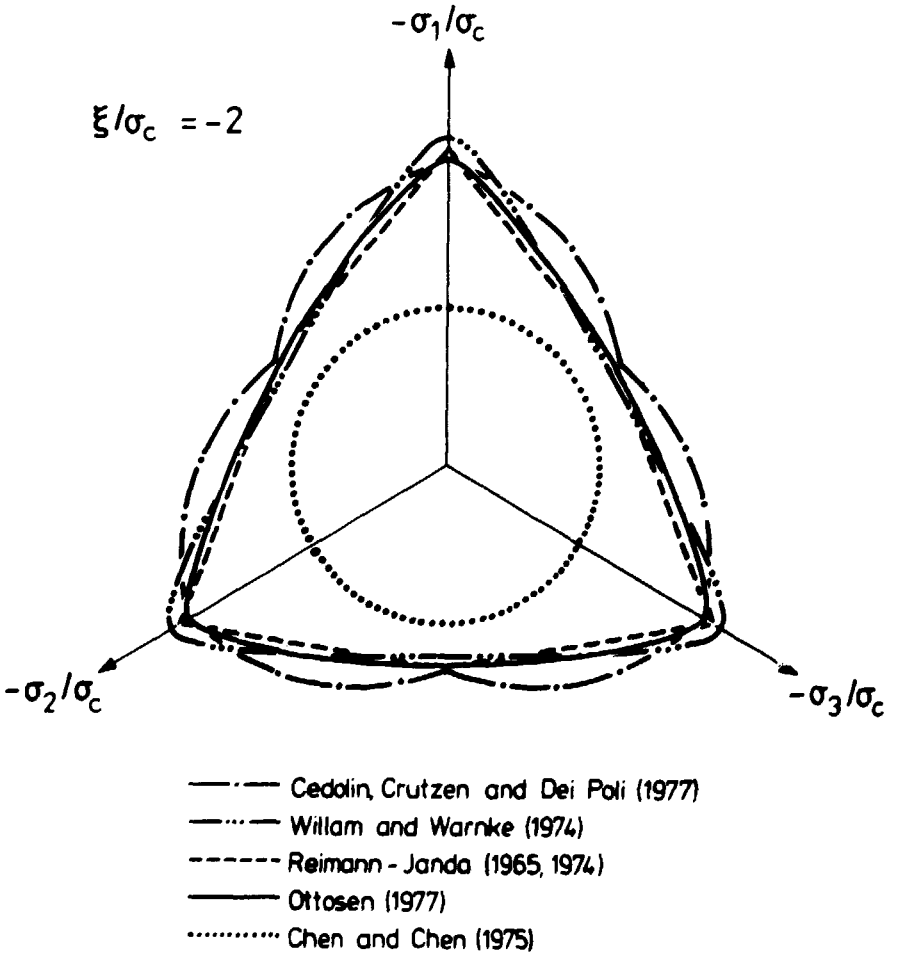

Fig. 2.1-3: Predicted shape in deviatoric plane.

(1965, 1974) and of Cedolin et al. (1977) both involve singular points, i.e. corners. In addition, the trace of the latter proposal is concave along the tensile meridian. As will appear later this concavity has large consequences. The proposal of Willam and Warnke (1974) and of the writer (1977) both correspond to smooth convex curves.

Great importance is attached to plane stress states, and fig. 4 a) shows a comparison for all criteria, except that of Cedolin et al. (1977) with the experimental results of Kupfer et al. (1969, 1973). All criteria in fig. 4 a) show good agreement with the experimental data especially those of Willam and Warnke (1974) and Ottosen (1977) even when tensile stresses occur. Com-

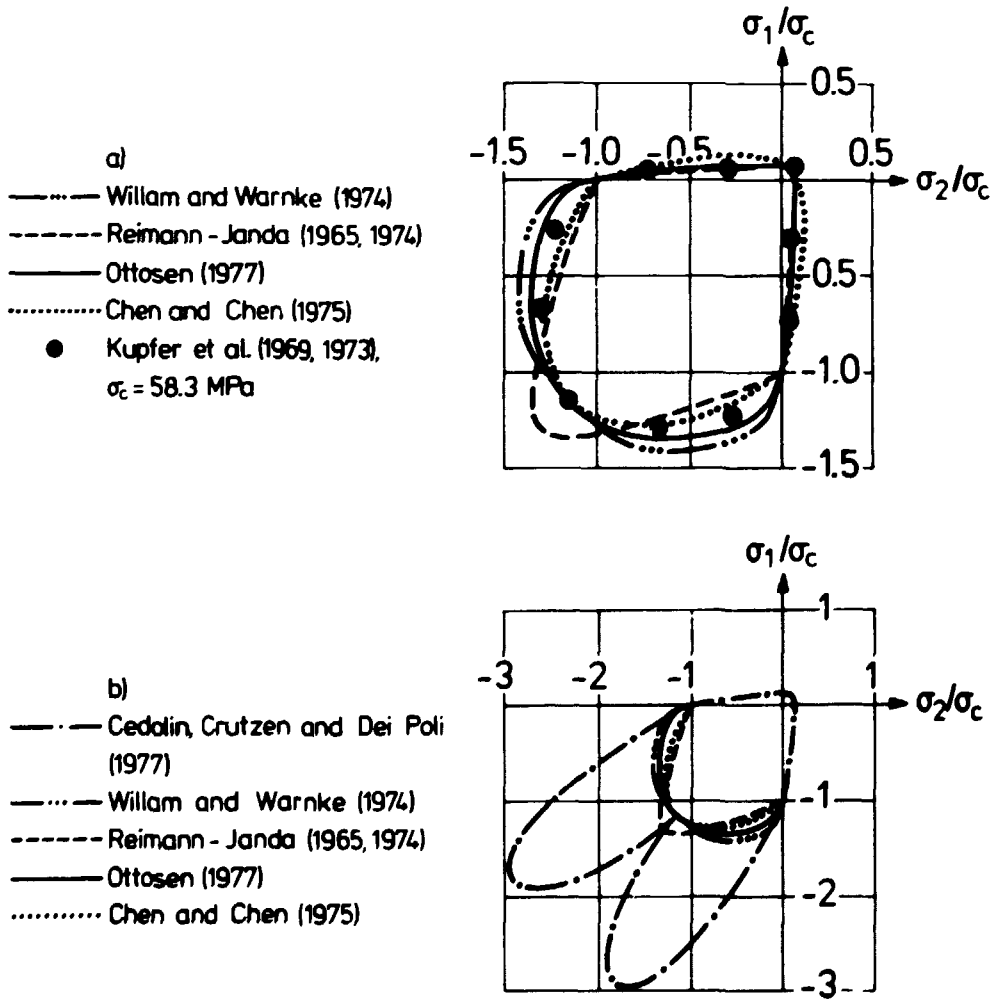

Fig. 2.1-4: Comparison of some failure criteria for plane stress states.

parisons of fig. 2 and 4 a) show that the model of Chen and Chen (1975) is much more suited for predicting biaxial failures than triaxial ones. For biaxial loading, the proposal of Cedolin et al. (1977) is compared with the other criteria in fig. 4 b). It appears that the influence of the concavity along the tensile meridian is ruinous to the obtained curve.

Comparison in general of figs. 3 and 4 reveals that even small changes in the form of the trace in the deviatoric plane have considerable effect on the biaxial failure curve. Indeed, the latter curve is the intersection of the failure surface with a plane that makes rather small angles to planes which are tangent to the failure surface in the region of interest. This emphasizes the need for a very accurate description of the trace in the deviatoric plane. In general, it may be concluded that fitness of a failure criterion can be estimated only when comparisons with experimental data are performed in at least three planes of different type.

2.1.3 The two adopted failure criteria

In the previous section it was shown that the failure criterion proposed by the writer (1977) is an attractive choice when considering criteria proposed quite recently. Let us now investigate this criterion together with the classical Coulomb criterion with tension cut-offs in more details as both criteria are implemented in the finite element program.

The criterion proposed by the writer (1977) uses explicitly the formulation of eq. (4) and suggests that

$$A \frac{J_2}{\sigma_c^2} + \lambda \frac{\sqrt{J_2}}{\sigma_c} + B \frac{I_1}{\sigma_c} - 1 = 0 \qquad (2.1\text{-}5)$$

in which A and B = parameters; and λ = a function of $\cos 3\theta$, $\lambda = \lambda(\cos 3\theta) > 0$. The value of $f(I_1, J_2, \cos 3\theta) < 0$ corresponds to stress states inside the failure surface. For $A > 0$, $B > 0$ it is seen that the meridians are curved (nonaffine), smooth and convex, and the surface opens in the negative direction of the hydrostatic axis. From eq. (5)

$$\frac{\sqrt{J_2}}{\sigma_c} = \frac{1}{2A}\left[-\lambda + \sqrt{\lambda^2 - 4A\left(B\frac{I_1}{\sigma_c} - 1\right)}\right] \qquad (2.1\text{-}6)$$

and it may be shown that when $r = 1/\lambda(\cos 3\theta)$ describes a smooth convex curve in the polar coordinates (r,θ), the trace of the failure surface in the deviatoric plane, as given by eq. (6) is also smooth and convex. When approaching the vertex of the failure surface (corresponding to hydrostatic tension) $\sqrt{J_2} \to 0$, which according to eq. (5) leads to

$$\frac{\sqrt{J_2}}{\sigma_c} \to \frac{1}{\lambda}\left(1 - B\frac{I_1}{\sigma_c}\right) \quad \text{i.e.} \quad \frac{\rho_t}{\rho_c} \to \frac{\lambda_c}{\lambda_t} \text{ for } \sqrt{J_2} \to 0 \qquad (2.1\text{-}7)$$

in which $\lambda_c = \lambda(-1)$ and $\lambda_t = \lambda(1)$ correspond to the compressive and tensile meridian, respectively. As λ_c/λ_t is later determined to be inside the range 0.54-0.58 (see for comparison, table 3), eq. (7) indicates a nearly triangular shape of the trace in the deviatoric plane for small stresses. Furthermore, eq. (6) implies $(\rho_t/\rho_c) \to 1$ for $I_1 \to -\infty$, i.e. for very high compressive stresses, the trace in the deviatoric plane becomes nearly circular. It was found that the function, $\lambda = \lambda(\cos 3\theta)$, could be adequately represented in the form

$$\begin{aligned} \lambda &= K_1 \cos\left[\tfrac{1}{3}\operatorname{Arccos}(K_2 \cos 3\theta)\right] && \text{for } \cos 3\theta \geq 0 \\ \lambda &= K_1 \cos\left[\tfrac{\pi}{3} - \tfrac{1}{3}\operatorname{Arccos}(-K_2 \cos 3\theta)\right] && \text{for } \cos 3\theta \leq 0 \end{aligned} \qquad (2.1\text{-}8)$$

in which K_1 and K_2 = parameters; K_1 is a size factor, while K_2 is a shape factor ($0 \leq K_2 \leq 1$). This form was originally derived by a mechanical analogy, as $r = 1/\lambda(\cos 3\theta)$ given by eq. (8) corresponds to the smooth convex contour lines of a deflected membrane loaded by a lateral pressure and supported along the edges of an equilateral triangle, cf. appendix A. Thus, $r = 1/\lambda(\cos 3\theta)$ represents smooth convex curves with an equilateral triangle and a circle as limiting cases.

The characteristics of the failure surface given by eqs. (5) and (8) are: (1) only four parameters used; (2) use of invariants makes determination of the principal stresses unnecessary; (3) the surface is smooth and convex with the exception of the vertex; (4) the meridians are parabolic and opens in the direction of the negative hydrostatic axis; (5) the trace in the deviatoric plane changes from nearly triangular to circular shape with increasing hydrostatic pressure; (6) it contains several earlier proposed criteria as special cases, in particular, the criterion of Drucker and Prager (1952) for A = 0, λ = constant, and the von Mises criterion for A = B = 0 and λ = constant.

In evaluating the four parameters A, B, K_1 and K_2 use has been made of the biaxial tests of Kupfer et al. (1969, 1973) and the triaxial results of Balmer (1949) and Richart et al. (1928). The parameters are determined so as to represent the following three failure states exactly: (1) uniaxial compressive strength σ_c; (2) biaxial compressive strength $\sigma_{cb} = 1.16\ \sigma_c$ corresponding to the tests of Kupfer et al. (1969, 1973) and (3) uniaxial tensile strength σ_t given by the σ_t/σ_c-ratio (dependence on this ratio is illustrated in tables 2 and 3). Finally, the method of least squares has been used to obtain the best fit of the compressive meridian for $\xi/\sigma_c \geq -5.0$ to the test results of Balmer (1949) and Richart et al. (1928), cf. fig. 5. The compressive meridian is hereby found to pass through the point $(\xi/\sigma_c, \rho/\sigma_c) = (-5.0, 4.0)$. The foregoing procedure implies values of the parameters as given in table 2. The values of K_1 and K_2 correspond to the those of λ_t and λ_c found in table 3.

Table 2.1-2: Parameter values and their dependence on the σ_t/σ_c-ratio.

σ_t/σ_c	A	B	K_1	K_2
0.08	1.8076	4.0962	14.4863	0.9914
0.10	1.2759	3.1962	11.7365	0.9801
0.12	0.9218	2.5969	9.9110	0.9647

Table 2.1-3: λ-values and their dependence on the σ_t/σ_c-ratio.

σ_t/σ_c	λ_t	λ_c	λ_c/λ_t
0.08	14.4725	7.7834	0.5378
0.10	11.7109	6.5315	0.5577
0.12	9.8720	5.6979	0.5772

Although the parameters A, B, K_1 and K_2 show considerable dependence on the σ_t/σ_c-ratio, the failure stresses, when only compressive stresses occur, are influenced only to a minor extent. Using $\sigma_t/\sigma_c = 0.10$ as reference, the difference amounts to less than 2.5%.

Comparison of predictions of the failure criterion with some experimental results has already been given in figs. 2 and 4. Fig. 5 shows a further comparison with some of the earlier applied experimental results, but now for a larger loading range. Fig. 6 contains additional experimental results of Chinn and Zimmerman (1965), Mills and Zimmerman (1970) and the mean of the test results of Launay et al. (1970, 1971, 1972). Comparisons of the last two figures indicate considerable scatter of the test results on the compressive meridian for $\xi/\sigma_c < -5.0$, the tendencies being opposite in the two last figures. Along the tensile meridian the failure criterion underestimates the results of Launay et al. (1970, 1971, 1972) and Chinn and Zimmerman (1965) for $\xi/\sigma_c > -6$, in accordance with the higher biaxial compressive strength determined in these tests (1.8 σ_c and 1.9 σ_c, respectively) compared with that used to determine the parameters of the failure criterion. Mills and Zimmerman (1970) determined the biaxial compressive strength to 1.3 σ_c.

If the compressive and tensile meridians are accurately represented, the trace of the failure surface in the deviatoric plane is confined to within rather narrow limits provided that the trace is a smooth, convex curve. This is especially pronounced when the ρ_t/ρ_c ratio is close to the minimum value 0.5. The ability of the considered failure surface to represent the experimental biaxial results of Kupfer et al. (1969, 1973) outside the

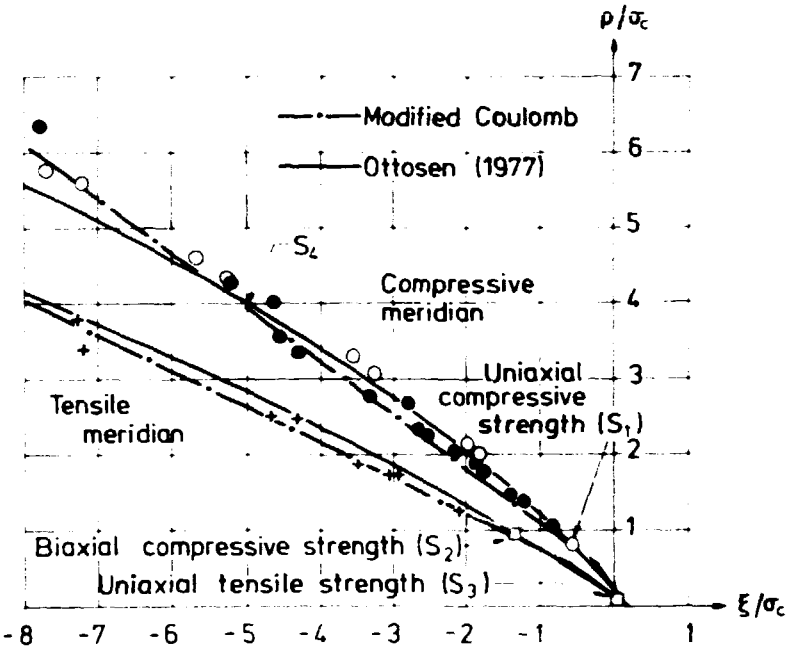

Fig. 2.1-5: Comparisons of test results by: Balmer (1949) o (Compressive); Richart et al. (1928) ● (Compressive), + (Tensile); Kupfer et al. (1969, 1973) ▫ (Tensile) (Failure stresses S_1, S_2, S_3 and S_4 determine parameters in writers failure criterion). $\sigma_t/\sigma_c = 0.1$ used in the criteria.

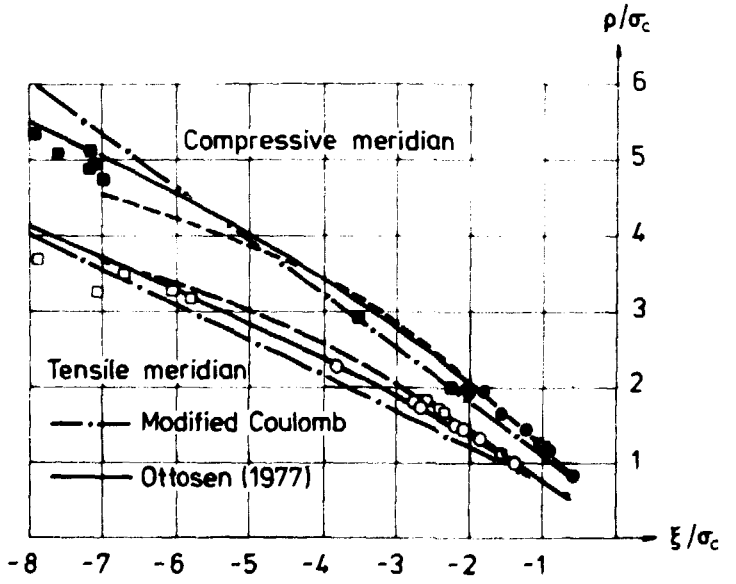

Fig. 2.1-6: Mean values of Launay et al. (1970, 1971, 1972) --- (Compressive), — — (Tensile); Chinn and Zimmerman (1965) ■ (Compressive), ▫ (Tensile); Mills and Zimmerman (1970) ● (Compressive) o (Tensile). $\sigma_t/\sigma_c = 0.1$ used in the criteria.

tensile and compressive meridians was shown previously in fig. 4. However, to facilitate comparison of the failure criteria considered there, not all available experimental results were given when tensile stresses are present. A more detailed comparison with the failure criterion considered now is therefore illustrated in fig. 7.

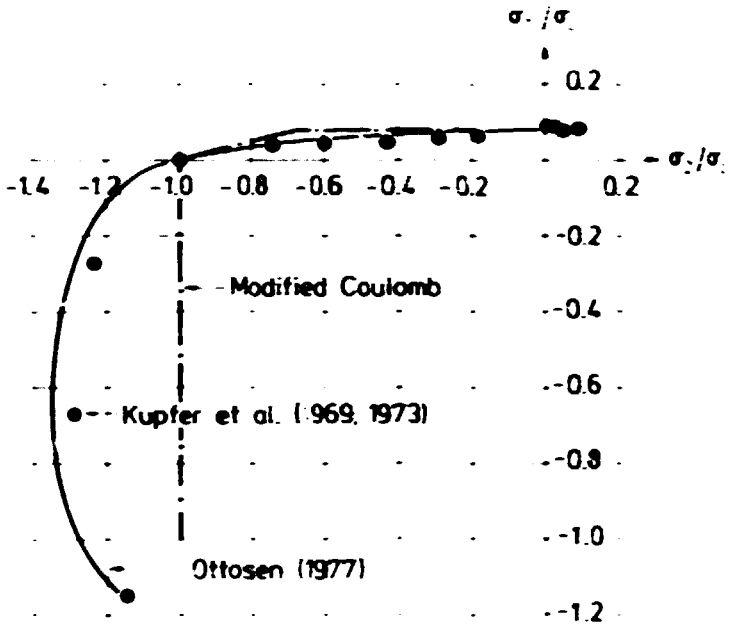

Fig. 2.1-7: Biaxial tests of Kupfer et al. (1969, 1973), σ_c = 58.3 MPa. $\sigma_t = 0.08\ \sigma_c$ used in both criteria.

The agreement is considered satisfactory, the largest difference occurring in compression when $\sigma_1/\sigma_2 \simeq 0.5$. In this case Kupfer et al. obtained $\sigma_2 = -1.27\ \sigma_c$ as the mean value of tests with σ_c ranging from 18.7 - 58.3 MPa; on the other hand the failure criterion with the parameters of table 2 gives - 1.35 σ_c, - 1.38 σ_c and - 1.41 σ_c for σ_t/σ_c = 0.08, 0.10, and 0.12, respectively. It is interesting to note that the classical biaxial tests of Wästlund (1937) with σ_c ranging from 24.5 - 35.0 MPa give $\sigma_2 = -1.37\ \sigma_c$ with almost the same biaxial strength (1.14 σ_c) as the results of Kupfer et al (1.16 σ_c).

Surmarizing, the failure criterion given by eqs. (5) and (8) contains the three stress invariants explicitly and it corresponds to a smooth convex surface with curved meridians which open in the negative direction of the hydrostatic axis. The trace in the deviatoric plane changes from an almost triangular to a more

circular shape with increasing hydrostatic pressure. The criterion has been demonstrated to be in good agreement with experimental results for different types of concrete and covers a wide range of stress states including those where tensile stresses occur. The formulation in terms of one function for all stress states facilitates its use in structural calculations and it has been shown that a sufficiently accurate calibration of the parameters in the criterion is obtained by knowledge of the uniaxial compressive strength σ_c and the uniaxial strength σ_t alone.

As mentioned previously, the other failure criterion implemented in the finite element program is the classical Coulomb criterion with tension cut-offs which consist of a combination of the Coulomb criterion suggested in 1773 and the maximum tensile stress criterion often attributed to Rankine, 1876. This dual criterion was originally proposed by Cowan (1953) but using the terminology of Paul (1961), it is usually termed the modified Coulomb criterion. It reads,

$$\begin{aligned} m\sigma_1 - \sigma_3 &= \sigma_c \\ \sigma_1 &= \sigma_t \end{aligned} \qquad (2.1\text{-}9)$$

where, as previously, $\sigma_1 \geq \sigma_2 \geq \sigma_3$ and tensile stress is considered positive. The criterion contains three parameters and it includes a cracking criterion given by the second of the above two equations. The coefficient m is related to the friction angle φ by $m = (1 + \sin\varphi)/(1 - \sin\varphi)$. Different m-values have been proposed in the past, but here we adopt the value

$$m = 4 \qquad (2.1\text{-}10)$$

corresponding to a friction angle equal to 37°. This value has been proposed both by Cowan (1953) and by Johansen (1958, 1959) and is applied almost exclusively in the Scandinavian countries.

As shown in fig. 8 the modified Coulomb criterion corresponds to an irregular hexagonal pyramid with straight meridians and with tension cut-offs. The trace in the deviatoric plane is shown in fig. 8 together with the other criterion implemented in the fin-

ite program. A comparison with this latter criterion and some experimental results is shown in figs. 5, 6 and 7.

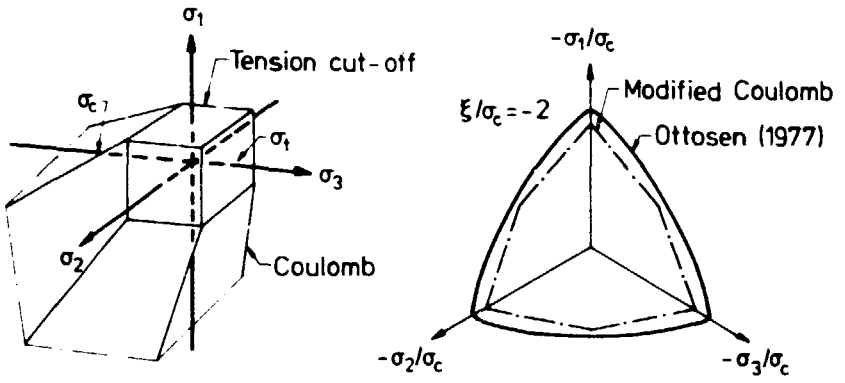

Fig. 2.1-8: Appearance of the modified Coulomb criterion.

It appears that for most stress states of practical interest the modified Coulomb criterion underestimates the failure stresses. This is quite obvious when considering for instance the case of plane stress, fig. 7. However, it is important to note that the modified Coulomb criterion provides a fair approximation that is comparable in accuracy to many recently proposed failure criteria and with the simplicity of the modified Coulomb criterion in mind it may be considered as quite unique. Note also that just like the other criterion implemented in the finite element program, calibration of the modified Coulomb criterion requires only knowledge of the uniaxial compressive strength σ_c and the uniaxial tensile strength σ_t for the concrete in question.

In conclusion, the two failure criteria implemented in the finite element program each provide realistic failure predictions for general stress states. While the criterion proposed by the writer (1977) is superior when considering accuracy the modified Coulomb criterion possesses an attractive simplicity.

2.1.4. Adopted cracking criteria

As the failure criterion proposed by the writer (1977) applies to all stress states, in terms of one equation, it must be augmented by a failure mode criterion to determine the possible ex-

istence of tensile cracks. Following the proposal of the writer (1979) we assume that the cracking occurs, firstly, if the failure criterion is violated and secondly, if $\sigma_1 \geq \sigma_t/2$ holds. Note that this crack criterion may be applied to any smooth failure surface.

The other failure criterion implemented in the finite element program - the modified Coulomb criterion - already includes a cracking criterion determined by $\sigma_1 \geq \sigma_t$.

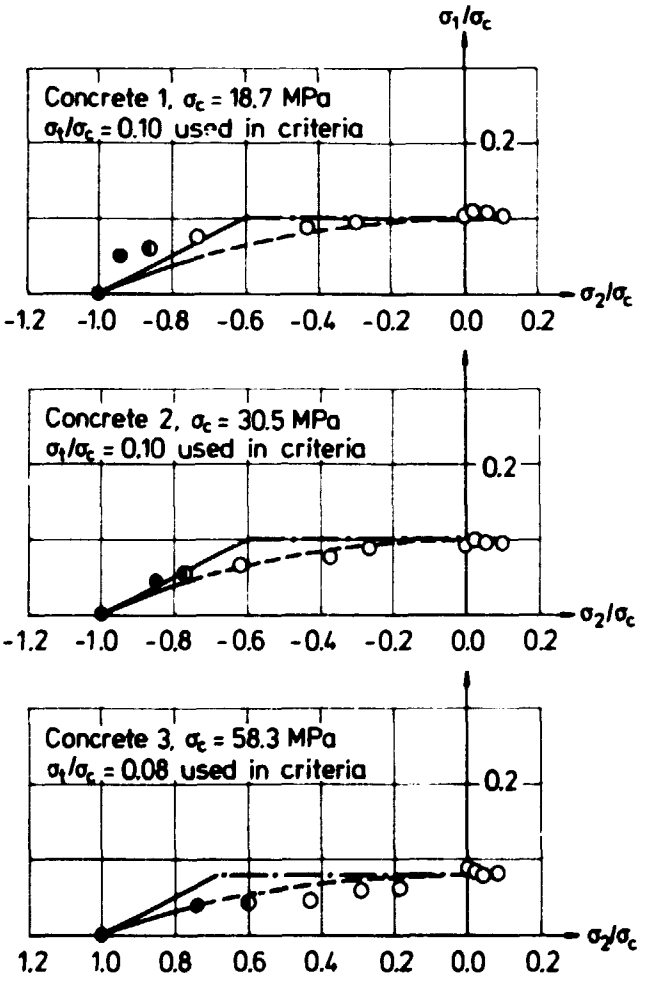

Fig. 2.1-9: Failure criteria and failure mode criteria compared with the biaxial results of Kupfer et al. (1969,1973). Writers proposal: tensile cracking indicated by ----. Modified Coulomb criterion: tensile cracking indicated by -·-. Test results: ● compressive crushing, o tensile cracking ◐ no particular mode.

Figure 9 contains the experimental results of Kupfer et al. (1969, 1973) for biaxial tensile-compressive loading of three different types of concrete. Both failure stresses and failure modes are indicated. In addition, the figure shows the corresponding failure curves together with their failure mode criteria using the two failure criteria implemented in the finite element program. It appears that the two failure mode criteria and the two failure criteria are in close agreement with the experimental evidence. In accordance with earlier conclusions the proposals of the writer are favourable when considering accuracy. The modified Coulomb criterion , on the other hand, possesses an attractive simplicity.

For both failure mode criteria it is assumed that the orientation of the crack plane is normal to the principal direction of σ_1. This assumption is also in good agreement with the aforementioned tests.

2.2. Stress-strain relations

Having discussed the strength of concrete in some detail, the stress-strain behaviour will now be dealt with. Ideally, a constitutive model for concrete should reflect the strain hardening before failure, the failure itself as well as the strain softening in the post-failure region. The post-failure behaviour has received considerable attention in the last years especially, where it has become evident that the calculated load capacity of a structure may be strongly influenced by the particular post-failure behaviour employed for the concrete; for example ideal plasticity with its infinite ductility might be an over-simplified model. This is just to say that redistribution of stresses in a structure must be dealt with in a proper way. These aspects will be considered in some detail in section 5. Moreover, the constitutive model should ideally be simple and flexible, i.e. different assumptions can easily be incorporated. The numerical performance of the model in a computer program should also be considered. Moreover, it should be applicable to all stress states and both loading and unloading should ideally be dealt

with in a correct way. Eventually, and as a very important feature, the model should be easy to calibrate to a particular type of concrete. For instance it is very advantageous if all parameters are calibrated by means of uniaxial data alone.

A model reflecting most of the above-mentioned features will be described in the following, but prior to this attention will be turned towards the large number of proposals for predicting the nonlinear behaviour of concrete that have appeared in the past. Plasticity models have been proposed; however because of their simplicity the bulk of the models are nonlinear elastic ones. A review of some models is given as follows:

Plasticity models based on linear elastic-ideal plastic behaviour using the failure surface as yield surface have been proposed by e.g. Zienkiewicz et al. (1969), Mroz (1972), Argyris et al. (1974) and Willam and Warnke (1974). A somewhat different approach still accepting linear elastic behaviour up to failure was put forward by Argyris et al. (1976) using the modified Coulomb criterion as failure criterion. Instead of a flow rule this model uses different stress transfer strategies when stresses exceed the failure state. A very essential feature is that different post-failure behaviours can be reflected in the model. To consider the important nonlinearities before failure, models using the theory of hardening plasticity have been proposed by e.g. Green and Swanson (1973), Ueda et al. (1974) and Chen and Chen (1975), all of whom neglect the important effect of the third stress invariant, while Hermann (1978) includes the effect. However, as these plasticity models all make use of Drucker's stability criterion (1951) they are not able to consider the strain softening effects occurring after failure. Coon and Evans (1972) applied a hypoelastic model of grade one, but this model also operates with two stress invariants only, and strains are inferred as infinite at maximum stress.

Incremental nonlinear elastic models based on the Hookean anisotropic formulation have been proposed for plane stress by Liu et al. (1972) and Link et al. (1974, 1975). The model of Darwin and Pecknold (1977) applicable for plane stresses can even be

used for cyclic loading in the post-failure region. In contrast to these proposals, similar models that now assume the incremental isotropic formulation neglect the stress-induced anisotropy, and softening and dilatation cannot be dealt with. This is because tangential values of Young's modulus and Poisson's ratio can never become negative or larger than 0.5, respectively. However, a tangential formulation facilitates the numerical performance regarding convergence in a computer code. A model based on this incremental and isotropic concept and applicable for general plane stresses was introduced by Romstad et al. (1974) using a multilinear approach. In the models proposed by Zienkiewicz et al. (1974) and Phillips et al. (1976) the tangential shear modulus variates as a function of the octahedral shear stress alone. In principle, a similar approach applicable for compressive stresses and valid until dilatation occurs was later applied by Riccioni et al. (1977), but in this model the influence of all the stress invariants on both the tangential bulk modulus and the tangential shear modulus was considered. Recently, Bathe and Ramaswamy (1979) proposed a model considering all stress invariants also and applicable for general stress states while the Poisson ratio was assumed to be constant.

Several nonlinear elastic models of the Hookean isotropic form using the secant values of the material parameters have also been put forward. An early proposal of Saugy (1969) considered the bulk modulus as a constant and the shear modulus as a function of the octahedral shear stress alone. For plane compressive stresses Kupfer (1973) and Kupfer and Gerstle (1973) assumed both these moduli to be functions of the octahedral shear stress. Palamiswamy and Shah (1974) and Cedolin et al. (1977) proposed models applicable to triaxial compressive stress states also. However only the influence of the first two stress invariants on the bulk and shear moduli are considered and the validity of the models is limited to stress states not too close to failure. Also the recent approach by Kotsovos and Newman (1978) neglects the influence of the third invariant. Schimmelpfennig (1975, 1976) made use of a model where the shear modulus changes. All stress invariants are considered but only compressive stress states can be dealt with, and dilatation is excluded.

All the nonlinear elastic models mentioned previously, except the proposals of Romstad et al. (1974), Darwin and Pecknold (1977), Bathe and Ramaswamy (1979) and to some extent, that of Riccioni et al. (1977), have to be argumented by a failure criterion that is formulated completely independently of the stress-strain relations presented. This results in a nonsmooth transition from the prefailure behaviour to the failure state. In addition, all these models, except again, the model of Romstad et al. (1974), Darwin and Pecknold (1977), Bathe and Ramaswamy (1979) and to some extent, the model of Cedolin et al. (1977), are valid only for a particular type of concrete. As a result, the models can only be calibrated to other types of concrete if, in addition to uniaxial results, biaxial or triaxial test results are also available for the concrete in question.

Recently, Bažant and Bhat (1976) extended to endochronic theory to include concrete behaviour. Very important characteristics such as dilatation, softening and realistic failure stresses are simulated and the model can be applied to general stress states even for cyclic loading. In a later version of the model, Bažant and Shieh (1978), even the nonlinear response to compressive hydrostatic loading was reflected. However, Sandler (1978) has questioned the uniqueness and stability of the endochronic equations and the modelling only through the value of the actual concrete's uniaxial compressive strength is another important aspect. This seems to be a rather crude approximation even for uniaxial compressive loading, as different failure strains and initial stiffnesses can be obtained for concrete possessing the same uniaxial compressive strength.

The following model proposed by the writer (1979) for the description of the nonlinear stress-strain relations of concrete is based on nonlinear elasticity, where the secant values of Young's modulus and Poisson's ratio are changed appropriately. Path-dependent behaviour is naturally beyond the possibilities of the model and the same holds also for a realistic response to unloading when nonlinear elasicity is used. However, from the way in which the model is implemented in the program, cf. section 4.6, its unloading characteristics is greatly improved compared

to that of nonlinear elasticity and the model indeed corresponds to the behaviour of a fracturing solid, Dougill (1976). Moreover, the described model is able to represent in a simple way most of the characteristics of concrete behaviour, even for general stress states. These features include: (1) the effect of all three stress invariants; (2) consideration of dilatation; (3) the obtaining of completely smooth stress-strain curves; (4) prediction of realistic failure stresses; (5) simulation of different post-failure behaviours and (6) the model applies to all stress states including those where tensile stresses occur. In addition, the model is simple to use, and calibration to a particular type of concrete requires only experimental data obtained by standard uniaxial tests. The construction of the model can conveniently be divided into four steps: (1) failure and cracking criteria; (2) nonlinearity index; (3) change of the secant value of Young's modulus and (4) change of the secant value of Poisson's ratio. The failure and cracking criteria utilized in this section are the ones proposed by the writer and dealt with in sections 2.1.3 and 2.1.4. In the finite element program the modified Coulomb criterion described previously is also used together with the following stress-strain model and it should be emphasized that any failure criterion can be employed in connection with the described constitutive model, and no change as such is necessary because the criterion in question is involved only through the determination of the nonlinearity index, as defined.

2.2.1. Nonlinearity index

Let us now define a convenient measure for the given loading in relation to the failure surface. First of all, we have to determine to which failure state the actual stress state should relate. Although there is an infinite number of possibilities, four essentially different types can be identified. To achieve a simple illustration, we will at present adopt as failure criterion the Mohr criterion shown in fig. 1 a), which also shows the actual stress state given by σ_1 and σ_3. Failure can be obtained by increasing the σ_1-value as shown by circle I, or alternatively by fixing the $(\sigma_1 + \sigma_3)/2$-value as shown by circle II. However, tensile stresses may then be involved in the failure

state as shown in fig. 1 a) and an evaluation of, e.g., a uniaxial compressive stress state, would depend on the tensile

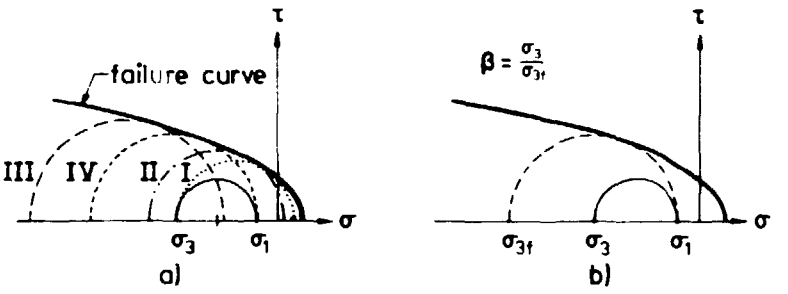

Fig. 2.2-1: Mohr diagrams. (a) Different ways to obtain failure; (b) Definition of nonlinearity index β.

strength, which seems invonvenient. A third method indicated by circle III, where all stresses are changed proportionally, is also rejected as, depending on the form of the failure curve, failure may not be obtained from some compressive stress states located outside the hydrostatic axis. However, failure can always be obtained by decreasing the σ_3-value as shown by circle IV, and this procedure is adopted here.

Next, we must determine a measure for the actual loading, and here we adopt the ratio of the actual stress, σ_3, to the corresponding value of that stress at failure, σ_{3f}, as shown in fig. 1 b). In summary, for an arbitrary choice of failure criterion, we define a measure for the actual loading, the nonlinearity index, β, by

$$\beta = \frac{\sigma_3}{\sigma_{3f}} \qquad (2.2\text{-}1)$$

in which σ_3 = the actual most compressive principal stress; and σ_{3f} = the corresponding failure value, provided that the other principal stresses, σ_1 and σ_2, are unchanged ($\sigma_1 \geq \sigma_2 \geq \sigma_3$). Thus, $\beta < 1$, $\beta = 1$ and $\beta > 1$ correspond to stress states located inside, on, and outside the failure surface, respectively.

The nonlinearity index, β, given by eq. (1), has the advantage

of being proportional to the stress for uniaxial compressive loading, i.e., it can be considered as an effective stress. Note that the nonlinearity index depends on all three stress invariants if the failure criterion does also. The β-values will later be used as a kind of measure for the actual nonlinearity; fig. 2, where the failure criterion proposed by the writer (1977) is applied and where contour lines for constant β-values are shown, demonstrates its convenience for this purpose. Fig. 2 a) shows meridian planes containing the compressive and tensile meridian. Points corresponding to the uniaxial compressive strength, S_1, and the biaxial compressive strength, S_2, are shown on these meridians, and failure states involve tensile stresses to the right of these points. Fig. 2 b) shows curves in a deviatoric plane. Note in fig. 2 a) that in contrast to the failure surface, sur-

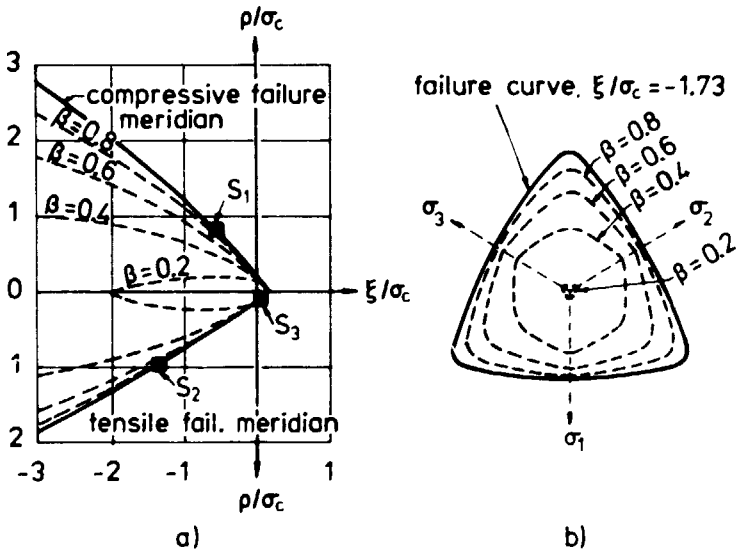

Fig. 2.2-2: Contour lines of constant β-values. (a) Meridian planes, S_1 = uniaxial compressive strength, S_2 = biaxial compressive strength, S_3 = uniaxial tensile strength; (b) Deviatoric plane. Failure criterion proposed by the writer (1977) is applied.

faces on which the nonlinearity index is constant are closed in the direction of the negative hydrostatic axis. For small β-values, these surfaces resemble the one that defines the onset of the stable fracture propagation, i.e. the discontinuity limit (see, for comparison, Newman and Newman (1973) and Kotsovos and

Newman (1977)).

When tensile stress occur, a modification of the definition of the nonlinearity index is required as concrete behaviour becomes less nonlinear, the more the stress state involves tensile stresses. For this purpose we transform the actual stress state $(\sigma_1, \sigma_2, \sigma_3)$, where at least σ_1 is a tensile stress, by superposing the hydrostatic pressure, $-\sigma_1$, obtaining the new stress state $(\sigma_1', \sigma_2', \sigma_3') = (0, \sigma_2 - \sigma_1, \sigma_3 - \sigma_1)$, i.e. a biaxial compressive stress state. The index β is then defined as

$$\beta = \frac{\sigma_3'}{\sigma_{3f}'} \qquad (2.2\text{-}2)$$

In which σ_{3f}' is the failure value of σ_3' provided that σ_1' and σ_2' are unchanged, i.e. the stress state $(\sigma_1', \sigma_2', \sigma_{3f}')$ is to satisfy the failure criterion. This procedure has the required effect, as shown in fig. 2 a), of reducing the β-values appropriately when tensile stresses occur and $\beta < 1$ will always apply. Point S_3 on fig. 2 a) corresponds to the uniaxial tensile strength, and $\beta = 0$ holds for hydrostatic tension. Contour surfaces for constant β-values are smooth, except for points where tensile stresses have just become involved.

2.2.2. Change of the secant value of Youngs's modulus

To obtain expressions for the secant value of Young's modulus under general triaxial loading, we begin with the case of uniaxial compressive loading. Here we approximate the stress-strain curve as proposed by Sargin (1971)

$$-\frac{\sigma}{\sigma_c} = \frac{-A\,\frac{\varepsilon}{\varepsilon_c} + (D-1)\,\left(\frac{\varepsilon}{\varepsilon_c}\right)^2}{1-(A-2)\,\frac{\varepsilon}{\varepsilon_c} + D\,\left(\frac{\varepsilon}{\varepsilon_c}\right)^2} \qquad (2.2\text{-}3)$$

Tensile stress and elongation are considered positive, and ε_c determines the strain at failure, i.e., $\varepsilon = -\varepsilon_c$ when $\sigma = -\sigma_c$. The parameter A is defined by $A = E_i/E_c$, in which $E_c = \sigma_c/\varepsilon_c$. The Young's moduli E_i and E_c are the initial modulus and the secant modulus at failure, respectively; D = a parameter mainly

affecting the descending curve in the post-failure region. Eq. (3) is a four-parameter expression determined by the parameters σ_c, ε_c, E_i, and D, and it infers that the initial slope is E_i, and that there is a zero slope at failure, where $(\sigma,\varepsilon) = (-\sigma_c, -\varepsilon_c)$ satisfies the equation. The parameter D determines the post-failure behaviour, and even though there are some indications of this behaviour, e.g. Karsan and Jirsa (1969), the precise form of this part of the curve is unknown and is in fact, not obtained by a standard uniaxial compressive test. Therefore, the actual value of D is simply chosen so that a convenient post-failure curve results. However, there are certain limitations to D, if eq. (3) is to reflect: (1) an increasing function without inflexion points before failure; (2) a decreasing function with at most one inflexion point after failure; (3) a residual strength equal to zero after sufficiently large strain. To achieve these features $A > 4/3$ must hold, and the parameter D is subject to the following restrictions

$$(1-\tfrac{1}{2}A)^2 < D \leq 1+A(A-2) \text{ when } A \leq 2;$$

$$0 \leq D \leq 1 \text{ when } A \leq 2$$

The requirement $A > 4/3$ is in practice not a restriction, and, in fact, eq. (3) provides a very flexible procedure to simulate the uniaxial stress-strain curve. For instance, the proposal of Saenz (1964) follows when D = 1, the Hognestad parabola (1951) follows when A = 2 and D = 0, and the suggestion of Desayi and Krishnan (1964) follows when A = 2 and D = 1. In addition, different post-failure behaviours can be simulated by means of the parameter D and this affects only the behaviour before failure insignificantly. This is shown in fig. 3, where A = 2 is assumed and where the limits of D are given by zero and unity.

Using simple algebra, eq. (3) can be solved to obtain the actual secant value E_s of Young's modulus. The expression for E_s contains the actual stress in terms of the ratio $-\sigma/\sigma_c$. For uniaxial compressive loading $\beta = -\sigma/\sigma_c$ holds, and the expression for E_s can therefore be generalized to triaxial compressive load-

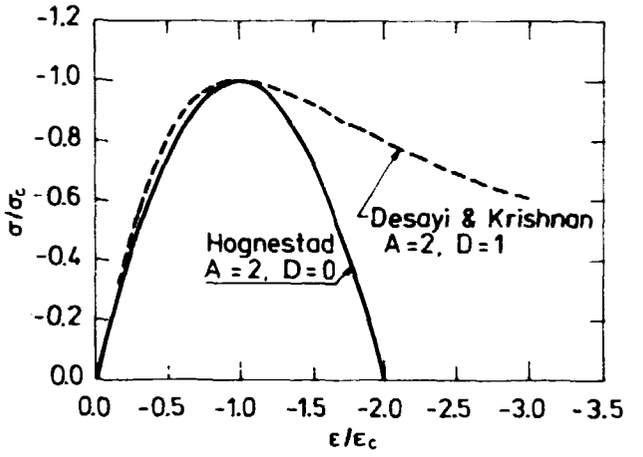

Fig. 2.2-3: Control of post-failure behaviour by means of parameter D in eq. (3).

ing, if we replace the ratio - σ/σ_c by β. We then obtain

$$E_s = \tfrac{1}{2}E_i - \beta(\tfrac{1}{2}E_i - E_f) \pm \sqrt{[\tfrac{1}{2}E_i - \beta(\tfrac{1}{2}E_i - E_f)]^2 + E_f^2\beta[D(1-\beta)-1]} \quad (2.2\text{-}4)$$

in which the positive and negative signs apply to the ascending and descending part of the curves, respectively. In eq. (4) the parameter value E_c, denoting the secant value of Young's modulus at uniaxial compressive failure, has been replaced by E_f, the secant value of Young's modulus at general triaxial compressive failure. By means of the aforementioned procedure, we obtain that the stress-strain curves for general triaxial compressing loading have the same features as the stress-strain curve of uniaxial compressive loading: (1) a correct initial slope; (2) a zero slope at failure; (3) the correct failure stresses when the failure strains are given; and (4) a realistic post-failure behaviour. Note, in particular, that we obtain correct failure stresses in the general triaxial compressive case by use of the nonlinearity index β, provided that a correct failure criterion is applied. This holds even if the value of the parameter E_f is incorrect. In fact, this parameter remains to be determined before eq. (4) can be applied. In general, the E_f value is a function of the type of loading, the type of concrete, etc. Considering general compressive loadings, it was found that a sufficiently accurate expression is

$$E_f = \frac{E_c}{1 + 4(A - 1)\, x} \qquad (2.2\text{-}5)$$

in which x represents the dependence on the actual loading and is given by $x = (\sqrt{J_2}/\sigma_c)_f - (\sqrt{J_2}/\sigma_c)_{f,c} = (\sqrt{J_2}/\sigma_c)_f - 1/\sqrt{3}$. The term $(\sqrt{J_2}/\sigma_c)_f$ denotes the failure value of the invariant $\sqrt{J_2}/\sigma_c$, where the failure stress state is that connected with the determination of the nonlinearity index, eq. (1). Correspondingly, $(\sqrt{J_2}/\sigma_c)_{f,c} = 1/\sqrt{3}$ is the value at failure for uniaxial compressive loading. Note that we presently deal only with compressive stress states, and we have $x \geq 0$, where $x = 0$ holds for uniaxial loading. The value $E_f = E_c$ holds when $x = 0$; otherwise $E_f < E_c$ applies. The dependence of E_f on the actual type of concrete is represented in eq. (5) by the parameters E_c and A.

Thus, when no tensile stresses occur, the actual secant value E_s is determined by eq. (4), in which the nonlinearity index is given by eq. (1), and the E_f value is given by eq. (5). When tensile stresses occur, the behaviour becomes more linear, and this is accomplished simply by again obtaining E_s from eq. (4). However, the nonlinearity index is now determined by eq. (2) and eq. (5) is replaced by the assumption $E_f = E_c$.

If cracking occurs, a completely brittle behaviour is assumed, and if only compressive stresses occur, the post-failure behaviour for the crushing of the concrete is controlled by eq. (4) through appropriate choice of the parameter D. The post-failure behaviour for intermediate stress states, where small tensile stresses are present but where there is neither cracking nor compressive crushing of the concrete, has apparently not been determined experimentally, but is conveniently obtained by the following hybrid procedure: At failure these intermediate stress states result in a nonlinearity index β_f, as determined by eq. (2), that is less than unity. As shown in fig. 4, the post-failure curve AB is then assumed to be obtained by translation of the part MN of the original descending branch of the curve parallel to the horizontal axis. The secant value E_s, corresponding to some actual β value is then easily shown to be determined by

$$E_s = \frac{\beta E_{MN} E_A E_M}{\beta E_A E_M + \beta_f E_{MN}(E_M - E_A)} \qquad (2.2\text{-}6)$$

in which E_{MN}, depending on β, is the secant value along the original post-failure curve MN obtained by means of eq. (4), using the negative sign. Likewise, the constants E_A and E_M are secant values at failure also determined by eq. (4) using the positive and negative sign, respectively, and the nonlinearity index value at failure, i.e. $\beta = \beta_f$. The preceding moduli are shown in fig. 4. Eq. (6) implies a gradual change of the post-failure behaviour, both when the stress state is changed towards purely compressive states, or towards stress states where cracking occurs.

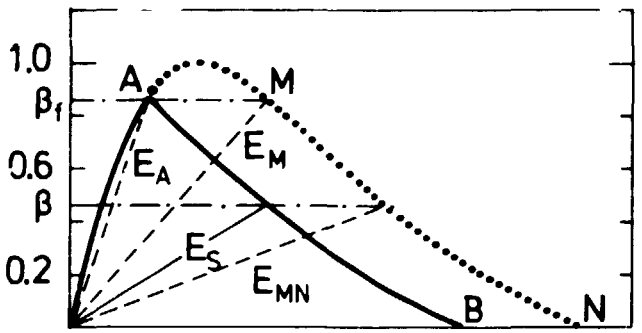

Fig. 2.2-4: Post-failure behaviour for intermediate stress states that do not result in cracking or compressive crushing of concrete.

2.2.3. Change of the secant value of Poisson's ratio

Let us now turn to the determination of the secant value υ_s of Poisson's ratio. Both for uniaxial and triaxial compressive loading we note that the volumetric behaviour is a compaction followed by a dilatation. The expression of υ_s for uniaxial compressive loading is therefore generalized to triaxial compressive loading by use of the nonlinearity index β. Hereby we obtain

$$\upsilon_s = \upsilon_i \text{ when } \beta \leq \beta_a$$

$$\upsilon_s = \upsilon_f - (\upsilon_f - \upsilon_i)\sqrt{1 - \left(\frac{\beta - \beta_a}{1 - \beta_a}\right)^2} \text{ when } \beta \geq \beta_a \qquad (2.2\text{-}7)$$

in which υ_i = the initial Poisson ratio; and υ_f = the secant value of Poisson's ratio at failure. Eq. (7) is shown in fig. 5.

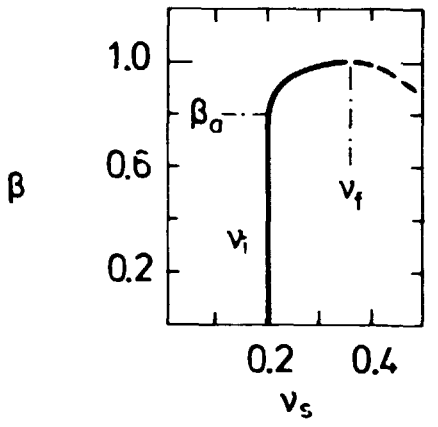

Fig. 2.2-5: Variation of secant value of Poisson's ratio.

The second of these equations, which represents one-quarter of an ellipse, is valid only until failure. Very little is known of the increase of υ_s in the post-failure region, but it is an experimental fact that dilatation continues here. Now, for a given change of the secant value E_s, there corresponds a secant value υ_s^*, so that the corresponding secant bulk modulus is unchanged. In this report, we decrease the E_s value by steps of 5% in the post-failure region, and to ensure dilatation in this region also we then simply put $\upsilon_s = 1.005\ \upsilon_s^*$ in each step, although other values may also be convenient. A similar approach is used for the intermediate stress states where tensile stresses are present but no cracking occurs. In the model, $\upsilon_s < 0.5$ must always hold, but this limit is achieved only far inside the post-failure region. In eq. (7), a fair approximation is obtained when the following parameter values are applied for all types of loading and concrete

$$\beta_a = 0.8; \qquad \upsilon_f = 0.36 \tag{2.2-8}$$

As before, the β value to be applied in eq. (7) is determined by eq. (1) when only compressive stresses occur, and by eq. (2) when tensile stresses are present.

In summary, the constitutive model is based on nonlinear elasticity, where the secant values of Young's modulus E_s, and Poisson's ratio υ_s, are changed appropriately. We select a failure criterion, and on this basis calculate the nonlinearity index

defined by eq. (1), when compressive stresses alone occur, and by eq. (2) when tensile stresses are present. Here we apply the failure criterion proposed by the writer (1977), but any criterion can be used, and the choice influences only the β value. The secant value E_s is given by eq. (4) coupled with eq. (5) when compressive stresses occur alone, and coupled with $E_f = E_c$ when tensile stresses are present. The secant value υ_s, is given by eqs. (7) and (8). The model is calibrated by six parameters: the two initial elastic parameters, E_i and υ_i, the two strength parameters, σ_c and σ_t, the ductility parameter ε_c, and finally the post-failure parameter D. While the D value is chosen, following earlier remarks, so that a convenient post-failure behaviour is obtained the other parameters are found from standard uniaxial tests. Let us now illustrate the abilities of the model by comparing its predictions with experimental results arrived at for different types of concrete under various loadings.

2.2.4. Experimental verification

The biaxial results of Kupfer (1973) including tensile stresses, are considered first. Fig. 6 shows the comparison between the predictions of the model and the experimental results. The concrete has a rather low strength. The following parameters were applied in the model: $E_i = 2.89 \cdot 10^4$ MPa, $\upsilon_i = 0.19$, $\sigma_c = 18.7$ MPa, $\sigma_t/\sigma_c = 0.1$, $\varepsilon_c = 1.87$ o/oo, and D = 0. Fig. 6 a) shows the cases of uniaxial and biaxial compressive loading, and fig. 6 b) shows the volumetric behaviour connected with these loadings. Fig. 6 b)

(a)

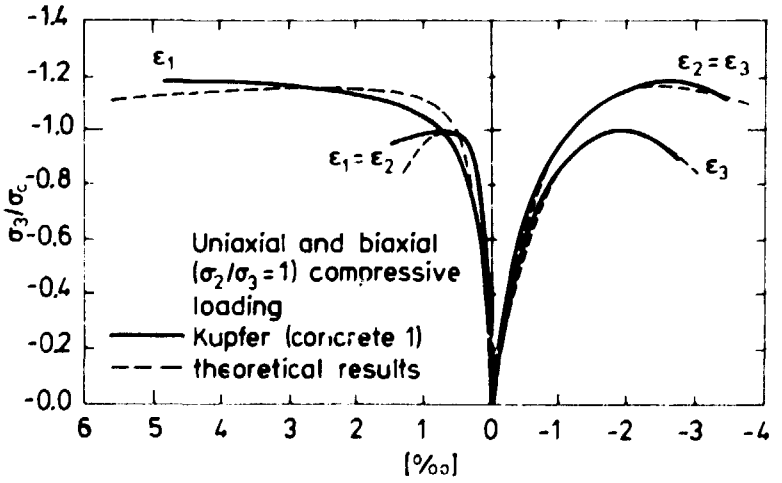

(b)

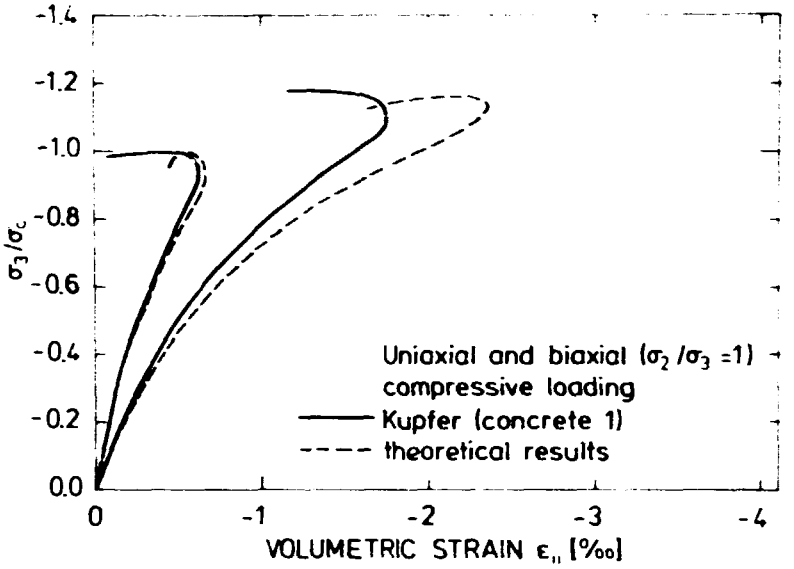

(c)

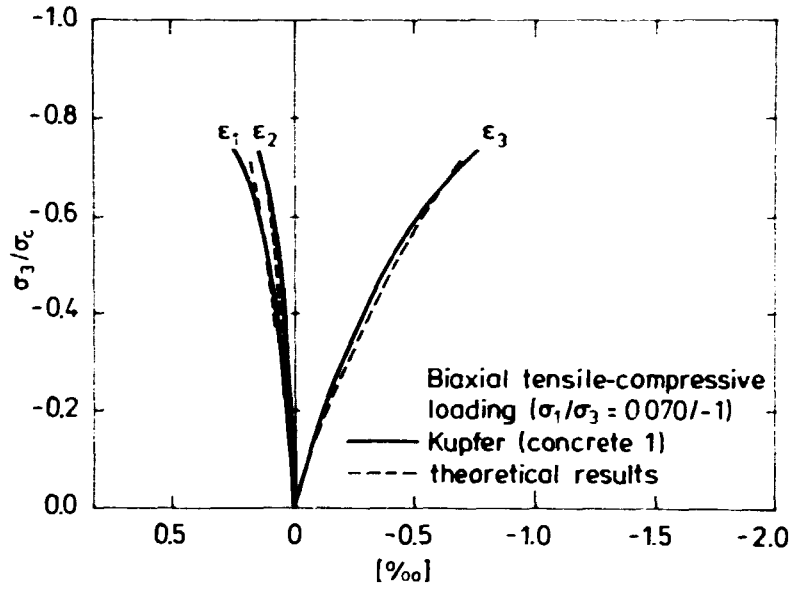

(d)

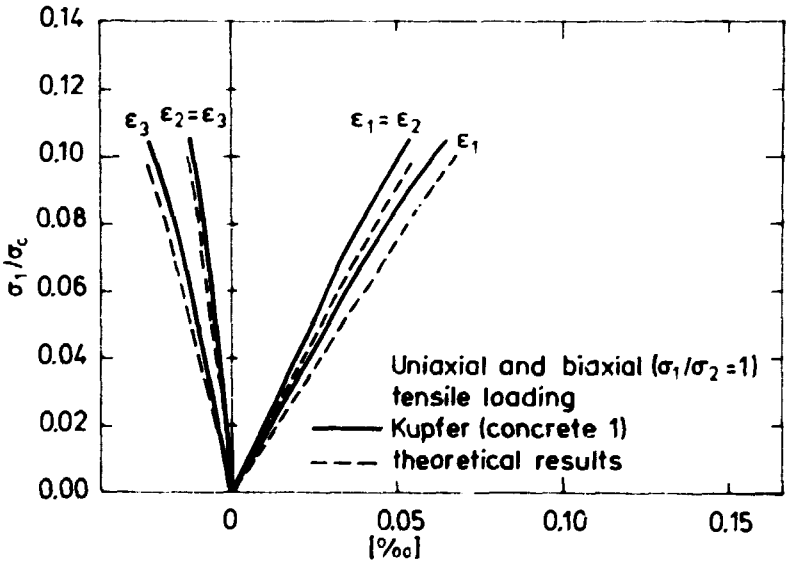

Fig. 2.2-6: Comparison between predictions of model and biaxial results of Kupfer (1973). (a) Compressive stress states; (b) Compressive stress states - volumetric behaviour; (c) Tensile-compressive loading; (d) Tensile stresses.

demonstrates that the model is able to simulate the dilatation that is characteristic for concrete loaded in compression. The behaviour of concrete becomes less nonlinear, the more the stress state involves tensile stresses; this fact is shown in fig. 6 c) for a biaxial tensile-compressive loading and in fig. 6 d) for uniaxial and biaxial tensile loadings. The loadings in fig. 6 c) and 6 d) result in cracking, i.e. a completely brittle failure.

Stress-strain curves for triaxial compressive loading obtained by means of the classical pressure chamber method and resulting in failure along the compressive meridian ($\sigma_1 = \sigma_2 > \sigma_3$) are shown in both figs. 7 and 8. To indicate their appearance, the predicted stress-strain curves on these figures are also indicated at the beginning of the post-failure region, even though no experimental data were given there.

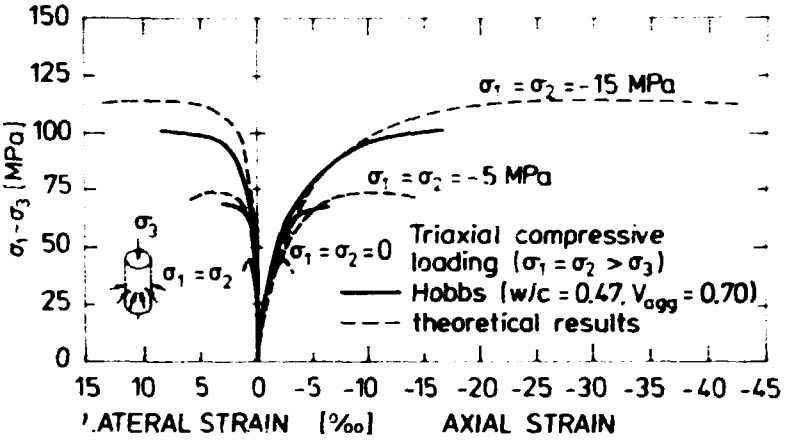

Fig. 2.2-7: Comparison between predictions of model and triaxial results of Hobbs (1974) - Compressive stress states.

The experimental results of fig. 7 are those of Hobbs (1974). The loading ranges from low to moderate triaxial compressive loading, and the concrete has a high strength. The following model parameters were applied in fig. 7: $E_i = 3.90 \cdot 10^4$ MPa, $\upsilon_i = 0.2$, $\sigma_c = 43.4$ MPa, $\sigma_t/\sigma_c = 0.08$, $\varepsilon_c = 2.27$ o/oo, and $D = 0.16$. The experimental results shown in fig. 8 are those of Ferrara et al. (1976). The loading ranges from moderate to very high triaxial compressive loading, and the concrete has a very high strength. The following model parameters were applied in fig. 8: E_i =

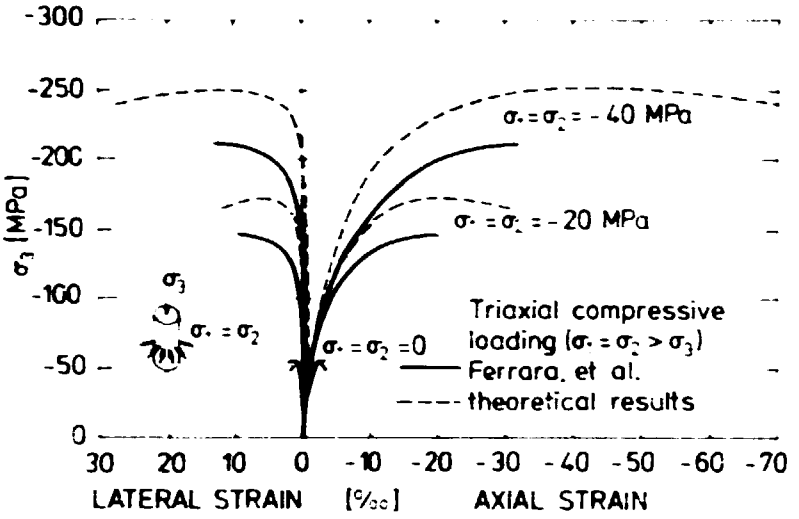

Fig. 2.2-8: Comparison between predictions of model and triaxial results of Ferrara et al. (1976) - Compressive stress states.

$4.40 \cdot 10^4$ MPa, $\nu_i = 0.16$, $\sigma_c = 56.9$ MPa, $\sigma_t/\sigma_c = 0.08$, $\varepsilon_c = 2.16$ o/oo, and D = 0.2. Some disagreement exists in fig. 8, but it appears that this disagreement is more connected to minor discrepancies between the predicted failure stresses and the actual ones than to the constitutive model as such.

Note that the model predictions in figs. 6, 7 and 8 are based purely on calibrations using uniaxial data alone.

In conclusion, the constitutive model proposed by the writer (1979) and investigated above provides realistic predictions for general stress states. Through use of the nonlinearity index relating the actual stress state to the failure surface, the model can be applied in connection with any failure criterion without change. Moreover, the model is simple to apply and implement in a computer program and calibration to a particular concrete is based purely on uniaxial data.

It may be of interest to note that a similar constitutive model has been constructed for rock salt, cf. Ottosen (1978) and Ottosen and Krenk (1979), and that close agreement with experimental results again was obtained.

2.3 Creep

Even though the finite element program and therefore also the present report concentrate on short-term loading of structures until failure occurs, nonlinearities due to time effects, i.e., creep strains, will be touched upon as the program enables one to deal with creep effects caused by simple load histories. This is done using the simple "effective E-modulus" concept described below.

For concrete structures subjected to normal loads it is usually assumed that concrete behaves like a linear viscoelastic material. For instance, the resulting proportionality between creep strains and stresses is generally considered as valid for uniaxial compressive loading provided the sustained stress is below half the short-term strength, cf. for instance Browne and Blundell (1972). Therefore for a constant uniaxial stress σ we have

$$\varepsilon^c = \varepsilon^{sp}\,\sigma \qquad (2.3\text{-}1)$$

where ε^c is the creep strain and ε^{sp} is termed in the specific creep function, i.e., the creep strain for unit stress. The specific creep function depends in general on time t and temperature T i.e. $\varepsilon^{sp} = \varepsilon^{sp}(t,T)$. If concrete is considered to be a homogeneous and isotropic material then two material parameters define the material also when creep strains are involved, cf. for instance Nielsen et al. (1977). These two parameters may be considered as the creep Young's modulus and the creep Poisson's ratio that now depend on time and temperature. Experiments show, cf. for instance Browne and Blundell (1972) and Hannant (1969) that Poisson's ratio during creep can be assumed to be equal to Poisson's ratio during short-term loading. This leaves Young's modulus during creep to be determined. For this purpose we consider a constant uniaxial stress state. The total strain ε consists of the elastic strain ε^e and the creep strain ε^c i.e.

$$\varepsilon = \varepsilon^e + \varepsilon^c$$

Using Hooke's law and eq. (1) we obtain

$$\varepsilon = \frac{\sigma}{E} + \varepsilon^{sp}\,\sigma \qquad (2.3\text{-}2)$$

where E is Young's modulus during short-term loading. From eq. (2) we derive

$$\varepsilon = E_{eff}\,\varepsilon$$

where

$$E_{eff} = \frac{E}{1 + E\,\varepsilon^{sp}} \qquad (2.3\text{-}3)$$

Hannant (1969) has shown that creep even under sustained triaxial loading can be estimated with close accuracy from uniaxial creep data using the above concept.

The modulus E_{eff} is termed the "effective E-modulus" as it appears that a creep calculation using the finite element program can be performed as a usual elastic calculation where the modulus E is simply replaced by E_{eff} according to eq. (3). It should be noted that this "effective E-modulus" concept assumes in principle that stresses are constant throughout the loading time, but even for constant loading, stress redistributions due to creep will in general occur in the structure thereby violating in principle the basis of the approach. Nevertheless, these latter stress changes are often quite small but it emphasizes that the "effective" E-modulus" concept must be utilized with caution. However the appeal of the method is its extreme simplicity.

Presently, the specific creep function available in the program is that proposed by Cederberg and David (1969) i.e.

$$\varepsilon^{sp} = 10^{-6}\,(0.4 + 0.086 \cdot T)\,\ln(1 + t)\quad [MPa]^{-1} \qquad (2.3\text{-}4)$$

where T is the temperature in ^{o}C and t the loading time in days. Moreover, the short-term modulus E in eq. (3) is assumed to depend on the temperature according to

$$E(T) = E_o \ (1.04 - 0.002 \cdot T) \qquad (2.3\text{-}5)$$

where E is the modulus at 20^{o}C. Eq. (5) was also proposed by Cederberg and David (1969).

With these few remarks no more attention will be drawn toward time-dependent behaviour of concrete as the primary concern of the present study is that of concrete structures loaded in the short-term until failure.

2.4. Summary

The present section 2 has primarily dealt with failure and non-linear behaviour of concrete when loaded in the short-term by general stress states. Different failure criteria and their agreement with experimental result have been discussed and it has been shown that the two failure criteria dealt with in section 2.1.3 and the failure mode criteria dealt with in section 2.1.4 provide a realistic approach to actual behaviour. In particular, it has been shown that the criterion of the writer (1977) is superior when considering accuracy, whereas the modified Coulomb criterion possesses an attractive simplicity. In section 2.2 a model for the stress-strain behaviour of concrete was outlined. This model, proposed by the writer (1979) and implemented in the finite element program, is based on nonlinear elasticity, where the secant values of Young's modulus and Poisson's ratio are changed appropriately.

The model simulates the nonlinear behaviour before failure, as the failure itself and as the post-failure behaviour. Smooth stress-strain curves are obtained, and different post-failure behaviours can easily be produced by changing one parameter, D, alone, while changing only the behaviour before failure insignificantly. In addition, the model reflects the dilatation that occurs when concrete is loaded in compression and the influence of all three

stress invariant is considered.

Through use of the nonlinearity index, β, relating the actual stress state to the failure surface, the model can be applied without change in connection with any failure criterion, and choice of an accurate failure criterion by itself assures predictions of realistic stress-strain curves. The constitutive model applies to all stress states, including those where tensile stresses are present. The model is determined by only six parameters that depend on the actual concrete. These are the initial elastic parameters, E_i and υ_i, the strength parameters σ_c and σ_t, the ducility parameter, ε_c, and the post-failure parameter, D. The calibration of the model is easily performed, as the D value is chosen to correspond with the anticipated post-failure behaviour. The other parameters are obtained by a standard uniaxial compressive, and a standard uniaxial tensile test. The flexibility of the model and its unified formulation makes it suitable for use in computer codes when investigating the sensivity of structures to certain specific parameters, e.g., the influence of different failure criteria, different post-failure behaviors, etc.; this will in fact be demonstrated in section 5. In the present section, however, it has been shown that the model predictions are in good agreement with experimental results over a wide range of stress states also including tensile stresses, and obtained by using very different types of concrete.

3. CONSTITUTIVE EQUATIONS FOR REINFORCEMENT AND PRESTRESSING

Plastic deformations of reinforcement embedded in the concrete and of unembedded reinforcement, i.e., springs can be dealt with in the finite element program. In practice, unembedded reinforcement often corresponds to ungrouted prestressed tendons, but prestressing of the springs is not mandatory. The following uniaxial stress-strain relations are assumed to apply for usual reinforce-

ment and for unembedded reinforcement:

a) usual reinforcement b) unembedded reinforcement

Fig. 3-1: Uniaxial stress-strain curves for usual reinforcement and for unembedded reinforcement.

I.e. a trilinear stress-strain curve applies to usual reinforcement while a quadrilinear stress-strain curve applies to unembedded reinforcement. The slope of the lines is arbitrary except that it is non-negative. In the present section emphasis is given not to the constitutive modelling as such, as it is quite trivial, but rather to a formulation that is computationally convenient in the finite element program.

As outlined in section 4.3 usual reinforcement may consist of bars or of membranes while unembedded reinforcement, i.e., springs, obviously are treated as uniaxial loading. In accordance with the formulation of the constitutive equations for concrete in terms of secant values of Young's modulus and Poisson's ratio, the constitutive equations for usual reinforcement are based on a total formulation instead of the generally more accurate incremental formulation. For usual bars carrying stresses in one direction only the two formulations coincide when loading alone is considered, but for membrane reinforcement differences exist. The incorrect response to unloading inherent in the total formulation employed is considered to be of minor importance as only structures subject to increasing external loading are dealt with. For unembedded reinforcement, i.e., springs, a different approach is followed that considers both loading and unloading in a correct way. This numerical approach is outlined in section 4.4 and no more attention will be given here to unembedded reinforcement

as the constitutive behaviour is fully described by fig. 3-1 b). In the present section we proceed with the total formulation of the plasticity theory as applied to membrane reinforcement.

The von Mises yield criterion is employed and considering in the first place the incremental formulation of isotropic hardening this means that the loading surfaces are given by

$$f = \left(\frac{3}{2}\, s_{ij}\, s_{ij}\right)^{\frac{1}{2}} = \sigma_e(\varepsilon^p) \qquad (3\text{-}1)$$

where s_{ij} as usual is the deviatoric stress tensor and σ_e is the equivalent stress. In accordance with the assumption of isotropic hardening σ_e depends on the equivalent plastic strain ε^p. The increment of equivalent plastic strain ε^p is defined by

$$d\varepsilon^p = \left(\frac{2}{3}\, d\varepsilon^p_{ij}\, d\varepsilon^p_{ij}\right)^{\frac{1}{2}} \qquad (3\text{-}2)$$

where ε^p_{ij} denotes the plastic strain tensor. For uniaxial loading, eq. (1) infers that $f = \sigma_{11} = \sigma_e$. Assuming the usual normality rule following for instance from Drucker's postulates (1951) we have

$$d\varepsilon^p_{ij} = d\lambda\, \frac{\partial f}{\partial \sigma_{ij}}$$

where $d\lambda$ is a positive function. Use of eq. (1) yields

$$d\varepsilon^p_{ij} = d\lambda\, \frac{3\, s_{ij}}{2\, \sigma_e} \qquad (3\text{-}3)$$

From the latter equation follows plastic incompressibility which in turn implies that for uniaxial loading eq. (2) results in $d\varepsilon^p = d\varepsilon^p_{11}$.

If eq. (3) is multiplied with itself we obtain

$$d\lambda = \left(\frac{2}{3}\, d\varepsilon^p_{ij}\, d\varepsilon^p_{ij}\right)^{\frac{1}{2}}$$

i.e.

$$d\lambda = d\varepsilon^p$$

By use of eq. (3) we have then derived the final incremental equations

$$d\varepsilon^p_{ij} = d\varepsilon^p \frac{3\, s_{ij}}{2\, \sigma_e} \qquad (3\text{-}4)$$

where $d\varepsilon^p$ is given by eq. (2) and σ_e by eq. (1).

If increasing proportional loading is considered it follows that

$$\varepsilon^p_{ij} = \varepsilon^p \frac{3\, s_{ij}}{2\, \sigma_e} \qquad (3\text{-}5)$$

where the ratio s_{ij}/σ_e is constant. From this equations follows that

$$\varepsilon^p = \left(\frac{2}{3}\, \varepsilon^p_{ij}\, \varepsilon^p_{ij}\right)^{\frac{1}{2}} \qquad (3\text{-}6)$$

Eqs. (5) and (6) hold exactly for increasing proportional loading. It is now assumed that they also apply to nonproportional loadings. However, while in the finite element program the reinforcement stresses are not directly determined, the total reinforcement strains are known as these are assumed to be identical to the concrete strains. It is therefore advantageous to derive explicitly the relation between reinforcement stresses and total strains. Noting that total strains ε_{ij} are composed of elastic strains ε^e_{ij} and plastic strains ε^p_{ij} i.e.

$$\varepsilon_{ij} = \varepsilon^e_{ij} + \varepsilon^p_{ij} \qquad (3\text{-}7)$$

and working only with principal stresses and strains which is allowable here inasmuch as the corresponding principal directions always are assumed to coincide, we therefore write

$$\varepsilon_1 = \frac{1}{E}\,(\sigma_1 - \upsilon(\sigma_2 + \sigma_3)) + \frac{\varepsilon^p}{2\sigma_e}\,(2\sigma_1 - \sigma_2 - \sigma_3)$$

$$\varepsilon_2 = \frac{1}{E}\,(\sigma_2 - \upsilon(\sigma_1 + \sigma_3)) + \frac{\varepsilon^p}{2\sigma_e}\,(2\sigma_2 - \sigma_1 - \sigma_3)$$

$$\varepsilon_3 = \frac{1}{E}\,(\sigma_3 - \upsilon(\sigma_1 + \sigma_2)) + \frac{\varepsilon^p}{2\sigma_e}\,(2\sigma_3 - \sigma_1 - \sigma_2)$$

where Hooke's law and eq. (5) are applied. Solving this equation system so that stresses are given in terms of strains and putting $\sigma_3 = 0$ in accordance with the assumption that plane stress exists in the membrane reinforcement we obtain

$$\varepsilon_3 = - \frac{S}{R-S} (\varepsilon_1 + \varepsilon_2) \tag{3-8}$$

and

$$\begin{bmatrix} \sigma_1 \\ \sigma_2 \end{bmatrix} = \frac{1}{R^2-S^2} \begin{bmatrix} R & S \\ S & R \end{bmatrix} \begin{bmatrix} \varepsilon_1 \\ \varepsilon_2 \end{bmatrix} \tag{3-9}$$

where

$$R = \frac{1}{E} + \frac{\varepsilon^p}{\sigma_e} \qquad S = \frac{\upsilon}{E} + \frac{\varepsilon^p}{2\sigma_e} \tag{3-10}$$

It is to be noted that while the principal strains ε_1 and ε_2 in the membrane plane are assumed to be identical to the corresponding concrete strains, as perfect bond is assumed, the principal strain ε_3 transverse to the membrane plane is given by eq. (8) and not by the corresponding concrete strain.

From eq. (9) the well known fact appears explicitly that the present formulation is identical to nonlinear elasticity. The constitutive equation (9) is equivalent to

$$\begin{bmatrix} \varepsilon_1 \\ \varepsilon_2 \end{bmatrix} = \frac{E}{1-\upsilon^2} \begin{bmatrix} 1 & \upsilon \\ \upsilon & 1 \end{bmatrix} \begin{bmatrix} \varepsilon_1 \\ \varepsilon_2 \end{bmatrix} + \begin{bmatrix} \sigma_{01} \\ \sigma_{02} \end{bmatrix} \tag{3-11}$$

where the initial stresses σ_{01} and σ_{02} are determined so that eqs. (9) and (11) result in identical stresses when the total strains are identical, i.e.,

$$\begin{bmatrix} \sigma_{01} \\ \sigma_{02} \end{bmatrix} = \left(\frac{1}{R^2-S^2} \begin{bmatrix} R & S \\ S & R \end{bmatrix} - \frac{E}{1-\upsilon^2} \begin{bmatrix} 1 & \upsilon \\ \upsilon & 1 \end{bmatrix} \right) \begin{bmatrix} \varepsilon_1 \\ \varepsilon_2 \end{bmatrix} \tag{3-12}$$

As the total strains are composed of elastic and plastic strains it follows from eq. (11) that

$$\begin{bmatrix} \varepsilon_1^p \\ \varepsilon_2^p \end{bmatrix} = -\frac{1}{E} \begin{bmatrix} 1 & -\upsilon \\ -\upsilon & 1 \end{bmatrix} \begin{bmatrix} \sigma_{01} \\ \sigma_{02} \end{bmatrix} \qquad (3\text{-}13)$$

Equation (11) and (12) form the basis for the initial stress method employed in the program for consideration to nonlinearities in membrane reinforcement, cf. section 4.3.2.

However, some further derivations are necessary as the finite element program directly determines only the total strains and also because the only quantities that are stored from the previous loading stage are the initial stresses. Parameters R and S present in eq. (12) and defined by eq. (10), however, require knowledge of the equivalent stress σ_e and the equivalent plastic strain ε^p both corresponding to the actual total strains. Using the plastic incompressibility, eq. (6) can be written

$$\varepsilon^p = \frac{2}{\sqrt{3}} \sqrt{\varepsilon_1^{p2} + \varepsilon_2^{p2} + \varepsilon_1^p \, \varepsilon_2^p} \qquad (3\text{-}14)$$

Through eqs. (13) and (14) the equivalent plastic strain ε^p and thereby also the equivalent stress σ_e can be determined, both corresponding to the previous loading stage. Obviously, an iteration sequence is necessary to determine the present values of ε^p and σ_e and different iteration schemes can be employed for this purpose. Here we make use of the proposal of Mendelson (1968) which has the advantage of quick convergence and applicability even in the case of ideal plasticity. In essence this proposal given below enables one to compute plastic strains from total strains without recourse to stresses.

Letting $e_{ij} = \varepsilon_{ij} - \frac{1}{3}\ _{ij}\ \varepsilon_{kk}$ and $e_{ij}^e = \varepsilon_{ij}^e - \frac{1}{3}\ \delta_{ij}\ \varepsilon_{kk}^e$ denote the deviatoric total strain and the deviatoric elastic strain, respectively, and noting that the plastic strain tensor ε_{ij}^p is purely deviatoric, eq. (7) yields

$$e_{ij} = e^{e}_{ij} + \varepsilon^{p}_{ij} \tag{3-15}$$

From Hooke's law follows

$$e^{e}_{ij} = \frac{s_{ij}}{2\,G}$$

where G is the shear modulus. Inserting this equation in eq. (15) and eliminating s_{ij} by means of eq. (5) gives

$$e_{ij} = \left(\frac{\sigma_e}{3G\varepsilon^p} + 1\right) \varepsilon^{p}_{ij} \tag{3-16}$$

Multiplication of eq. (16) with itself yields

$$\varepsilon^p = e_{et} - \frac{\sigma_{e(\varepsilon^p)}}{3G} \tag{3-17}$$

where eq. (6) has been used and where the equivalent total strain e_{et} is defined by

$$e_{et} = \left(\frac{2}{3}\, e_{ij}\, e_{ij}\right)^{\frac{1}{2}}$$

which using the definition of deviatoric total strain can be written

$$e_{et} = \frac{\sqrt{2}}{3} \sqrt{(\varepsilon_1 - \varepsilon_2)^2 + (\varepsilon_1 - \varepsilon_3)^2 + (\varepsilon_2 - \varepsilon_3)^2} \tag{3-18}$$

Moreover, as the stress-plastic strain curve obtained from uniaxial loading and derived from fig. 3-1 a) determines σ_e as a unique function of ε^p, equation (17) is the expression sought, as it determines the equivalent plastic strain ε^p as a function of e_{et} determined by the total strains. The iteration sequence is then as follows:

From the present values of the total strains ε_1 and ε_2 and from the values of σ_e and ε^p from the previous loading stage a ε_3-value is determined through eq. (8). The equivalent total strain e_{et} is then evaluated by means of eq. (18). Knowing e_{et} and σ_e, eq. (17) determines a new value of ε^p and thereby also a new value of σ_e. This iteration loop is continued until values for ε^p and σ_e that are in suffficiently close agreement with the pre-

sent values of total strains ε_1 and ε_2 are obtained. The initial stresses in question can then be determined through eq. (12).

For uniaxial reinforcement bars the approach is much simpler. As perfect bond is assumed, the axial strain ε is directly determined in the finite element program. Through the uniaxial stress-strain curve of fig. 3-1 a) the corresponding stress is determined, i.e.,

$$\sigma = \sigma(\varepsilon)$$

This constitutive equation is equivalent to

$$\sigma = E\varepsilon + \sigma_0$$

where the initial stress is given by

$$\sigma_0 = \sigma(\varepsilon) - E\varepsilon \qquad (3\text{-}19)$$

No iteration sequence is involved here.

Summarizing, the constitutive equations for usual embedded reinforcement corresponds to nonlinear elasticity. The numerical considerations of plastic deformation are applied using the initial stress method outlined in section 4.3.2. For a given loading stage, the finite element program determines the total strains in the reinforcement plane. For membrane reinforcement the corresponding initial stresses are given by eq. (12) while the initial stress for uniaxial reinforcement bars is given by eq. (19).

4. FINITE ELEMENT MODELLING

In this section the finite element formulation of the AXIPLANE-program described by the writer (1980) is given. This pro-

gram is applicable for axisymmetric, plane stress and plane strain structures. Triangular elements are utilized for simulation of concrete, while one- and two- dimensional elements simulate arbitrarily located reinforcement bars and membranes. Linear displacement functions are used in all elements resulting in perfect bond between concrete and steel. Figure 1 shows the available axisymmetric elements while figs. 2 and 3 show the plane stress and plane strain elements, respectively. These

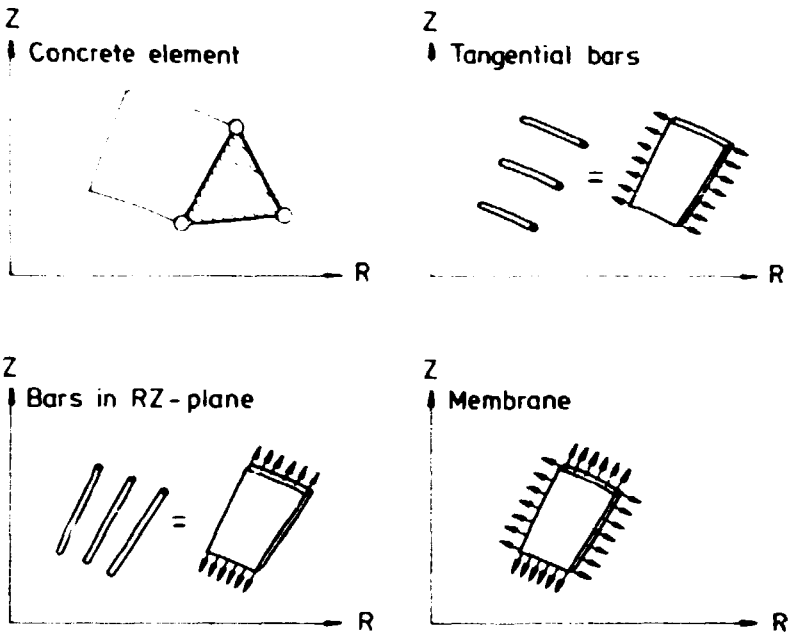

Fig. 4-1: Axisymmetric elements.

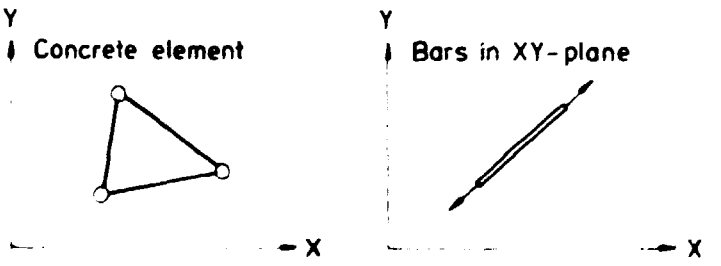

Fig. 4-2: Plane stress elements.

figures also illustrate how the discrete reinforcement bars are smeared out to equivalent "shells" possessing identical volumina and stiffness characteristics as the bars. It is apparent that

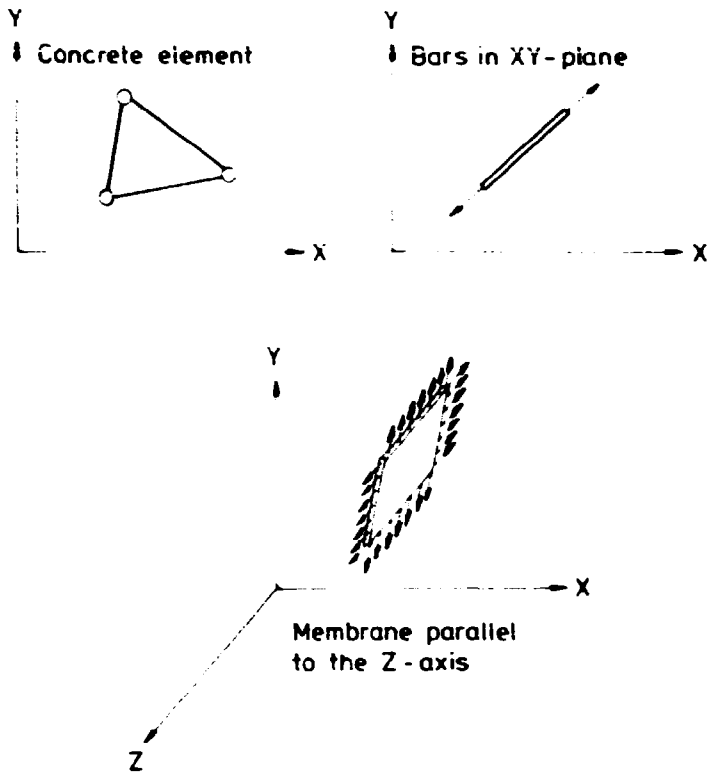

Fig. 4.3: Plane strain elements.

from a finite element point of view, the modelling is very simple. It also follows that the program is most suited for analysis of massive structures while slender structures acting primarily in bending represent problems that are unfitted for use of the program.

In section 4.1 following, the fundamental equations in the finite element displacement method will be derived. Then, sections 4.2, 4.3 and 4.4 will treat the axisymmetric elements in detail. The formulation of the plane elements follow very much the same lines and they will therefore be treated only schematically in section 4.5. Finally, the computational schemes employed in the program will be considered in section 4.6.

4.1. Fundamental equations of the finite element method

This section briefly outlines the fundamental equations of the finite element displacement method. The Galerkin method is util-

ized in this formulation for the following reasons: (1) it operates directly with the differential equations in question and no corresponding functional or potential function is needed opposed to the Rayleigh-Ritz method; and (2) it demonstrates clearly which equations are satisfied exactly and which only approximately. The present section takes some advantage of the work of Zienkiewicz (1977) pp. 42-92. Cartesian coordinates are assumed and tensor notation is used for lower indices with Latin letters ranging from 1 and 3 and Greek letters ranging from 1 to n or from 1 to n^e.

Five basic equations define the response when a structure is loaded. Three of these are field equations to be satisfied throughout the whole volume of the structure while the last two equations define the boundary conditions. Let us first consider the field equations starting with the equilibrium equations

$$\sigma_{ij,j} + \tilde{b}_i = 0 \qquad (4.1\text{-}1)$$

where σ_{ij} is the stress tensor and $\tilde{b}_i$ denotes the specified volume forces. Only static problems are considered. A tilda indicates that the quantity in question is prescribed. The symmetry of the stress tensor $\sigma_{ij} = \sigma_{ji}$ follows from equilibrium of moments; this symmetry will be tacitly assumed in the following therefore being exactly satisfied. Assuming small strains these are defined by

$$\varepsilon_{ij} = \frac{1}{2} (u_{i,j} + u_{j,i}) \qquad (4.1\text{-}2)$$

where ε_{ij} is the symmetric strain tensor and u_i denotes the displacements. The stresses and strains are related through the constitutive equation

$$\sigma_{ij} = D_{ijkl} (\varepsilon_{kl} - \varepsilon^0_{kl}) + \sigma^0_{ij} \qquad (4.1\text{-}3)$$

where D_{ijkl} is the elasticity tensor that might depend on stresses, strains and time. The symmetry properties $D_{ijkl} = D_{jikl} = D_{ijlk}$ follow from the symmetry of σ_{ij} and ε_{ij}. Moreover, to achieve symmetric stiffness matrices for the finite elements,

the material is assumed to be hyperelastic (Green-elastic) possessing a strain energy function so that $D_{ijkl} = D_{klij}$ holds. The terms ε^0_{kl} and σ^0_{ij} in the constitutive equation denote initial strains due to shrinkage, thermal expansions, etc. and initial stresses, respectively. More realistic constitutive equations than the above might well be used in the finite element formulation, but for the present purpose, eq. (3) suffices.

Having defined the field equations, the boundary conditions will be set up. For this purpose we divide the total boundary S of the structure into two regions, a region S_t where surface forces, tractions, are specified and a region S_u where displacements are prescribed. The static boundary conditions specify that

$$\sigma_{ij}\, n_j = \tilde{t}_i \quad \text{on } S_t \tag{4.1-4}$$

where n_j is the outward unit vector normal to the boundary and $\tilde{t}_i$ denotes the given tractions. The kinematic boundary conditions specify that

$$u_i = \tilde{u}_i \quad \text{on } S_u \tag{4.1-5}$$

where $\tilde{u}_i$ is the prescribed displacements. If the structural response satisfies the equations (1)-(5) then the true solution has been established. Let us now consider a reformulation of some of these equations.

Satisfaction of the equilibrium equations all through the structure is equivalent to

$$\int_V u^*_i\, (\sigma_{ij,j} + \tilde{b}_i)\, dV = 0 \tag{4.1-6}$$

when u^*_i is any arbitrary function that can be considered as a displacement. The term dV denotes an infinitesimal volume. From this equation follows

$$\int_V [(u^*_i\, \sigma_{ij})_{,j} - u^*_{i,j}\, \sigma_{ij}]dV + \int_V u^*_i\, \tilde{b}_i\, dV = 0$$

Use of Gauss's divergence theorem yields

$$\int_S u_i^* \sigma_{ij} n_j \, dS - \int_V u_{i,j}^* \sigma_{ij} \, dV + \int_V u_i^* \bar{b}_i \, dV = 0$$

where dS denotes an infinitesimal surface. Use of eq. (2) and the symmetry of σ_{ij} gives

$$\int_V \sigma_{ij} \varepsilon_{ij}^* \, dV - \int_V u_i^* \bar{b}_i \, dV - \int_S u_i^* \bar{\sigma}_{ij} n_j \, dS = 0 \qquad (4.1\text{-}7)$$

where the strain tensor ε_{ij}^* corresponds to the displacements u_i^*. The last term can be split into integrations over S_t and S_u. In region S_t the static boundary condition eq.(4) holds while in region S_u the geometric boundary condition eq.(5) applies. These latter prescribed displacements correspond to some tractions, which however are unknown. Therefore in region S_u we can write

$$\sigma_{ij} n_j = t_i^r \quad \text{on } S_u \qquad (4.1\text{-}8)$$

where the index r suggests that these tractions are the unknown reaction forces. Integrating the last term in eq. (7) over S_t and S_u and using eqs. (4) and (8) we derive

$$\int_V \sigma_{ij} \varepsilon_{ij}^* \, dV - \int_V u_i^* \bar{b}_i \, dV - \int_{S_t} u_i^* \bar{t}_i \, dS - \int_{S_u} u_i^* t_i^r \, dS = 0 \qquad (4.1\text{-}9)$$

This equation states the principle of virtual work. Note that u_i^* are completely arbitrary displacements. In the derivation of the virtual work equation use has been made of the equilibrium relation, eq. (1), the definition of the strain tensor, eq. (2) and the static boundary condition, eq. (4), so that these equations may be replaced by the virtual work expression, eq. (9). In the virtual work equation, no consideration has been taken to the constitutive condition.

In a state of equilibrium given by the displacements u_i, the stress tensor σ_{ij} depends on u_i and satisfies the equilibrium condition, eq. (1). Suppose now that an approximation u_i^a to u_i is found where upper index a, in general, is related to approximative quantities. Then a corresponding approximative strain

tensor ε^a_{ij} follows which in turn determines an approximative stress tensor σ^a_{ij} through the constitutive equation. It is obvious, however, that this stress tensor will not in all points of the structure satisfy the equilibrium condition, eq. (1), as no means have been taken for this purpose. However, the method of Galerkin ensures an approximative satisfaction of these equilibrium equations. Let us now consider this procedure in some detail.

The true displacements u_i are approximated by

$$u_i \simeq u^a_i = N_{i\alpha}\, a_\alpha \qquad \alpha = 1, 2.....n \qquad (4.1\text{-}10)$$

where the tensor $N_{i\alpha}$ depends on position and is assumed to be known while the coefficients a_α are to be determined. It is convenient to consider these coefficients as displacements of some points distributed all over the structure. These points are termed nodal displacements. Obviously, to obtain an accurate approximation by the available n degrees of freedom, the nodal points should be distributed closely where large changes in the displacement field are expected. It is a crucial feature of the finite element method that the approximative displacement functions given by the tensor $N_{i\alpha}$ and, in a finite element context, termed shape functions are not the same all through the structure, but render different expressions for each subdomain or element, the total of which covers the whole structure. Moreover, the finite element method assumes that within each element, the approximative displacements can be expressed solely by the nodal displacements located within or on the boundary of the element in question. However, with these remarks in mind we will retain the formulation given by eq. (10).

The approximative strain tensor follows from eqs. (2) and (10) i.e.

$$\varepsilon^a_{ij} = B_{ij\alpha}\, a_\alpha \qquad \alpha = 1, 2.....n \qquad (4.1\text{-}11)$$

where the tensor $B_{ij\alpha}$ depends on position and follows from knowledge of $N_{i\alpha}$. Through the constitutive condition eq. (3), the

tensor ε^a_{ij} determines the approximative stress tensor σ^a_{ij}. Consider now eq. (6) when use is being made of the σ^a_{ij} tensor i.e.

$$\int_V u^*_i \, (\sigma^a_{ij,j} + \tilde{b}_i) \, dV = 0 \qquad (4.1\text{-}12)$$

As $\sigma^a_{ij,j} + \tilde{b}_i$ in general differs from zero, this equation cannot be satisfied for <u>any</u> displacements u^*_i. However, if we consider a <u>finite</u> set of functions for u^*_i only, then eq. (12) may be satisfied. It also follows that certain continuity restrictions have to be placed on u^*_i and u^a_i enabling the integral to be evaluated, cf. Zienkiewicz (1977) pp. 46-47 and pp.63-65. The term $\sigma^a_{ij,j} + \tilde{b}_i$ defines a residual and as u^*_i serves the purpose of weighting functions for the residuals, a method based on the approximative satisfaction of the equilibrium equation envisaged by eq. (12) is often termed a method of weighted residuals. The Galerkin method consists of a particular choice for the weighting functions namely

$$u^*_i = N_{i\alpha} \, a^*_\alpha \qquad \alpha = 1, 2.....n \qquad (4.1\text{-}13)$$

where the tensor $N_{i\alpha}$ is the same as that for used for the approximative displacements, cf. eq. (10). The n coefficients a^*_α are completely arbitrary, but as only n linear independent choices for a^*_α exist, eq. (13) determines n linear independent functions.

Corresponding to eq. (13) we have

$$\varepsilon^*_{ij} = B_{ij\alpha} \, a^*_\alpha \qquad \alpha = 1, 2.....n \qquad (4.1\text{-}14)$$

Inserting eqs. (13) and (14) into the virtual work equation given by eq. (9) and utilizing also the approximative stress tensor, we derive

$$\int_V B_{ij\alpha} \, a^*_\alpha \, \sigma^a_{ij} \, dV - \int_V N_{i\alpha} \, a^*_\alpha \, \tilde{b}_i \, dV - \int_{S_t} N_{i\alpha} \, a^*_\alpha \, \tilde{t}_i \, dS$$

$$- \int_{S_u} N_{i\alpha} \, a^*_\alpha \, t^r_r \, dS = 0 \qquad \alpha = 1, 2.....n$$

As this homogeneous equation holds for any of the n linear independent choices of a^*_α , it possesses only the trivial solution given by the n equations

$$\int_V B_{ij\alpha}\, \sigma^a_{ij}\, dV - \int_V N_{i\alpha}\, \tilde{b}_i\, dV - \int_{S_t} N_{i\alpha}\, \tilde{t}_i\, dS - \int_{S_u} N_{i\alpha}\, t^r_i\, dS = 0$$

$\alpha = 1, 2.....n$

Use of the constitutive condition eq. (3) and eq. (11) finally leads to

$$\left(\int_V B_{ij\alpha}\, D_{ijkl}\, B_{kl\beta}\, dV\right)a_\beta - \int_V B_{ij\alpha}\, D_{ijkl}\, \varepsilon^0_{kl}\, dV + \int_V B_{ij\alpha}\, \sigma^0_{ij}\, dV$$

$$- \int_V N_{i\alpha}\, \tilde{b}_i\, dV - \int_{S_t} N_{i\alpha}\, \tilde{t}_i\, dS - \int_{S_u} N_{i\alpha}\, t^r_i\, dS = 0$$

α and $\beta = 1, 2.....n$ (4.1-15)

These are the equations that determine the unknown displacements a_α. For every α-value ($\alpha = 1, 2.....n$) i.e. for every degree of freedom there corresponds one equation. All terms are known except the last one that represent the reaction forces corresponding to the prescribed displacements. These displacements must be dictated before eq. (15) can be solved. However, the last term in eq. (15) contributes only to the equation in question provided a prescribed displacement is related to the considered degree of freedom. Therefore, a convenient way to dictate the geometrical boundary conditions is simply to ignore the last term in eq. (15) and then replace the effected equations by ones that directly state the prescribed displacements. Thereby, rearrangements of eq. (15) are avoided and symmetry of the equation system is retained. The actual procedure is described in section 4.6. Therefore, in the following, the last term in eq. (15) will be ignored as due regard to its influence will be taken at a later stage.

Eq. (15) refers to the whole structure. Traditionally, however a corresponding equation is set up for each element and then ap-

propriate assembly rules using the superposition principle are applied to obtain the total equation system. In the following, this approach will be adopted.

Within each element eq. (10) degenerates to

$$u_i^{ae} = N_{i\alpha}^e \, a_\alpha^e \qquad \alpha = 1, 2.....n^e \quad (4.1\text{-}16)$$

where the upper index e expresses that an element is considered. The element possesses an n^e-degree of freedom represented by the nodal displacements a_α^e of the element. As adjacent elements most often share nodal points some of the nodal displacement appear in different a_α^e- vectors.

Corresponding to eqs. (2) and (16) we have

$$\varepsilon_{ij}^{ae} = B_{ij\alpha}^e \, a_\alpha^e \qquad \alpha = 1, 2.....n^e \quad (4.1\text{-}17)$$

Ignoring the last term in eq. (15) and carrying out the integrations element by element assuming appropriate smoothness of the involved functions we then derive

$$\sum_{e=1}^{m} \left[\left(\int_{v^e} B_{ij\alpha}^e \, D_{ijkl}^e \, B_{kl\beta}^e \, dV \right) a_\beta^e - \int_{v^e} B_{ij\alpha}^e \, D_{ijkl}^e \, \varepsilon_{kl}^0 \, dV + \right.$$

$$\left. \int_{v^e} B_{ij\alpha}^e \, \sigma_{ij}^0 \, dV - \left[\int_{v^e} N_{i\alpha}^e \, \tilde{b}_i \, dV - \int_{S_t^e} N_{i\alpha}^e \, \tilde{t}_i \, dS \right] \right] = 0$$

$$\alpha \text{ and } \beta = 1, 2.....n^e \qquad (4.1\text{-}18)$$

where m is the number of elements. This equation in itself also contains the assembly rules for connection of all the elements. For each element the equation yields

$$K_{\alpha\beta}^e \, a_\beta^e = F_\alpha^{be} + F_\alpha^{pe} + F_\alpha^{te} + F_\alpha^{\varepsilon 0 e} + F_\alpha^{\sigma 0 e}$$

$$\alpha \text{ and } \beta = 1, 2.....n^e \qquad (4.1\text{-}19)$$

where

$$\int_{v^e} B^e_{ij\alpha}\, D^e_{ijkl}\, B^e_{kl\beta}\, dV = K^{\alpha}_{\alpha\beta} \qquad (4.1\text{-}20)$$

is the symmetric stiffness tensor of the element

$$\int_{v^e} N^e_{i\alpha}\, \tilde{b}_i\, dV = F^{be}_{\alpha} \qquad (4.1\text{-}21)$$

is the body force vector. Discrete point forces P_i can be treated by this formulation, but are conveniently treated separately by use of eq. (22) which follows from eq. (21).

$$\sum N^e_{i\alpha}\, P_i = F^{pe}_{\alpha} \qquad (4.1\text{-}22)$$

is the discrete point force vector. The tensor $N^e_{i\alpha}$ is evaluated at the location of the point force in question and the summation is extended over all point forces located within the element.

$$\int_{S^e_t} N^e_{i\alpha}\, \tilde{t}_i dS = F^{te}_{\alpha} \qquad (4.1\text{-}23)$$

is the traction force vector.

$$\int_{v^e} B^e_{ij\alpha}\, D^e_{ijkl}\, \varepsilon^0_{kl}\, dV = F^{\varepsilon 0 e}_{\alpha} \qquad (4.1\text{-}24)$$

is the force vector due to initial strains.

$$-\int_{v^e} B^e_{ij\alpha}\, \sigma^0_{ij}\, dV = F^{\sigma 0 e}_{\alpha} \qquad (4.1\text{-}25)$$

is the force vector due to initial stresses.

By means of the fundamental equation given by eq. (19) the original problem has been transformed into a form relating nodal displacements linearly to forces that can be vizualized as located at the nodal points. As previously mentioned, an equation completely analogous to this equation and valid for the whole structure can be set up; introduction of the geometrical boundary conditions will then establish the final linear equation system

for the structure, where the nodal displacements are the unknown variables. Solution of this equation system determines these nodal displacements which, for each element, determine the displacements through

$$u_i^e = N_{i\alpha}^e \, a_\alpha^e \qquad \alpha = 1, 2.....n^e \quad (4.1\text{-}26)$$

The nodal displacements also determine the strains in an element through

$$\varepsilon_{ij}^e = B_{ij\alpha}^e \, a_\alpha^e \qquad \alpha = 1, 2.....n^e \quad (4.1\text{-}27)$$

and the stresses in an element are determined by

$$\sigma_{ij}^e = D_{ijkl}^e \, (\varepsilon_{kl}^e - \varepsilon_{kl}^{0e}) + \sigma_{ij}^{0e} \qquad (4.1\text{-}28)$$

This means that all quantities of interest have been determined. Referring now to the statement of the original problem given by eqs. (1)-(5), it appears that the field equations given by eqs. (2) and (3) are exactly satisfied, viz. eqs. (27) and (28). Moreover, the geometrical boundary conditions given by eq. (5) have also been satisfied exactly, as these were directly imposed on the equation system (it is assumed that the employed shape functions are able to satisfy these geometrical boundary conditions between the nodal points as well). However, the static boundary conditions given by eq. (4) and the equilibrium equations within the structure and given by eq. (1) are satisfied only in a global sense through the use of Galerkin's method while local violations of these equations in general are present.

4.2. Concrete element

Section 4.2.1. presents a standard formulation of the axisymmetric triangular element with linear shape functions, cf. for instance Zienkiewicz (1977) pp. 119-134, while the important section 4.2.2. deals with the necessary modifications when cracking occurs in this element that represents the concrete. Ample reference will be made to the preceeding section, but matrix notation

will now be employed and upper indices will be dropped for convenience. A double bar indicates a matrix while a single bar denotes a vector.

4.2.1. Basic derivations

The considered element is shown in fig. 1, where the Z-axis corresponds to the axis of rotation. Each of the three nodal points i, j and m located at the corners of the triangle possesses

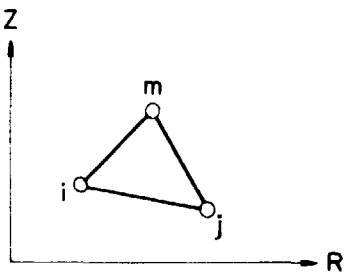

Fig. 4.3-1: Triangular axisymmetric concrete element.

two degrees of freedom: translations u and v in the radial and vertical direction, respectively. The displacement vector $\bar{u}$ is defined as

$$\bar{u} = \begin{bmatrix} u \\ v \end{bmatrix} \qquad (4.2\text{-}1)$$

The nodal displacements are given by the vector

$$\bar{a} = \begin{bmatrix} u_i \\ v_i \\ u_j \\ v_j \\ u_m \\ v_m \end{bmatrix} \qquad (4.2\text{-}2)$$

As displacements within the element are assumed to be uniquely defined by the nodal displacements we have

$$\bar{u} = \bar{\bar{N}}\,\bar{a} \qquad (4.2\text{-}3)$$

where the (2 x 6) matrix $\bar{\bar{N}}$ contains the shape functions. As linear shape functions are assumed we have

$$\bar{\bar{N}} = \frac{1}{2\Delta}\begin{bmatrix} a_i+b_i r+c_i z & 0 & a_j+b_j r+c_j z & 0 & a_m+b_m r+c_m z & 0 \\ 0 & a_i+b_i r+c_i z & a_j+b_j r+c_j z & 0 & a_m+b_m r+c_m z \end{bmatrix} \quad (4.2\text{-}4)$$

where the coefficients are given by

$$a_i = r_j z_m - r_m z_j$$

$$b_i = z_j - z_m$$

$$c_i = r_m - r_j$$

and a_j, b_j, c_j and a_m, b_m, c_m are obtained using cyclic permutations of i, j and m. The term 2Δ denotes twice the area of the triangle and we have

$$2\Delta = a_i + a_j + a_m$$

The strains are given by the vector

$$\bar{\varepsilon} = \begin{bmatrix} \varepsilon_Z \\ \varepsilon_R \\ \varepsilon_\theta \\ \gamma_{RZ} \end{bmatrix} \quad (4.2\text{-}5)$$

containing the vertical, radial, circumferential and the engineering shearing strain, respectively. Differentiating eq. (3) and using eq. (4) yield

$$\bar{\varepsilon} = \bar{\bar{B}}\,\bar{a} \quad (4.2\text{-}6)$$

where the (4 x 6) matrix $\bar{\bar{B}}$ is given by

$$\bar{\bar{B}} = \frac{1}{2\Delta}\begin{bmatrix} 0 & c_i & 0 & c_j & 0 & c_m \\ b_i & 0 & b_j & 0 & b_m & 0 \\ \frac{a_i}{r}+b_i+\frac{c_i z}{r} & 0 & \frac{a_j}{r}+b_j+\frac{c_j z}{r} & 0 & \frac{a_m}{r}+b_m+\frac{c_m z}{r} & 0 \\ c_i & b_i & c_j & b_j & c_m & b_m \end{bmatrix} \qquad (4.2\text{-}7)$$

It appears that all strains except the tangential strain are constant within an element. However, in the present report this variation of the tangential strain is ignored and instead, as an approximation, the value at the centroid of the element is applied. The stresses are given by the vector.

$$\bar{\sigma} = \begin{bmatrix} \sigma_Z \\ \sigma_R \\ \sigma_\theta \\ \tau_{RZ} \end{bmatrix} \qquad (4.2\text{-}8)$$

with obvious notation. The usual elastic constitutive equation is assumed to hold, i.e.

$$\bar{\sigma} = \bar{\bar{D}}\ (\bar{\varepsilon} - \bar{\varepsilon}_o) \qquad (4.2\text{-}9)$$

where $\bar{\bar{D}}$ is a (4x4) symmetric matrix termed the constitutive or material matrix and $\bar{\varepsilon}_o$ is a vector containing initial strains due to temperature. As the strains within an element are constant the same follows for the stresses. It is here assumed that the $\bar{\bar{D}}$-matrix may depend on the stress state and time. For an isotropic material we have

$$\bar{\bar{D}} = \frac{E}{(1+\nu)\ (1-2\nu)}\begin{bmatrix} 1-\nu & \nu & \nu & 0 \\ \nu & 1-\nu & \nu & 0 \\ \nu & \nu & 1-\nu & 0 \\ 0 & 0 & 0 & \frac{1-2\nu}{2} \end{bmatrix} \qquad (4.2\text{-}10)$$

where E and ν are Young's modulus and Poisson's ratio, respectively, that might depend on the stress state and time. The change

of E and ν depending on stress state is given in sections 2.2.2 and 2.2.3, respectively, and a simple approach that considers time effects, i.e. creep, is dealt with in section 2.3. The initial strain vector caused by themal expansion of an isotropic material is

$$\bar{\varepsilon}_o = \alpha\Delta T \begin{bmatrix} 1 \\ 1 \\ 1 \\ 0 \end{bmatrix} \qquad (4.2\text{-}11)$$

where α is the coefficient of themal expansion and ΔT is the mean temperature rise in the element. The AXIPLANE-program includes as a subroutine a completely independent finite element program that determines stationary and transient temperature fields using the same triangular elements dealt with in this section. Thus, corresponding stationary and transient temperature stresses may be considered directly. This temperature program is developed by Andersen (1968a, 1968b) and will not be considered here.

Evaluation of the different terms in eq. (4.1-19) involves integration over the element volume. However, as the element is very simple, many elements and therefore also small elements are necessary for an accurate calculation. Consequently, as a fair approximation, kernels are evaluation at the centroid of the element and multiplied by the approximate element volume. Corresponding to eq. (4.1-19), we have for the element in question

$$\bar{\bar{K}}\ \bar{a} = \bar{F}_b + \bar{F}_p + \bar{F}_t + \bar{F}_{\varepsilon_o}$$

where the element stiffness matrix is given by eq. (4.1-20) using eqs. (7) and (19) i.e.

$$\bar{\bar{K}} = \int_{\text{el.vol}} \bar{\bar{B}}^T\ \bar{\bar{D}}\ \bar{\bar{B}}\ dV \simeq \bar{\bar{B}}^T\ \bar{\bar{D}}\ \bar{\bar{B}}\ 2\pi\ r_m\Delta \qquad (4.2\text{-}12)$$

Here r_m is the mean radius of the element and, as previously mentioned, the matrix $\bar{\bar{B}}$ is evaluated at the centroid of the triangle. The index T denotes the transpose of a matrix. Body forces $\bar{b}$ due to gravity in the direction of the Z-axis may be dealt with in the program, i.e.,

$$\bar{b} = \begin{bmatrix} 0 \\ b_Z \end{bmatrix}$$

Using eq. (4.1-21) and eq. (4) we obtain

$$\bar{F}_b = \int_{\text{el.vol}} \bar{\bar{N}}^T \bar{b}\, dV \simeq \bar{\bar{N}}^T \bar{b}\, 2\pi\, r_m \Delta = \frac{2\pi r_m \Delta b_Z}{3} \begin{bmatrix} 0 \\ 1 \\ 0 \\ 1 \\ 0 \\ 1 \end{bmatrix}$$

where the matrix $\bar{\bar{N}}$ is evaluated at the centroid of the triangle. Nodal forces due to prescribed discrete point forces $\bar{P}$ located within the element are given by eq. (4.1-22) and eq. (4), i.e.,

$$\bar{F}_p = \Sigma\, \bar{\bar{N}}^T \bar{P} \qquad (4.2\text{-}13)$$

where the summation extends over the number of discrete point forces $\bar{P}$ and where the matrix $\bar{\bar{N}}$ is evaluated at the location of the point force in question. Nodal forces due to prescribed traction forces $\bar{t}$ are given by eq. (4.1-23) and eq. (4), i.e.

$$\bar{F}_t = \int_{\substack{S_t\text{- area of} \\ \text{the element}}} \bar{\bar{N}}^T \bar{t}\, ds$$

and nodal forces due to temperature expansion are given by eq. (4.1-24), i.e.

$$\bar{F}_{\varepsilon_o} = \int_{\text{el.vol}} \bar{\bar{B}}^T \bar{\bar{D}}\, \bar{\varepsilon}_o\, dV \simeq \bar{\bar{B}}^T \bar{\bar{D}}\, \bar{\varepsilon}_o\, 2\pi r_m \Delta$$

where the $\bar{\bar{B}}$-matrix is given by eq. (7) and evaluated at the centroid of the triangle while $\bar{\bar{D}}$ and $\bar{\varepsilon}_o$ are given by eqs. (10) and (11).

4.2.2. Cracking in the concrete element

Suppose now that tensile cracks according to the cracking criteria of section 2.1.4. initiate within the element. The present section deals with the corresponding modifications in the finite element approach of the concrete triangular axisymmetric element.

Due to rotational symmetry only two types of cracks can exist, namely radial cracks where the crack plane follows a radial plane and circumferential cracks where the crack plane forms a rotational symmetric surface. These two types of cracks are il-

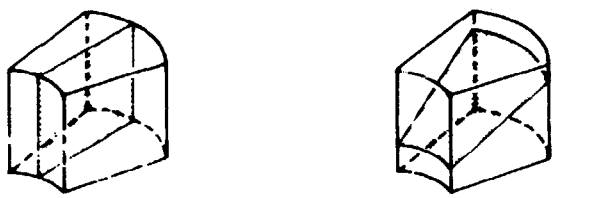

Fig. 4.2-2: Type of cracks in an axisymmetric structure.

lustrated in fig. 2. In addition, combinations of these cracks are possible namely: a radial crack together with a circumferential crack, two circumferential cracks with different directions of the crack planes and finally these last named two circumferential cracks together with a radial crack.

When a crack forms then in principle a discontinuous displacement field results. However, this can be represented only in the finite element approach either by forcing the cracks to follow the boundary of the elements and then introducing new nodal points along these boundaries so that separation can occur, or by allowing the cracks to propagate through the elements and then define new elements and nodal points so that representation of

the discontinuity of the displacement field can be modelled. These approaches to cracking are often termed discrete crack modelling. The first method was proposed by Nilson (1968) as an extension of the model of Ngo and Scordelis (1967) who considered only predefined cracks. Obviously this first method places severe restrictions on the possible crack directions and it is almost abandoned today. The second method is physically attractive, but like the first method it implies considerable computational effort as a complete redefinition of the structure is necessary. However, very recent progress in the latter approach to cracking has been given by Grootenboer (1979).

Apart from the discontinuity in the displacement field another crucial feature of cracking is that the material loses its ability to carry tensile load normal to the crack plane. This very important aspect may easily be incorporated in the finite element formulation as it can be accomplished simply by appropriately changing the constitutive matrix $\bar{\bar{D}}$ when determining stresses from strains and when evaluating the element stiffness matrix compare eqs. (9) and (12). This procedure was proposed by Zienkiewics and Cheung (1967) and Rashid (1968) and constitutes the most often applied consideration to cracking.

In the present report we also adopt this cracking model that is often termed the smeared or continuous cracking approach as the discontinuity in the displacement field is ignored while the inability of concrete to carry tensile load normal to a crack plane is considered by changing the $\bar{\bar{D}}$-matrix from an expression corresponding to isotropic material behaviour to an appropriate anisotropic formulation. Moreover, it is assumed that when a crack forms in an element it intersects the complete element.

Following Mohraz and Schnobrich (1970) we consider the strain state at an arbitrary point. The strain vector $\bar{\varepsilon}$ referred to the original RZ-coordinate system is related to the strain vector $\bar{\varepsilon}'$ referred to the rotated R'Z'-coordinate system, cf. fig. 3, through

$$\bar{\varepsilon}' = \bar{\bar{T}}\ \bar{\varepsilon} \qquad (4.2\text{-}14)$$

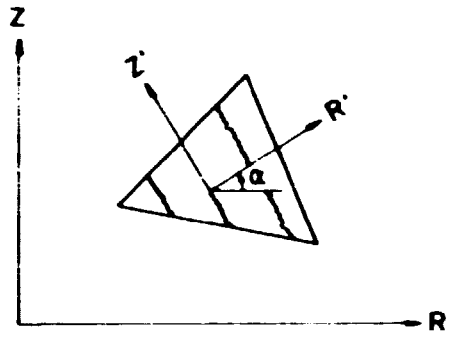

Fig. 4.2-3: Cracking in an element

where

$$\bar{\bar{T}} = \begin{bmatrix} \cos^2\alpha & \sin^2\alpha & 0 & -\frac{1}{2}\sin 2\alpha \\ \sin^2\alpha & \cos^2\alpha & 0 & \frac{1}{2}\sin 2\alpha \\ 0 & 0 & 1 & 0 \\ \sin 2\alpha & -\sin 2\alpha & 0 & \cos 2\alpha \end{bmatrix} \qquad (4.2\text{-}15)$$

The elastic energy in an infinitesimal volume element dV is given by $\frac{1}{2}\,\bar{\varepsilon}^T\,\bar{\sigma}\,dV$ irrespective of the applied coordinate system; i.e.

$$\bar{\varepsilon}^T\,\bar{\sigma} = \bar{\varepsilon}'^T\,\bar{\sigma}' \qquad (4.2\text{-}16)$$

applies, where the prime indicates that reference is made to the rotated R'Z'-coordinate system. Ignoring for convenience initial stresses and strains we have in accordance with eq. (9)

$$\bar{\sigma}' = \bar{\bar{D}}'\,\bar{\varepsilon}' \qquad (4.2\text{-}17)$$

By use of this equation, $\bar{\sigma}'$ can be eliminated from eq. (16) and use of eq. (14) then yields

$$\bar{\varepsilon}^T\,\bar{\sigma} = \bar{\varepsilon}^T\,\bar{\bar{T}}^T\,\bar{\bar{D}}'\,\bar{\bar{T}}\,\bar{\varepsilon}$$

From this equation and the relation

$$\bar{\sigma} = \bar{\bar{D}}\ \bar{\varepsilon} \qquad (4.2\text{-}18)$$

we derive the transformation formula

$$\bar{\bar{D}} = \bar{\bar{T}}^T\ \bar{\bar{D}}'\ \bar{\bar{T}} \qquad (4.2\text{-}19)$$

Suitable expressions for the $\bar{\bar{D}}'$-matrix will now be investigated for different types of cracks. Before cracking isotropic behaviour exists determined by the two parameters E and ν. After cracking a stratified material results where it is reasonable to assume that a plane of isotropy parallel to the crack plane is present. Following Lekhnitskii (1963) such a material is termed transverse-isotropic and it is characterized by five parameters. It is obviously not trivial how to determine these parameters knowing in advance the isotropic parameters E and ν alone, and various procedures may be found in the literature.

Consider first a circumferential crack where the crack plane forms a rotational symmetric surface, compare fig. 2. Just before cracking we have an isotropic material, i.e., the $\bar{\bar{D}}'$-matrix in eq. (17) relating the stress vector $\bar{\sigma}'$ and the strain vector $\bar{\varepsilon}'$ is given by eq. (10). Moreover, the principal stresses in the RZ-plane are assumed to follow the directions of the R'-and Z'-axis. The $\sigma_{R'}$-stress is then a principal stress and it is assumed that it is the largest principal stress. As the crack plane is assumed to be normal to this stress it follows the direction of the Z'-axis as shown in fig. 3. After cracking, the inability of the material to carry tensile load in the R'-direction is obtained by replacing all coefficients in the corresponding row of the $\bar{\bar{D}}'$-matrix with zeros. As the constitutive matrix is symmetric the corresponding column consists also of zeros. In the plane of isotropy now created, it is assumed that plane stress conditions exists. Before cracking the shear stiffness in the RZ-plane along the direction of the crack plane is given by the shear modulus $G = E/2(1+\nu)$. After cracking, it is assumed that only the shear stiffness ηG, where $0 \leq \eta \leq 1$ applies, is

retained along the crack plane. With these assumptions the $\bar{\bar{D}}'$-matrix, as given by eq. (10) and applicable before cracking, is modified to

$$\bar{\bar{D}}'_C = \frac{E}{1-\nu^2}\begin{bmatrix} 1 & 0 & \nu & 0 \\ 0 & 0 & 0 & 0 \\ \nu & 0 & 1 & 0 \\ 0 & 0 & 0 & \eta\frac{1-\nu}{2} \end{bmatrix} \qquad (4.2\text{-}20)$$

where index C denotes that this constitutive matrix refers to the formation of a circumferential crack. This expression corresponds to that proposed by Suidan and Schnobrich (1973). The factor η termed the shear retention factor after Hand et al. (1973) is subject to much controversy, but for convenience a detailed discussion will be postponed to the end of this section. If $\eta = 0$ the crack plane is assumed to be completely smooth while $\eta = 1$ implies that formation of a crack does not influence the shear stiffness of the material. In the program the value $\eta = 0.01$ will be applied universally, except for certain sensitivity studies.

Transformation of eq. (20) from the R'Z'-coordinate system to the RZ-coordinate system is given by eq. (19) with ample use of eq. (15). The result is

$$D_C = \frac{E}{1-\nu^2}\begin{bmatrix} \cos^4\alpha+K\sin^2 2\alpha & \sin^2\alpha\cos^2\alpha-K\sin^2 2\alpha & \nu\cos^2\alpha & -\tfrac{1}{2}\sin 2\alpha\cos^2\alpha+K\sin 2\alpha\cos 2\alpha \\ & \sin^4\alpha+K\sin^2 2\alpha & \nu\sin^2\alpha & -\tfrac{1}{2}\sin 2\alpha\sin^2\alpha-K\sin 2\alpha\cos 2\alpha \\ \text{symmetric} & & 1 & -\tfrac{1}{2}\sin 2\alpha \\ & & & \frac{1}{4}\sin^2 2\alpha+K\cos^2 2\alpha \end{bmatrix} \qquad (4.2\text{-}21)$$

where

$$K = \eta\frac{1-\nu}{2} \qquad (4.2\text{-}22)$$

Considering formation of a radial crack where the crack plane follows a radial plane, use of the assumptions just outlined results in

$$\bar{\bar{D}}_R = \bar{\bar{D}}'_R = \frac{E}{1 - \nu^2} \begin{bmatrix} 1 & \nu & 0 & 0 \\ \nu & 1 & 0 & 0 \\ 0 & 0 & 0 & 0 \\ 0 & 0 & 0 & \frac{1-\nu}{2} \end{bmatrix} \tag{4.2-23}$$

where index R indicates that this constitutive matrix refers to a radial crack. Obviously no transformation of coordinates is involved.

If both a radial and a circumferential crack exist, we derive

$$\bar{\bar{D}}'_{CR} = E \begin{bmatrix} 1 & 0 & 0 & 0 \\ 0 & 0 & 0 & 0 \\ 0 & 0 & 0 & 0 \\ 0 & 0 & 0 & \frac{\eta}{2(1+\nu)} \end{bmatrix} \tag{4.2-24}$$

Use of the transformation formula eq. (19) and of eq. (15) infers

$$\bar{\bar{D}}_{CR} = E \begin{bmatrix} \cos^4\alpha+M\sin^2 2\alpha & \sin^2\alpha\cos^2\alpha-M\sin^2 2\alpha & 0 & -\tfrac{1}{2}\sin 2\alpha\cos^2\alpha+M\sin 2\alpha\cos 2\alpha \\ & \sin^4\alpha+M\sin^2 2\alpha & 0 & -\tfrac{1}{2}\sin 2\alpha\sin^2\alpha-M\sin 2\alpha\cos 2\alpha \\ \text{symmetric} & & 0 & 0 \\ & & & \frac{1}{4}\sin^2 2\alpha+M\cos^2 2\alpha \end{bmatrix} \tag{4.2-25}$$

where

$$M = \frac{\eta}{2(1+\nu)} \tag{4.2-26}$$

Consideration is also taken to secondary cracks where for in-

stance one circumferential crack already exists and according to the crack criterion a new circumferential crack is formed that has a different direction than the first crack. In that situation it is assumed that all load carrying capacity in the RZ-plane is lost, i.e.,

$$\bar{\bar{D}}_{CC} = \bar{\bar{D}}'_{CC} = E \begin{bmatrix} 0 & 0 & 0 & 0 \\ 0 & 0 & 0 & 0 \\ 0 & 0 & 1 & 0 \\ 0 & 0 & 0 & 0 \end{bmatrix} \qquad (4.2\text{-}27)$$

Obviously no transformation is involved. Similarly, if both two circumferential cracks and a radial crack develop in an element, the material loses its carrying capacity in all directions and the constitutive matrix degenerates to the null matrix, i.e.,

$$\bar{\bar{D}}_{CCR} = \bar{\bar{D}}'_{CCR} = \begin{bmatrix} 0 & 0 & 0 & 0 \\ 0 & 0 & 0 & 0 \\ 0 & 0 & 0 & 0 \\ 0 & 0 & 0 & 0 \end{bmatrix} \qquad (4.2\text{-}28)$$

The above approach infers that the resistance of the material to carry tensile load normal to the crack plane is exactly zero. However, this may give rise to an ill-conditioned finite element equation system and in the program 0.5% of the stiffness normal to a crack plane and existing just before cracking is therefore retained.

In the program it is also assumed that once a crack is developed it will remain open with a fixed direction. This seems to be a reasonable assumption as we are dealing only with structures subject to increasing loadings. However, assuming closing of a crack when the strain normal to the crack plane becomes compressive the problem of crack healing has been dealt with by e.g. Phillips and Zienkiewics (1976) and Marchertas et al. (1978). In case of cyclic loading, a more refined model has been proposed by Arnesen et al. (1979).

Let us now consider the question of shear transfer across a crack surface in more detail. The ability of shear transfer is here considered through the shear retention factor η, compare eq. (20). Obviously, this factor which models the aggregate interlock is a nonlinear function of crack width, relative displacement tangential to the crack plane and the nature of the crack surface. Also, the η-value is expected to decrease with increasing crack widths so that for small widths the η-value is close to its upper limit, $\eta = 1$, and for large crack widths the η-value is close to its lower limit, $\eta = 0$. An expression reflecting this dependency of the crack width and neglecting the influence of other variables was proposed, e.g., by Cedolin and Dei Poli (1977). For simplicity, however, we will make use of the often adopted extreme simplification here and consider the shear retention factor as a fixed value. Much discussion has been and is devoted to a suitable choice of this value to ensure its applicability in structural analysis. Some physical arguments justifying to some extent the value employed in the present study will now be put forward.

As the relations between stresses and strains for stress conditions where cracking is impending are almost linear and as the crack plane is assumed to be normal to the largest principal stress, small shear strains along the crack direction can be expected both before and immediately after creation of the crack. Therefore, even though the η-value can be expected to be close to unity for small crack widths, the actual transferred shear stresses just after cracking are probably so small that for the structural response it does not seem to imply drastically simplifications when a small η-value is used. On the other hand, for loadings close to structural collapse, large crack widths can be expected and a small η-value may then be assumed. These arguments suggest a small η-value to be applied universally. An η-value equal to zero would correspond to an extreme physical situation and it might also imply an ill-conditioned finite element equation system. We will therefore make use of the value $\eta = 0.01$. The influence of other η-values will be investigated in section 5.3. Hand et al. (1973) analyzing a rectangular slab subject to bending and torsion until failure is reached found

very little sensitivity to η-values ranging from 0.2 to 1.0 but noticed in accordance with previous remarks that a value equal to zero was unacceptable for numerical reasons. They then arbitrarily selected an η-value equal to 0.4. Yuzugullu and Schnobrich (1973) investigated the deflections and cracking of a shear wall frame system for $\eta = 0$, $\eta = 0.125$, $\eta = 0.25$ and $\eta = 1.00$. Very little influence of the η-value on the deflections and a minor influence on the cracking were observed and even $\eta = 0$ was accepted as a value. The applicability of $\eta = 0$ may be caused by a uniform reinforcement mesh preventing the equation system to be ill-conditioned. The conclusions of Yuzugullu and Schnobrich are in favour of η between 0.125 and 0.25 but apparently no consideration to failure loads was taken. Lin and Scordelis (1975) found no influence of the η-value on the ultimate loads of a circular slab, a square slab and a hyperbolic paraboloid shell. This finding even applies for η ranging from zero to unity. On the other hand Cedolin and Dei Poli (1977) analyzing a beam failing in shear observed an extreme sensitivity of the η-value on the calculated failure loads. For $\eta = 0.25$ they determined a failure load twice as large as that determined when $\eta = 0.025$ was utilized.

The above findings are in accordance with the intuitively acceptable assumption that the calculated response of structures loaded primarily in bending is insensitive to the value of η while the theoretical response of structures loaded primarily in shear shows some dependency of the η-value. However, as shown in section 5.3, the present investigation finds this dependency of η to be much less than that found by Cedolin and Dei Poli (1977).

Apart from the above discussion of choice of a suitable η-factor an additional assumption inherent in the adopted cracking approach should be noted. It follows from the manipulation of the $\bar{D}$-matrix relating stresses and strains in performing consideration to cracks. However, the stress and strain tensors are symmetric and considering for the moment only shear strains, no distinction is therefore made as to whether these shear strains are a result of relative displacements tangential to the crack plane or they are caused instead by nonuniform relative displace-

ments normal to the crack plane. Using the cracking approach followed here, the stiffness related to these two displacement fields would be identical, but in reality much less stiffness would be related to shear parallel to the crack plane than to shear normal to the crack plane.

Terminating this section, attention should be drawn to a new cracking concept proposed very recently by Bažant and Gamborova (1979,a,b) and termed the "rough crack approach". This procedure evades much of the drawbacks of the method adopted here and encompasses apparently most of the essential features of cracking.

4.3. Reinforcement elements

This section deals with the finite element formulation of the three types of axisymmetric reinforcement elements shown in fig. 1, namely, tangential reinforcement where the reinforcement bars are located circumferentially, RZ-reinforcement where the bars are located in the RZ-plane and membran reinforcement with dimensions both in the circumferential direction and in the RZ-plane. It is to be emphazised that arbitrarily located reinforce-

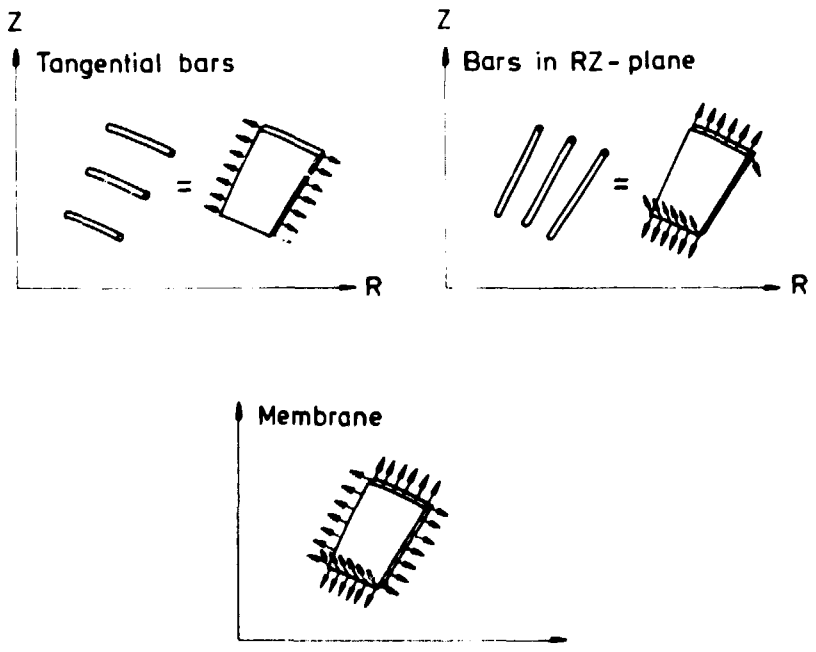

Fig. 4.3-1: Axisymmetric reinforcement elements

ment is treated here. However, before proceeding further it is of interest to reveiw various concepts that are employed when considering the effect of reinforcement.

As reinforcement and concrete follow very different constitutive equations a separate treatment of the two materials is necessary in the finite element formulation. However, different approaches to consider the effect of reinforcement exist. Assuming perfect bond between concrete and reinforcement the "smeared" approach assumes that the reinforcement bars are distributed uniformly all over the region occupied by the involved elements. From these anisotropic homogeneous elements and taking advantage of concrete strains being equal to reinforcement strains, constitutive matrices for the reinforced concrete elements can be derived that consider the directional effect of the reinforcement. This approach has been employed e.g. by Cervenka and Gerstle (1971) and by Suidan and Schnobrich (1973). For inhomogeneous reinforcement arrangements problems may arise when determining the concrete elements involved. Moreover, the specific location of the reinforcement is accounted for only within certain limits that depend on the type and size of the concrete elements.

Another approach which often is termed the discrete idealization employs different elements for concrete and reinforcement. Moreover, reinforcement elements and concrete elements share nodal points. This approach considers the specific reinforcement location, and additional "link" elements that connect concrete and reinforcement may be applied. The use of such link element as proposed by Ngo and Scordelis (1967) opens for consideration to slip and bond failure. Ngo and Scordelis used a linear relation while nonlinear slip relations have been utilized by e.g. Nilson (1968) and Cedolin and Dei Poli (1977). When slip effects are ignored the considered approach is very common in various computer programs, cf. for instance Bathe and Ramaswamy (1979), but an obvious drawback is the requirement that reinforcement elements and concrete elements have to share nodal points. This places severe restrictions on the finite element mesh.

A third approach in considering the effect of reinforcement is

the "embedded" concept where reinforcement can be located arbitrarily within the concrete elements. Assuming consistent displacements for reinforcement elements and concrete elements the displacements and thereby the response of the reinforcement can be described by the nodal displacements of the concrete element. The advantage is that reinforcement can be located at will but assumption of perfect bond is inherent in the approach. In the present report this latter consideration for reinforcement is employed. A quite similar formulation was given by Zienkiewicz et al. (1972), but the present concept in its original form and the corresponding procedures in the finite element program were given by Tingleff (1969, 1973).

Figure 1 illustrates how the discrete reinforcement bars are smeared out to equivalent "shells" possessing volumina and stiffness characteristics identical to those of the bars. This means that all three elements can be treated in the same way except for their different stiffness characteristics. In general all three types of reinforcement will therefore be referred to as bars.

In addition to the in-plane forces of the bar, transverse forces, i.e., dowel forces, may develop as a result of cracking. Relative displacements parallel to a crack plane result mainly in local bending of the bar as well as local crushing of the concrete in the vicinity of the bar. Such crushing of the concrete might be simulated by suitable link elements which, however, is beyond the possibilities of the present approach. Local bending of a bar could in principle be considered, but this would require knowledge of the displacement fields of two subsequent triangular elements. As a result nodal points are coupled that generally do not interact. This coupling would in general almost double the band width of the equation system thereby increasing the computer time inadmissibly, at least for the equation solver used here. The only possibility to deal with dowel action, therefore, is to consider the shear stiffness of the bar. The corresponding shear forces that might be present in RZ- and membrane reinforcement are shown in fig. 1. This approach to consider dowel action is evaluated in sections 5.1 and 5.3 and it is shown there that

even though some features of dowel action are indeed reflected, the approach is in general not preferable.

As concrete and reinforcement is assumed to follow each other, the full shear capacity of the bars is to be considered. While this assumption is fair for uncracked regions, it is obvious that as a result of cracking relative deformations parallel to the crack plane will be localized to the vicinity of the crack where local bending of the reinforcement is initiated and where local crushing of the concrete may be present. As a result, the stiffness of the bar parallel to the crack plane is considerably lower than that given by the original shear stiffness. This effect can be accounted for in the program by using the term κG where $0 \leq \kappa \leq 1$ instead of the original shear modulus G of the reinforcement material. Due to simplicity we employ a constant κ-value and as the shear capacity of reinforcement bars is insignificant when no cracking is present a realistic κ-value might be determined by means of calibration calculations on a structure where cracking and dowel action dominate the response. Such calculations are performed in section 5.1 and, as previously mentioned, it is found there that neglect of dowel shear, i.e., $\kappa = 0$, constitutes in fact the most preferable value. This finding is supported by the calculations in section 5.3. Consequently, except for certain sensitivity studies the value $\kappa = 0$ is always employed in the program.

The objective of the following considerations is to determine the stiffness contributions of reinforcement elements to the involved triangular elements. In section 4.3.1 only linear material response is considered. Section 4.3.2 then treats the necessary modifications when plastic strains develop. Moreover, when temperature stresses are present the contribution from the reinforcement to the nodal forces of the involved triangular elements are also determined in section 4.3.1.

4.3.1. Elastic deformation of reinforcement

Every reinforcement bar is located along an arbitrary straight line. From the start and end point of each bar a special search

routine developed by Tingleff (1969) determines the intersection points with all involved triangular elements. Two such intersection points for a particular triangular element are shown as point A and B in fig. 2. The distance between A and B is termed

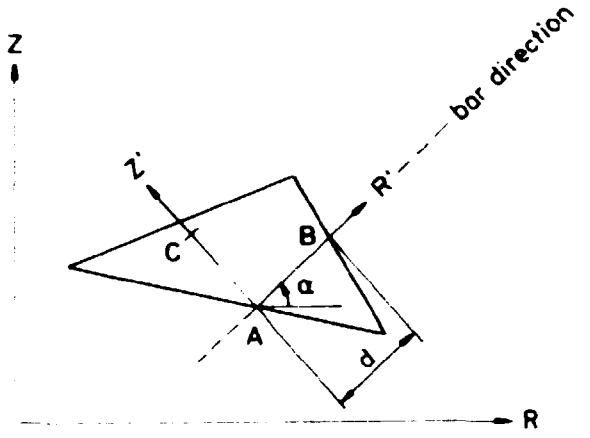

Fig. 4.3-2: Reinforcement bar intersecting a triangular element

d. The figure also indicates a local coordinate system R'Z' located at point A and with the R'-axis in the bar direction. The displacements of point A and B determine the in-plane forces in the reinforcement element. To determine the shear strain and thereby the shear stress an additional point is necessary. Point C located on the Z'-axis at a distance d from point A is used for this purpose. First, the reinforcement element is treated in the local R'Z'-coordinate system. Then a transformation to the global RZ-coordinate system is performed and finally the response of the reinforcement element is described by the nodal displacements of the involved triangular element. Let us first treat the reinforcement element in the local R'Z'-plane.

The displacements in the R'-direction and in the Z'-direction are given by

$$\bar{u}' = \begin{bmatrix} u' \\ v' \end{bmatrix}$$

where the prime(') in general indicates that reference is made to the local R'Z'-coordinate system. Similarly, the displacements

at point A, B and C are given by

$$\bar{a}'_b = \begin{bmatrix} u'_A \\ v'_A \\ u'_B \\ v'_B \\ u'_C \\ v'_C \end{bmatrix} \tag{4.3-1}$$

where index b in general indicates that a reinforcement bar is considered. The points A, B and C are the nodal points of the reinforcement element and the vector $\bar{a}'_b$ contains therefore the nodal displacements. In accordance with the triangular element concept, we work with a linear displacement field i.e.

$$u' = \alpha_1 + \alpha_2 r' + \alpha_3 z'$$

$$v' = \alpha_4 + \alpha_5 r' + \alpha_6 z'$$

To determine the constants α_1 ..... α_6 the displacement values at point A(r' = z' = 0), B(r' = d, z' = 0) and C(r' = 0, z' = d), i.e., the nodal points, are applied. It follows that

$$\begin{aligned} u' &= u'_A + \tfrac{1}{2}(u'_B - u'_A)r' + \tfrac{1}{2}(u'_C - u'_A)z' \\ v' &= v'_A + \tfrac{1}{2}(v'_B - v'_A)r' + \tfrac{1}{2}(v'_C - v'_A)z' \end{aligned} \tag{4.3-2}$$

The corresponding reinforcement strains of interest are

$$\bar{\varepsilon}'_b = \begin{bmatrix} \varepsilon'_R \\ \varepsilon'_\theta \\ \gamma'_{RZ} \end{bmatrix} = \begin{bmatrix} \dfrac{\partial u'}{\partial r'} \\ \varepsilon_\theta = \dfrac{u}{r} = \dfrac{1}{r}(u'\cos\alpha - v'\sin\alpha) \\ \dfrac{\partial u'}{\partial z'} + \dfrac{\partial v'}{\partial r'} \end{bmatrix} \tag{4.3-3}$$

where the angle α denotes the inclination of the local R'Z'-coordinate system with the global RZ-coordinate system, cf. fig. 2. The term r denotes the radial distance of the particular point of interest in the global RZ-coordinate system. Moreover, as reinforcement is assumed to have small dimensions in the direction of the Z'-axis, the variation of $\varepsilon'_\theta = \varepsilon_\theta$ due to different z'-values can be ignored. Use of eqs. (1), (2) and (3) then results in

$$\bar{\varepsilon}'_b = \bar{\bar{B}}'_b \, \bar{a}'_b \tag{4.3-4}$$

where

$$\bar{\bar{B}}'_b = \begin{bmatrix} -\frac{1}{d} & 0 & \frac{1}{d} & 0 & 0 & 0 \\ \frac{1-\frac{r'}{d}}{r}\cos\alpha - \frac{1-\frac{r'}{d}}{r}\sin\alpha & \frac{r'}{rd}\cos\alpha - \frac{r'}{rd}\sin\alpha & 0 & 0 \\ -\frac{1}{d} & -\frac{1}{d} & 0 & \frac{1}{d} & \frac{1}{d} & 0 \end{bmatrix}$$

As expected, all strains except the tangential strain are constant within the reinforcement bar. Similarly to the treatment of the triangular element in section 4.2 the variation along the bar of the tangential strain is ignored and as an approximation the value at the center of the bar element is used. At this center r' = d/2 applies and denoting the global radial distance of the center by r* the above expression for the matrix $\bar{\bar{B}}'_b$ simplifies to

$$\bar{\bar{B}}'_b = \begin{bmatrix} -\frac{1}{d} & 0 & \frac{1}{d} & 0 & 0 & 0 \\ \frac{\cos\alpha}{2r^*} - \frac{\sin\alpha}{2r^*} & \frac{\cos\alpha}{2r^*} - \frac{\sin\alpha}{2r^*} & 0 & 0 \\ -\frac{1}{d} & -\frac{1}{d} & 0 & \frac{1}{d} & \frac{1}{d} & 0 \end{bmatrix} \tag{4.3-5}$$

Corresponding to the reinforcement strains of interest the stresses in a bar are given by

$$\bar{\sigma}'_b = \begin{bmatrix} \sigma'_R \\ \sigma'_\theta \\ \tau'_{RZ} \end{bmatrix}$$

The stress-strain relations are as usual given by

$$\bar{\sigma}'_b = \bar{\bar{D}}'_b \ (\bar{\varepsilon}'_b - \bar{\varepsilon}'_{ob}) \qquad (4.3\text{-}6)$$

where the material matrix $\bar{\bar{D}}'_b$ and the initial strain vector $\bar{\varepsilon}'_{ob}$ due to temperature take different forms depending on the reinforcement type.

For tangential reinforcement that carries forces only in the tangential direction, cf. fig. 1 a), we have

$$\bar{\bar{D}}'_{b,tan.} = E \begin{bmatrix} 0 & 0 & 0 \\ 0 & 1 & 0 \\ 0 & 0 & 0 \end{bmatrix} \qquad \bar{\varepsilon}'_{ob,tan.} = \alpha\Delta T \begin{bmatrix} 0 \\ 1 \\ 0 \end{bmatrix} \qquad (4.3\text{-}7)$$

where, as usual, E is Young's modulus, α the coefficient of thermal expansion and ΔT the mean temperature rise of the bar element in question.

RZ-reinforcement, cf. fig. 1 b), carries load in the RZ-plane. In addition to the load in the bar direction, shear stresses due to dowel action might be considered, i.e.

$$\bar{\bar{D}}'_{b,RZ} = E \begin{bmatrix} 1 & 0 & 0 \\ 0 & 0 & 0 \\ 0 & 0 & \frac{\kappa}{2(1+\nu)} \end{bmatrix} \qquad \bar{\varepsilon}'_{ob,RZ} = \alpha\Delta T \begin{bmatrix} 1 \\ 0 \\ 0 \end{bmatrix} \qquad (4.3\text{-}8)$$

where ν is Poisson's ratio for the reinforcement material and κ is factor, $0 \leq \kappa \leq 1$, which implies that the full shear capacity of the reinforcement cannot be utilized due to, for instance, local crushing of the concrete. As explained previously

the value $\kappa = 0$ is always assumed except for certain sensitivity studies cf. also sections 5.1 and 5.3.

Membrane reinforcement, cf. fig. 1 c), carries load both in the tangential direction and in the RZ-plane. Like the RZ-reinforcement, shear stresses in the RZ-plane due to dowel action might be considered, i.e.,

$$\bar{\bar{D}}'_{b,mem.} = \frac{E}{1-\nu^2}\begin{bmatrix} 1 & \nu & 0 \\ \nu & 1 & 0 \\ 0 & 0 & \frac{\kappa(1-\nu)}{2} \end{bmatrix} \qquad \bar{\varepsilon}'_{ob,mem.} = \alpha\Delta T\begin{bmatrix} 1 \\ 1 \\ 0 \end{bmatrix} \tag{4.3-9}$$

where in general the value $\kappa = 0$ again is assumed.

From the standard finite element formulation given by eqs. (4.1-19) to (4.1-25) and noting the constitutive equation (6) the reinforcement element is described by

$$\bar{\bar{K}}'_b \, \bar{a}'_b = \bar{F}'_{\varepsilon_o b} \tag{4.3-10}$$

where the reinforcement element stiffness matrix is given by $\bar{\bar{K}}'_b$, the nodal displacements $\bar{a}'_b$ are given by eq. (1) and the vector $\bar{F}'_{\varepsilon_o b}$ describes the nodal forces due to temperature loading. The stiffness matrix is given by

$$\bar{\bar{K}}'_b = \int_{\text{bar vol.}} \bar{\bar{B}}'^{T}_b \, \bar{\bar{D}}'_b \, \bar{\bar{B}}'_b \, dV \approx \bar{\bar{B}}'^{T}_b \, \bar{\bar{D}}'_b \, \bar{\bar{B}}'_b \, 2\pi r^* dt \tag{4.3-11}$$

where $\bar{\bar{B}}'_b$ is given by eq. (5) and $\bar{\bar{D}}'_b$ is given by eqs. (7)-(9). The term t denotes the thickness of the "shell" possessing the same volume and stiffness as the bars. The nodal forces due to temperature loading are given by

$$\bar{F}'_{\varepsilon_o b} = \int_{\text{bar vol.}} \bar{\bar{B}}'^{T}_b \, \bar{\bar{D}}'_b \, \bar{\varepsilon}'_{ob} \, dV \approx \bar{\bar{B}}'^{T}_b \, \bar{\bar{D}}'_b \, \bar{\varepsilon}'_{ob} \, 2\pi r^* dt \tag{4.3-12}$$

the reinforcement element, i.e. point A, B and C in fig. 2. Let us now describe the reinforcement element when reference is made to the nodal points of the involved triangular element.

As perfect bond is assumed the following relations exist, cf. eq. (4.2-3)

$$\bar{u}_A = \bar{\bar{N}}_A \bar{a} \; ; \quad \bar{u}_B = \bar{\bar{N}}_B \bar{a} \; ; \quad \bar{u}_C = \bar{\bar{N}}_C \bar{a} \tag{4.3-17}$$

where $\bar{u}_A$ is the displacements at point A, the matrix $\bar{\bar{N}}_A$ is given by eq. (4.2-4) where the coordinates of point A are applied and $\bar{a}$ contains the nodal displacements of the involved triangular element. Similar expressions hold for point B and C. Equation (17) leads to

$$\bar{a}_b = \begin{bmatrix} \bar{\bar{N}}_A \\ \bar{\bar{N}}_B \\ \bar{\bar{N}}_C \end{bmatrix} \bar{a} \tag{4.3-18}$$

Similarly, from eq. (4.2-13) follows

$$\bar{F}_{\epsilon_o r} = \left[\bar{\bar{N}}_A^T \; \bar{\bar{N}}_B^T \; \bar{\bar{N}}_C^T\right] \bar{F}_{\epsilon_o b} \tag{4.3-19}$$

where $\bar{F}_{\epsilon_o r}$ are the equivalent nodal forces due to reinforcement at the nodal points of the involved triangular element. The index r indicates that reinforcement is considered. Premultiplication of eq. (15) with the matrix $\left[\bar{\bar{N}}_A^T \; \bar{\bar{N}}_B^T \; \bar{\bar{N}}_C^T\right]$ and use of eqs. (18) and (19) yields

$$\left[\bar{\bar{N}}_A^T \; \bar{\bar{N}}_B^T \; \bar{\bar{N}}_C^T\right] \bar{\bar{L}}^T \bar{\bar{K}}_b \bar{\bar{L}}^T \begin{bmatrix} \bar{\bar{N}}_A \\ \bar{\bar{N}}_B \\ \bar{\bar{N}}_C \end{bmatrix} \bar{a} = \bar{F}_{\epsilon_o r} \tag{4.3-20}$$

This equation states the contribution of the reinforcement element to the involved triangular element with respect to stiff-

ness and nodal forces if temperature stresses are present. The stiffness contribution $\bar{\bar{K}}_r$ is

$$\bar{\bar{K}}_r = \left[\bar{\bar{N}}_A^T \; \bar{\bar{N}}_B^T \; \bar{\bar{N}}_C^T\right] \bar{\bar{L}}^T \; \bar{\bar{K}}_b' \; \bar{\bar{L}} \begin{bmatrix} \bar{\bar{N}}_A \\ \bar{\bar{N}}_B \\ \bar{\bar{N}}_C \end{bmatrix} \tag{4.3-21}$$

and the contribution to nodal forces if temperature stresses are present is

$$\bar{F}_{\varepsilon_o r} = \left[\bar{\bar{N}}_A^T \; \bar{\bar{N}}_B^T \; \bar{\bar{N}}_C^T\right] \bar{\bar{L}}^T \; \bar{F}'_{\varepsilon_o b} \tag{4.3-22}$$

To reduce computer time it is convenient to give closed form expressions for the terms $\bar{\bar{L}}^T \; \bar{\bar{K}}_b' \; \bar{\bar{L}}$ and $\bar{\bar{L}}^T \; \bar{F}'_{\varepsilon_o b}$ present in eqs. (21) and (22), respectively. The matrix $\bar{\bar{L}}$ is given by eq. (14), $\bar{\bar{K}}_b'$ is given by eq. (11) while $\bar{F}'_{\varepsilon_o b}$ is given by eq. (12). After tedious matrix multiplications the following results are obtained:

Tangential reinforcement:

$$\bar{\bar{L}}^T \; \bar{\bar{K}}_b' \; \bar{\bar{L}} = \frac{\pi dt \; E}{2r^*} \begin{bmatrix} 1 & 0 & 1 & 0 & 0 & 0 \\ & 0 & 0 & 0 & 0 & 0 \\ & & 1 & 0 & 0 & 0 \\ & & & 0 & 0 & 0 \\ \text{symmetric} & & & & 0 & 0 \\ & & & & & 0 \end{bmatrix}$$

$$\bar{\bar{L}}^T \; \bar{F}'_{\varepsilon_o b} = \pi dt \; E \; \alpha \Delta T \begin{bmatrix} 1 \\ 0 \\ 1 \\ 0 \\ 0 \\ 0 \end{bmatrix}$$

RZ-reinforcement:

$$\bar{\bar{L}}^T \bar{\bar{K}}'_b \bar{\bar{L}} = \frac{2\pi r^* t\ E}{d}$$

$$\begin{bmatrix}
c^2+g(1-2sc) & sc+g(c^2-s^2) & -c^2+g(sc-s^2) & -sc+g(sc-c^2) & g(sc-c^2) & g(s^2-sc) \\
 & s^2+g(1+2sc) & -sc+g(sc+s^2) & -s^2-g(sc+c^2) & -g(sc+c^2) & -g(s^2+sc) \\
 & & c^2+gs^2 & sc-gsc & -gsc & -gs^2 \\
\text{symmetric} & & & s^2+gc^2 & gc^2 & gsc \\
 & & & & gc^2 & gsc \\
 & & & & & gs^2
\end{bmatrix}$$

where

$$s = \sin\alpha; \quad c = \cos\alpha; \quad g = \frac{\kappa}{2(1+\nu)}$$

and in accordance with previous remarks the value $\kappa = 0$ is always employed, except for certain sensitivity studies.

$$\bar{\bar{L}}^T \bar{\bar{F}}'_{\varepsilon_o b} = 2\pi r^* t\ E\ \alpha\Delta T \begin{bmatrix} -\cos\alpha \\ -\sin\alpha \\ \cos\alpha \\ \sin\alpha \\ 0 \\ 0 \end{bmatrix}$$

Membrane reinforcement:

$$\bar{\bar{L}}^T \bar{\bar{K}}_b' \bar{\bar{L}} = \frac{2\pi r^* t d\, E}{1-\nu^2}$$

$$\begin{bmatrix}
\frac{c^2}{d^2} + \frac{h}{d^2}(1-2sc) & \frac{sc}{d^2} - \frac{\nu s}{2r^* d} & -\frac{c^2}{d^2} + \frac{1}{4r^{*2}} & -\frac{sc}{d^2} + \frac{\nu s}{2r^* d} & \frac{h}{d^2}(sc-c^2) & \frac{h}{c^2}(s^2-sc) \\
-\frac{\nu c}{r^* i} + \frac{1}{4r^{*2}} & +\frac{h}{d^2}(c^2-s^2) & +\frac{h}{d^2}(sc-s^2) & +\frac{h}{d^2}(sc-c^2) & & \\
 & \frac{s^2}{d^2} & -\frac{sc}{d^2} - \frac{\nu s}{2r^* d} & -\frac{s^2}{d^2} & -\frac{h}{d^2}(sc+c^2) & -\frac{h}{d^2}(s^2+sc) \\
 & +\frac{h}{d^2}(1+2sc) & +\frac{h}{d^2}(sc+s^2) & -\frac{h}{d^2}(sc+c^2) & & \\
 & & \frac{c^2}{d^2} + \frac{h}{d^2}s^2 & \frac{sc}{d^2} - \frac{h}{d^2}sc & -\frac{h}{d^2}sc & -\frac{h}{d^2}s^2 \\
 & & +\frac{1}{4r^{*2}} + \frac{\nu c}{r^* d} & +\frac{\nu s}{2r^* d} & & \\
\text{symmetric} & & & \frac{s^2}{d^2} + \frac{h}{d^2}c^2 & \frac{h}{d^2}c^2 & \frac{h}{d^2}sc \\
 & & & & \frac{h}{d^2}c^2 & \frac{h}{d^2}sc \\
 & & & & & \frac{h}{d^2}s^2
\end{bmatrix}$$

where

$$s = \sin\alpha; \quad c = \cos\alpha; \quad h = \frac{\kappa(1-\nu)}{2}$$

and in accordance with previous remarks the value $\kappa = 0$ is always employed, except for certain sensitivity studies. It appears that the stiffness contributions due to dowel shear are

identical to those for RZ-reinforcement.

$$\bar{\bar{L}}^T \bar{F}'_{\varepsilon_o b} = 2\pi r^* dt \frac{E}{1-\nu} \alpha \Delta T \begin{bmatrix} -\frac{1}{d}\cos\alpha + \frac{1}{2r^*} \\ -\frac{1}{d}\sin\alpha \\ \frac{1}{d}\cos\alpha + \frac{1}{2r^*} \\ \frac{1}{d}\sin\alpha \\ 0 \\ 0 \end{bmatrix}$$

These expressions together with eqs. (21) and (22) constitute the final finite element formulation when elastic behaviour of reinforcement is assumed. The next section deals with the finite element formulation when the reinforcement is loaded into the plastic region.

4.3.2. Plastic deformation of reinforcement

As already mentioned in section 3, the initial stress method is employed in the finite element program when considering plastic deformation of the reinforcement. In essence this method reformulates the original constitutive equation

$$\bar{\sigma} = \bar{\bar{D}}(\bar{\varepsilon})\ \bar{\varepsilon} \qquad (4.3\text{-}23)$$

where $\bar{\bar{D}}(\bar{\varepsilon})$ is the nonlinear material matrix that depends on the strain state, into the equivalent equation

$$\bar{\sigma} = \bar{\bar{D}}\ \bar{\varepsilon} + \bar{\sigma}_o \qquad (4.3\text{-}24)$$

Here $\bar{\bar{D}}$ is the usual constant material matrix while $\bar{\sigma}_o$ are the initial stresses determined so that eqs. (23) and (24) result in identical stresses when the strains are identical. The initial stresses are therefore determined by

$$\bar{\sigma}_o = (\bar{\bar{D}}(\bar{\varepsilon}) - \bar{\bar{D}})\ \bar{\varepsilon}$$

Finite element formulation using eq. (23) results in a stiffness matrix that depends on the unknown displacements and as solution of the resulting equation system therefore necessarily involves iterations, the inverse of the coefficient matrix of the equation system has in principle to be determined in each iteration. This is very time-consuming so instead the finite element formulation can use eq. (24) resulting in a constant coefficient matrix while only the nodal forces due to the initial stresses are changed in the iteration process. The contribution to the nodal forces due to the initial stresses is, cf. eqs. (4.1-19) and (4.1-25)

$$\bar{F}_{\sigma_o} = - \int_V \bar{\bar{B}}^T \bar{\sigma}_o \, dV \qquad (4.3\text{-}25)$$

This initial stress method was proposed by Zienkiewicz et al. (1969) and as shown by Zienkiewicz (1977) p. 459 it corresponds to the modified Newton-Raphson method.

Let us now determine the nodal force contribution due to plastic deformation of the reinforcement using this initial stress method. It should be noted that the corresponding implementation in the finite element program was performed mainly by Herrmann (1975). Moreover, as the primary reinforcement forces are those located in the reinforcement plane, and to facilitate the calculations the influence of shear tresses due to dowel action on the plastic deformation of the reinforcement is ignored.

Firstly, the forces at the nodes of the reinforcement element are determined in the local R'Z'-coordinate system, cf. fig. 2. Secondly, these forces are transformed to the global RZ-coordinate system and then they are transferred to the nodes of the involved triangular element. The forces at the nodes of the reinforcement element are determined by means of eq. (25), i.e.,

$$\bar{F}'_{\sigma_o b} = - \int_{\text{bar vol.}} \bar{\bar{B}}_b'^T \bar{\sigma}'_{ob} \, dV \simeq \bar{\bar{B}}_b'^T \bar{\sigma}'_{ob} \, 2\pi r^* dt \qquad (4.3\text{-}26)$$

where the same notation as in the previous section is applied (i.e. the prime (') indicates that reference is made to the local R'Z'-coordinate system, and index b indicates that reinforcement bars are considered). Moreover, r* is the global radial distance of the centre of the reinforcement element, t is the thickness and d is the length, cf. fig. 2. In eq. (26) the matrix $\bar{\bar{B}}'_b$ is given by eq. (5) while the initial stress vector $\bar{\sigma}'_{ob}$ takes different forms depending on the reinforcement type.

For tangential reinforcement, cf. fig. 1 a), we have

$$\bar{\sigma}'_{ob} = \begin{bmatrix} 0 \\ \sigma_o \\ 0 \end{bmatrix} \qquad (4.3\text{-}27)$$

where σ_o is given by eq. (3-19). For RZ-reinforcement, cf. fig. 1 b), we have

$$\bar{\sigma}'_{ob} = \begin{bmatrix} \sigma_o \\ 0 \\ 0 \end{bmatrix} \qquad (4.3\text{-}28)$$

where σ_o again is given by eq. (3-19). For membrane reinforcement, cf. fig. 1 c), we have

$$\bar{\sigma}'_{ob} = \begin{bmatrix} \sigma_{o1} \\ \sigma_{o2} \\ 0 \end{bmatrix} \qquad (4.3\text{-}29)$$

where σ_{o1} and σ_{o2} are given by eq. (3-12), i.e. the stress σ_{o1} is directed in the R'-direction while σ_{o2} is the tangential stress.

Transformation of the force vector $\bar{F}'_{\sigma_o b}$ from the local coordinate system to the global coordinate system and subsequent transformation of these forces located at the nodal points A, B and C of fig. 2 to the nodes of the involved triangular element follow

exactly the same lines as the transformations of the force vector $\bar{F}'_{\varepsilon_o b}$ caused by temperature stresses and dealt with in the previous section. Therefore an expression similar to eq. (22) holds, i.e.,

$$\bar{F}_{\sigma_o r} = [\bar{\bar{N}}_A^T \; \bar{\bar{N}}_B^T \; \bar{\bar{N}}_C^T] \; \bar{\bar{L}}^T \; \bar{F}'_{\sigma_o b} \qquad (4.3\text{-}30)$$

where $\bar{F}_{\sigma_o r}$ is the equivalent nodal force vector due to reinforcement at the nodes of the involved triangular element. The index r indicates that reinforcement is considered. As given previously the matrix $\bar{\bar{N}}_A$ is described by eq. (4.2-4) where the coordinates of point A are applied. The matrices $\bar{\bar{N}}_B$ and $\bar{\bar{N}}_C$ are given similarly. The matrix $\bar{\bar{L}}$ is given by eq. (14) and $\bar{F}'_{\sigma_o b}$ by eq. (26).

To reduce computer time it is convenient to give a closed form expression for the term $\bar{\bar{L}}^T \; \bar{F}'_{\sigma_o b}$ present in eq. (30). After trivial matrix multiplications we obtain:

Tangential reinforcement:

$$\bar{\bar{L}}^T \; \bar{F}'_{\sigma_o b} = -\pi dt \; \sigma_o \begin{bmatrix} 1 \\ 0 \\ 1 \\ 0 \\ 0 \\ 0 \end{bmatrix}$$

where σ_o is expressed by eq. (3-19).

RZ-reinforcement:

$$\bar{\bar{L}}^T \; \bar{F}'_{\sigma_o b} = -2\pi r^* t \; \sigma_o \begin{bmatrix} -\cos\alpha \\ -\sin\alpha \\ \cos\alpha \\ \sin\alpha \\ 0 \\ 0 \end{bmatrix}$$

where σ_o again is given by eq. (3-19).

Membrane reinforcement:

$$\bar{L}^T \bar{F}'_{\sigma_o b} = -2\pi r^* dt \begin{bmatrix} -\frac{\sigma_{o1}}{d}\cos\alpha + \frac{\sigma_{o2}}{2r^*} \\ -\frac{\sigma_{o1}}{d}\sin\alpha \\ \frac{\sigma_{o1}}{d}\cos\alpha + \frac{\sigma_{o2}}{2r^*} \\ \frac{\sigma_{o1}}{d}\sin\alpha \\ 0 \\ 0 \end{bmatrix}$$

These expressions together with eq. (30) constitute the nodal force contributions within the initial stress method when plastic deformation of reinforcement is present.

4.4. Prestressing

In principle two types of prestressing exist namely grouted and ungrouted prestressing. For grouted prestressing perfect bond between concrete and tendon is assumed to exist. This type of prestressing can therefore be dealt with by a combination of prescribed fixed line forces and usual reinforcement elements as described in the previous sections. Naturally, only a certain part of the nonlinear stress-strain curve for the tendon material is utilized when specifying the nonlinear stress-strain curve for these reinforcement elements, as consideration has to be taken to the initial prestressing force; but apart from that treatment of grouted prestressing is straightforward. It should also be noted that as a result of the assumed rotational symmetry even ungrouted circumferential prestressing is treated as grouted prestressing. However, consideration to ungrouted straight tendons located in the RZ-plane requires special features not

dealt with until now. In principle, such considerations could be performed using spring elements that could be formulated similarly to usual reinforcement elements. However, as concrete and tendon deform independently except at the anchor regions such a formulation would couple nodal points that in general are far from each other. As a result a very large bandwidth of the equation system would exist making such a formulation prohibitive. Instead, after specification of the initial prestressing forces, attention is focussed directly to the additional tendon forces caused by deformations. In the program the dependence between these forces and the relative deformations of the ends of the tendons is specified as the quatrolinear dependence shown in fig. 3-1 b) where as before consideration has to be taken to the initial prestressing force. The corresponding nodal forces then depend on the unknown displacements and this infers that an iterative process is necessary even when material behaviour is linear. As we are dealing here mainly with short-term loadings this is considered to be only a minor disadvantage as changes in tendon forces caused by deformations are usually of interest only for loadings where material nonlinearities are involved and where iterations therefore necessarily must be performed. It is to be noted that unloading is treated correctly.

4.5. Plane stress and strain versus axisymmetric formulation

Until now only the axisymmetric finite elements have been dealt with. However, the formulation both of plane stress and plane strain elements follows very much the same lines and they will therefore be treated only schematically in this section. Naturally the objective for the derivation of plane elements is to achieve formulations that are, as far as possible, analogous to the axisymmetric case so that, except for certain modifications, identical subroutines can be utilized in the computer program.

Let us first consider the plane strain concrete element and let the tangential stress and strain correspond to quantities in the longitudinal direction of the structure, i.e., according to the plane strain assumption we have $\varepsilon_0 = 0$. Now, the displacements

within the element are still given by eqs. (4.2-3) and (4.2-4). Therefore, the condition $\varepsilon_\theta = 0$ can be obtained simply by replacing all elements in the third row of the $\bar{\bar{B}}$-matrix given by eq. (4.2-7) with zeros. Then correct strain values follow and as the constitutive matrix $\bar{\bar{D}}$ given by eq. (4.2-10) also applies for plane strain the correct stiffness matrix is obtained directly. Correct expressions for strains, stresses and nodal forces hold even when temperature loading is present. Therefore, the plane strain concrete element is formulated completely identical to the axisymmetric element just by modifying the $\bar{\bar{B}}$-matrix as stated above.

Turning to the plane stress concrete element located with its plane in the RZ-plane we have $\sigma_\theta = 0$ according to the plane stress assumption. As before, the displacements within the element are given by eqs. (4.2-3) and (4.2-4). Using the standard transformation formula, cf. for instance Timoshenko and Goodier (1951) p. 34, and replacing E with $E(1+2\nu)/(1+\nu)^2$ and ν with $\nu/(1+\nu)$ then the $\bar{\bar{D}}$-matrix for plane strain transforms to the $\bar{\bar{D}}$-matrix for plane stress except for the third row and column that correspond to σ_θ and ε_θ, respectively. If the $\bar{\bar{B}}$-matrix is modified as for plane strain then $\varepsilon_\theta = 0$ follows, but it is easily shown that the true plane stress stiffness matrix is obtained and if the third row of the initial strain vector $\bar{\varepsilon}_o$ given by eq. (4.2-11) is set to zero then correct nodal forces due to temperature loading also result. Except for σ_θ and ε_θ the true stresses and strains are obtained as well and finally σ_θ is therefore simply set to zero while ε_θ is made directly equal to $-\nu(\varepsilon_R+\varepsilon_Z)/(1-\nu) + (1+\nu)\alpha\,\Delta T/(1-\nu)$. When cracking is involved, and obviously no radial cracks can be present, no temperature loading is considered and ε_θ is then made equal to $-\nu\,\varepsilon_p$ where ε_p is the strain parallel to the crack direction. This is just to say that ε_θ is independent of the strain normal to the crack plane and that isotropic properties exist along the crack plane. A similar expression was suggested by Phillips and Zienkiewicz (1976). Summarizing, the plane stress concrete element is obtained from the axisymmetric element by modifying the $\bar{\bar{B}}$-matrix as for plane strain. Moreover, the above-mentioned transformations for E and ν are applied and the initial strain vector due

to temperature loading is modified as stated above. Then calculations completely identical to the axisymmetric element result in the correct stiffness matrix and nodal forces due to temperature loading. Also the stresses and strains follow except that correct values for σ_θ and ε_θ are prescribed directly.

Considering reinforcement elements and treating first the plane strain case then, referring to fig. 4-3, RZ-reinforcement and membrane reinforcement can be applied. Obviously, no changes at all are necessary for the RZ-reinforcement. For membrane reinforcement the stiffness due to dowel shear is identical to that of RZ-reinforcement as when axisymmetry exists. From the condition $\varepsilon_\theta = 0$ we infer that the rest of the stiffness of membrane reinforcement corresponds to the stiffness of RZ-reinforcement - excluding contributions from dowel shear - multiplied by the factor $1/(1-\nu^2)$. The contribution from membrane reinforcement to nodal forces when temperature loading is present follows also from the condition $\varepsilon_\theta = 0$ and is easily shown to be identical to that of RZ-reinforcement multiplied by the factor $1/(1-\nu)$. When plastic deformation of membrane reinforcement occurs initial stresses are obtained if σ_{o2}, the tangential initial stress, is set to zero, cf. eq. (4.3-29). This result is also a simple implication of the condition $\varepsilon_\theta = 0$.

The only plane stress reinforcement considered is RZ-reinforcement, cf. fig. 4-2. Obviously no modifications compared to the axisymmetric case are involved.

With the above modifications all subroutines and statements of the axisymmetric formulation in the computer program apply for the plane elements also thereby ensuring a unified treatment that has obvious advantages not only from a programming point of view, but also when testing the validity of the computer program.

4.6. Computational schemes

Having described the constitutive models and the finite element theory employed in the AXIPLANE-computer program, attention will

now be directed towards numerical aspects related to the implementation of these matters.

The AXIPLANE-program is written in Algol and runs at Risø's Burrough B-6700 computer using single precision that considers 11 significant digits. Now, essentially the finite element modelling described in the previous sections results in an equation system with 2n degrees of freedom where n is the number of nodal points, i.e.

$$\bar{\bar{K}}\,\bar{a} = \bar{\bar{F}} \qquad (4.6\text{-}1)$$

Here $\bar{\bar{K}}$ denotes the total symmetric stiffness matrix, the vector $\bar{a}$ contains all the nodal displacements, while the vector $\bar{F}$ contains the nodal forces. This equation refers to the RZ-coordinate system. However, in accordance with the discussion in section 4.1 the geometric boundary conditions still remain to be considered.

Suppose that the nodal displacement a_j in either the R- or Z-direction is prescribed as $a_j = \gamma$. In accordance with the method described by Zienkiewicz and Cheung (1967) p. 233 the corresponding j-th equation in the equation system (1) is then modified by multiplying the diagonal stiffness term K_{jj} with the factor 10^{10} and by replacing the right hand side with the quantity then obtained multiplied by γ. This means that equation j in the equation system (1) is replaced by

$$K_{j1}a_1+K_{j2}a_2+\ldots+K_{jj}\cdot 10^{10}a_j+\ldots+K_{j,2n-1}a_{2n-1}$$

$$+K_{j,2n}a_{2n} = K_{jj}\cdot 10^{10}\gamma \qquad (4.6\text{-}2)$$

where no summation convention is utilized. As all other terms than that containing a_j contribute insignificantly, this equation yields as a very close approximation the attempted expression $a_j = \gamma$. The advantages of the method are that symmetry of the coefficient matrix continues and no rearrangements of the equations are involved.

If displacements are prescribed in other directions than the R- or Z-axis, i.e., if skewed kinematic constraints are present then eq. (1) has to be transformed to the R'Z'-coordinate shown in fig. 1. After that a modification corresponding to eq. (2) is performed and a retransformation back to the original RZ-

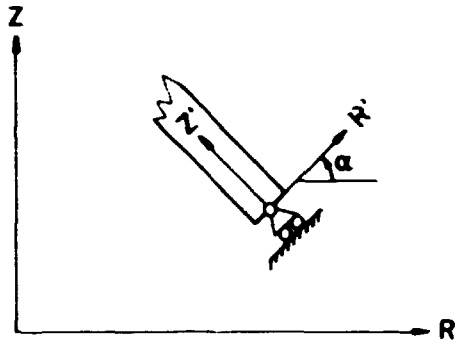

Fig. 4.6-1: Skewed geometrical constraint

coordinate system is then carried out. The result of these trivial matrix multiplications may be found in appendix B.

Having then introduced the prescribed displacements for a fixed stiffness matrix $\bar{\bar{K}}$ and a fixed force vector $\bar{F}$ standard routines are available for solution of the equation system (1). In the present case, the equation solver is termed BANDSYMEQ and is available at Risø's computer, Sørensen (1968). As the name indicates, this solver takes advantage of the symmetry and banded structure of the stiffness matrix. A direct solution is applied that uses the square-root method, i.e., a Cholesky decomposition of the stiffness matrix into triangular matrices. Special care is taken to minimize rounding-off errors.

Different strategies exist for determining the structural response when material behaviour becomes nonlinear. In the present case as a nonlinear elastic model is utilized for the concrete and as a secantial formulation has been employed so that dilatation and softening of concrete can be considered, the equation system (1) is set up and solved when the force vector $\bar{F}$ includes the total loadings applied to the structure. This means that a

total formulation as opposed to an incremental formulation is employed. However, for each loading level iterations are carried out until the constitutive equations for concrete, reinforcement and prestressing are in accordance with the total loading in question. This procedure is sketched in fig. 2.

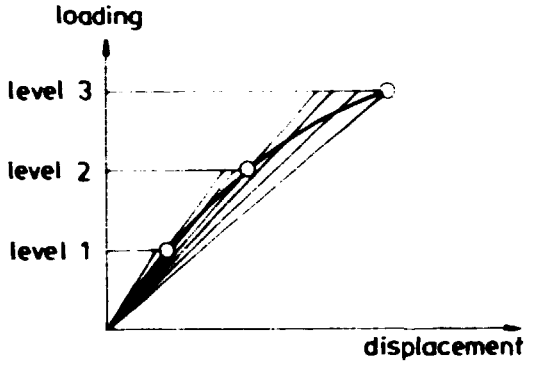

Fig. 4.6-2: Numerical solution of the nonlinear equation system

All nonlinearities can in principle be treated by the initial stress method where, as described in section 4.3.2, the stiffness matrix $\bar{\bar{K}}$ is maintained constant while the force vector $\bar{F}$ is modified appropriately. This approach enables a quick solution of the nonlinear equation system (1), but when nonlinear material behaviour becomes dominant it is known that convergence proceeds rather slowly. This is illustrated in fig. 3 where identical plastic strains exist at points A and B and where the predictions C and D are shown after 4 iterations. Therefore, to improve convergence an occasional updating of the total stiffness matrix is appropriate, cf. for instance Phillips and Zienkiewics (1976). A general acceptable criterion for determining when updating should occur is apparently not available. However, as cracking of concrete as opposed to the gradual development of plastic strains is an irreversible distinct phenomenon, it seems convenient to update the stiffness matrix every time cracking occurs. Moreover, plastic strains in concrete as well as cracking in concrete in general develop simultaneously in most structures when the loading is increased. Therefore, the extreme choice to treat all concrete nonlinearities by directly changing the total stiffness matrix $\bar{\bar{K}}$ and to treat all nonlinearities present in reinforcement and prestressing by appropriate

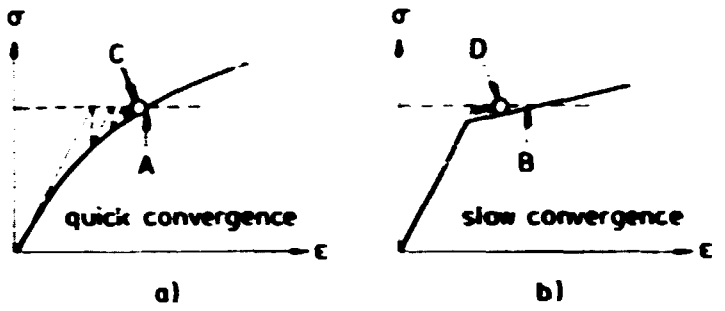

Fig. 4.6-3: Performance of the initial stress method for
a) Slightly curved stress-strain curve
b) Stress-strain curve with an almost flat part.

modifications of the force vector $\bar{F}$ has been employed here.

Tracing the nonlinear behaviour of a structure starts with a linear elastic solution. At the load level in question, concrete stresses determine whether cracking occurs and they also determine those secant values of Young's modulus, E_s, and Poisson's ration, ν_s, that are in accordance with the constitutive equations. If the utilized value of Young's modulus E is 5% larger than the E_s-value then a new Young's modulus equal to 0.95 E is employed. Likewise, if the utilized Poisson's ratio ν is 5% smaller than the ν_s-value then a new Poisson's ratio equal to 1.05ν is employed. The same alternation of the two material parameters occurs if the stress state violates the failure criterion provided that no cracking occurs. In the post-failure region when softening occurs if the utilized Young's modulus E is smaller than the E_s-value a new modulus equal to 0.95 E is utilized and at the same time Poisson's ratio ν is increased to 1.05ν. However, to avoid ill-conditioning of the equation system the maximum allowable value of Poisson's ratio is set at 0.45 in accordance with the findings of Huang (1969). For crushing of the concrete it is also possible in the program to disregard softening in the post-failure region. This extreme assumption of no-softening corresponds to infinite ductility at failure and, as above, the actual values of E and ν are decreased and increased 5%, respectively, if the stress state in

question violates the failure criterion.

As a nonlinear elastic model for concrete is employed here, loading and unloading follow in principle identical stress-strain curves. However, as a result of the above-mentioned numerical procedure, unloading follows the straight line from the stress point in question towards the origin. This is illustrated in fig. 4 and even though this unloading behaviour is still a

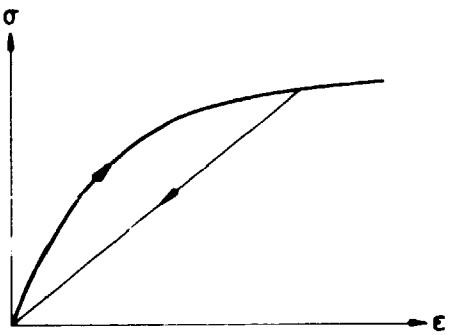

Fig. 4.6-4: Loading and unloading behaviour of concrete model (fracturing solid)

very crude approximation to reality it is certainly preferable to the ideal nonlinear elastic behaviour. Indeed, the behaviour shown in fig. 4 is classified as a fracturing solid according to Dougill (1976).

It should be noted that as the secantial values of Young's modulus and Poisson's ratio as determined by the constitutive equation steadily decreases and steadily increases, respectively, as the stress state approaches failure, the procedure outlined above is always numerically stable and convergent.

Considering embedded reinforcement the program determines the total concrete strains which in turn determine the corresponding initial stresses in the reinforcement as described previously. If these initial stresses have changed more than 1% the new initial stress values are then employed and a corresponding modification of the force vector $\bar{F}$ is carried out.

Unembedded reinforcement, i.e., springs which most often represent prestressed tendons, are considered directly through the corresponding forces. These forces depend on the relative displacements of the ends of the springs and if the force alteration is larger than 2% then the new spring forces are employed and the force vector $\bar{F}$ is updated appropriately.

From the obtained nodal displacements the strains and stresses within a triangular element are determined. As the result of the employed simple element these stress and strain values are constant within each element. It is well known, cf. for instance Zienkiewicz (1977) pp. 103-105 and pp. 127-130, that much better accuracy is related to stresses and strains at the nodal points determined simply as the mean values from the surrounding elements. This approach is also employed in the program.

From this we conclude that as the stress state determines crack initiation, cracking is related to a nodal point. It is assumed that cracking at a nodal point affects all surrounding elements which have not previously been cracked in the same way. In the afore-mentioned averaging process only those elements are used that are in the same cracking condition as the considered nodal point. It should be recalled that to avoid ill-conditioning of the equation system, 0.5% of the stiffness normal to a crack plane and present just before cracking is retained. When plastic deformation of the concrete occurs at a nodal point, the material parameters are changed accordingly in all surrounding elements not previously affected in the present iteration.

For analysis of a structure and to achieve a response that depends on the loading history, the load increments have in principle to be as small as possible so that the initiated cracks are as few as possible. The effect of these cracks and development of plastic strains may then in turn for the same loading cause additional cracking due to stress redistribution. If the load increments are too large cracking may be initiated in large regions at once and the effect of stress redistribution caused by previous cracking and plastic strains is distorted and the dependence of loading history is lost. This may result in a

premature failure load. However, if no or insignificant cracking occurs very large load increments can be utilized. In the examples considered in the following section load increments around 2-4% of the ultimate load were employed.

The failure load is determined as the load in which a large number of iterations is insufficient to satisfy both the constitutive equations and the static equilibrium. This means that large displacements occur corresponding to the maximum point on the forec-displacement curve having a horizontal tangent. In the present case 25 iterations are chosen as the limiting value.

It should be recalled that in the standard version of the program, the shear retention factor η in cracked elements is $\eta = 0.01$. Moreover, no dowel action of the reinforcement is considered, i.e., the value of κ is $\kappa = 0$.

5. EXAMPLES OF ANALYSIS OF CONCRETE STRUCTURES

While the previous sections have described in detail the theoretical basis of the AXIPLANE-program, the present section will treat examples of application of the program. In these examples, all of which represent realistic structures difficult to investigate by other theoretical means, a comparison with experimental evidence will be carried out, so that the applicability of the program can be evaluated. Moreover, apart from this obvious aspect much effort will be placed on investigating the structural behaviour of the analyzed concrete structures. In fact, the AXIPLANE-program offers quite unique possibilities for gaining insight in the load carrying mechanism of concrete structures since not only is detailed information available throughout the loading history, but different assumptions can easily be incorporated enabling sensitivity studies to be carried out.

These two objectives: (1) evaluation of the applicability of the

program and (2) attainment of insight into the structural behaviour are maintained in the analysis of the considered structures. It should also be emphasized that these structures all represent very difficult cases to investigate by other theoretical means and this benchmark-aspect should be borne in mind when evaluating predictions versus experimental evidence. The structures considered here are all loaded to their ultimate capacity, the quantity of primary concern here.

The next section treats quadratic panels with isotropic and orthogonal reinforcement loaded by tensile forces skewed to the reinforcement. The analysis focuses on aspects of reinforcement bar modelling and in particular on simulation of lateral bar stiffness.

In section 5.2, a thick-walled closure for a reactor pressure vessel is considered. It represents a structure where large triaxial compressive stresses as well as cracking are present. The influence of different failure criteria and post-failure behaviours is investigated.

Section 5.3 deals with the important cases of beams failing in shear. Beams both with and without shear reinforcement are considered, and of special interest are aggregate interlock, secondary cracks, influence of the magnitude of tensile strength and dowel action.

Finally, section 5.4 contains an analysis of a specific pull-out test, the so-called LoK-test. The influence of the uniaxial compressive strength, the ratio of tensile strength to compressive strength, different failure criteria and post-failure behaviours are investigated and special attention is given to the failure mode.

5.1. Panel

This first example of analysis of a concrete structure is an introductory one dealing primarily with different aspects of re-

inforcement bar modelling. The influence of the shear stiffness that might be attributed to reinforcement bars will receive particular attention. As discussed previously in section 4.3, relative displacements parallel to a crack plane result mainly in local bending of the bar as well as in local crushing of the concrete in the vicinity of the bar. However, these phenomena are not simulated in the program. Instead it is possible to consider some bar shear stiffness and the present section evaluates the use of such a shear stiffness. Obviously, use of the original shear modulus G of the bar material is expected to overestimate the bar stiffness parallel to the crack plane and therefore the modulus κG is applied where $0 \leq \kappa \leq 1$. The influence of different κ-values is investigated in the following.

For this purpose we consider a quadratic panel with uniform thickness as shown in fig. 1. It appears that reinforcement bars are located in two directions perpendicular to each other. This isotropic reinforcement consists of deformed Ø 8 bars (nominal area = 53.3 mm^2) with a distance of 100 mm. This corresponds to a reinforcement ratio = 0.666%. A uniform tensile loading corresponding to the force F is applied and the reinforcement forms the angle α to the loading direction. For $\alpha = 0$, 10^o, 20^o, 30^o and 40^o this arrangement was tested by Peter (1964), and of special interest are the vertical displacement δ_v and the horizontal displacement δ_u shown in fig. 1. To eliminate a possible influence from the boundaries of the panel, these displacements are referred to the measuring region shown. The horizontal displacement corresponds to a shear deformation that develops except when $\alpha = 0^o$.

The considered panels were termed S 2r 0, S 2r 10, S 2r 20, S 2r 30 and S 2r 40 with $\alpha = 0$, 10^o, 20^o, 30^o and 40^o, respectively. However, as no horizontal displacement values were available for S 2r 10 and S 2r 20, the experimental results for the panels S 2r 10, W and S 2r 20, W were employed instead. The only difference between these sets of panels is that the latter ones include some additional reinforcement along the boundary of the panel in the force direction. However, to facilitate comparison the analysis is based on the S 2r 10 and S 2r 20 panels. The

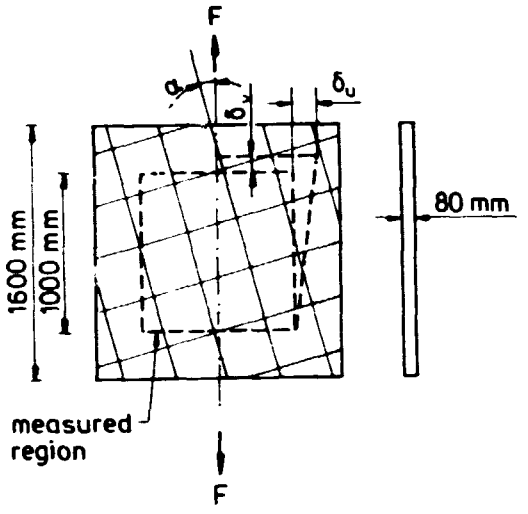

Fig. 5.1-1: Configuration of panel tested by Peter (1964)

finite element modelling uses two triangular plane stress elements only. The reinforcement is simulated by means of two bars in each direction. The thickness of these bars is determined so that the employed bar volume corresponds to the given one.

The same concrete mix and storing was applied for all panels. Even so, testing of concrete specimens indicated some scatter from panel to panel; however, to facilitate comparison the mean parameter values are applied in the analysis. Of the measured parameters only the uniaxial tensile strength σ_t = 1.74 MPa assumed to be equal to the measured Brazilian splitting strength and the initial Young's modulus $E_i = 2.45 \cdot 10^4$ MPa are of interest. Poisson's ratio was assumed to be ν_i = 0.2. The experimentally determined stress-strain curve for the reinforcement bars was simulated by a trilinear curve as shown in fig. 2. The full strength of the bars occurs when the strain is around 80 0/00; due to inhomogenities, etc., in the panels this stress value is not expected to be reached for all bars in one direction even at failure load. The approximation employed can be considered as a reasonable approach to reality.

For a fixed force F = 350 kN let us first consider the horizontal displacement δ_u and vertical displacement δ_v as functions of the angle α. This is shown in figs. 3 and 4 both for the ex-

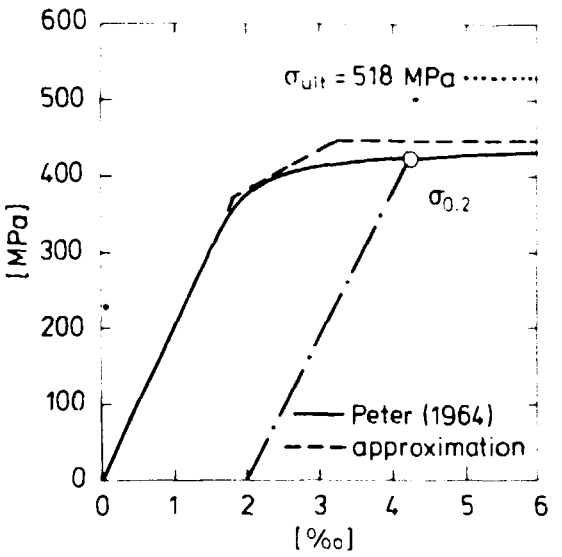

Fig. 5.1-2: Experimental and approximated stress-strain curve for bar material.

perimental values and for the predicted values using different κ-values. It should be recalled that for $\alpha = 10^{\circ}$ and 20° the experimental panels include vertical reinforcement not considered in the analysis. It is also important to note that the loading causes cracks so large that aggregate interlock can hardly be present, i.e., all forces along the crack planes must be attributed to the reinforcement bars. As an illustration, the largest horizontal displacement occurs experimentally for $\alpha = 30^{\circ}$. Experimentally the mean crack width was determined to be 0.44 mm and assuming that all horizontal displacements occurred along the crack planes the maximum mean horizontal displacement along a crack plane was determined to be 0.11 mm which is quite small compared to the crack width.

From the horizontal displacements shown in fig. 3 it appears that an optimal value of κ seems to be located in the range $\kappa = 0.10$-0.25. However, fig. 4 indicates that the predicted vertical displacements are strongly dependent also on the κ-value. This constitutes in fact a major objection against the method used here for considering the lateral stiffness of a reinforcement bar, as in reality the axial and lateral stiffnesses of a bar are quite independent. Obviously, the axial bar stiffness is the matter of major importance and even small κ-values between

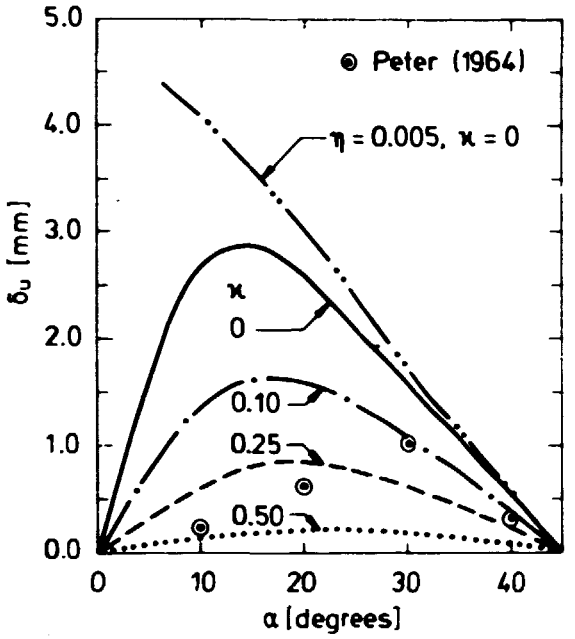

Fig. 5.1-3: Experimental and predicted horizontal displacement δ_u for fixed force = 350 kN.

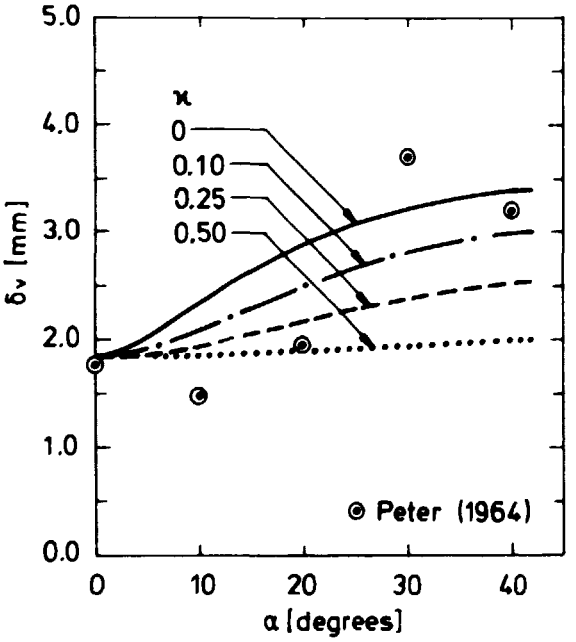

Fig. 5.2-4: Experimental and predicted vertical displacements δ_v for fixed force = 350 kN.

0.10 and 0.25 result in vertical displacements that are quite independent of the angle α. In addition, as plastic deformations of reinforcement bars are treaced here independently of the shear stresses, in principle when $\kappa > 0$ the panels have an infinitely

large failure capacity when $\alpha \neq 0$. A further disadvantage of using κ-values larger than zero is that the lateral bar stiffness then depends on the shear strain that may be a result not only of displacements normal to the bar direction, but also of displacements parallel to this direction. Based on the above and on findings in section 5.3, the value $\kappa = 0$, i.e., no lateral bar stiffness, will therefore be employed universally in the program except for certain sensitivity studies related to beams failing in shear, cf. section 5.3. It can therefore be concluded that consideration to lateral bar stiffness should be treated through its bending stiffness. However, within the practical limitations of the present program discussed in section 4.3 such an approach is not applicable here.

On the other hand, the value $\kappa = 0$ results in a considerable overestimate of the horizontal displacements as shown in fig. 3. However, this is presumed to be of minor importance as the panels are very special structures where only the bars contribute to the very small lateral stiffness. In most other structures such a situation will not arise as cracks usually do not cross a whole section and sufficient restraint along the crack plane is therefore easily established by the uncracked concrete.

As previously discussed in section 4.2.2 the shear retention factor η is assumed to be 1%. However, in fig. 3 the consequence of using the smaller value $\eta = 0.5\%$ is also indicated and it appears that very large overestimations then result for small α-values. In fact, as demonstrated earlier by Cervenka and Gerstle (1971), the value $\eta = 0$ gives rise to a discontinuity for $\alpha = 0$, as an infinitely small α-value results in infinitely large horizontal displacements. Apart from the previous arguments given in section 4.2.2 the aforementioned support the employed η-value equal to 1%.

For $\kappa = 0$ the predictions for vertical displacements are compared with experimental values in fig. 5 as a function of loading. As mentioned previously the panels with $\alpha = 10^{\circ}$ and 20° include vertical reinforcement not included in the analysis. Even so, the experimental values are remarkably smaller than the

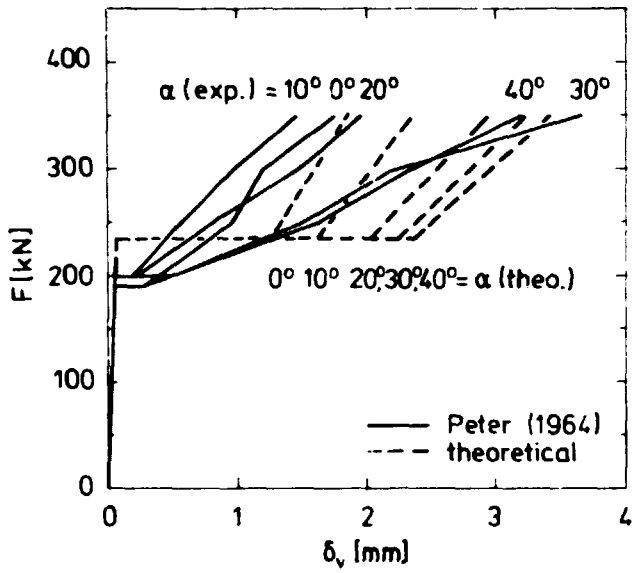

Fig. 5.1-5: Experimental and predicted (κ = 0) vertical displacements δ_v.

predicted ones just after cracking. This is a consequence of the so-called "tension stiffening effect" reflecting that in reality discrete cracks develop and that the concrete between these cracks is still bonded to the bar thereby contributing to the stiffness. In general, however, the experimental data support the prediction.

As discussed in section 4.6 the predicted failure loads are determined as the loads where the force-vertical displacement curve becomes horizontal. In the present case failure is determined solely by the bars where infinite ductility was assumed. However, as discussed in section 4.6 the analysis also includes a slight stiffness contribution from the concrete as 0.5% of the stiffness normal to the crack plane and present just before cracking is always retained for numerical reasons. This is to avoid a possible ill-conditioned equation system, but is in principle not necessary here as the cracks are crossed by bars. However, as the panels only posses a reinforcement percent equal to 0.67% this small retained concrete stiffness results in force-vertical displacement curves possessing a small slope even when all reinforcement is at full yield. It is important to note

that in all other structures where concrete in compression also contributes to the failure load a horizontal force-displacement curve at failure will be predicted as a result of the considered softening behaviour of the concrete in the post-failure region. The calculated failure loads of the panels are determined with the above-mentioned in mind and a comparison with experimental failure loads is given in the following table.

Table 5.1-1: Calculated and experimental failure loads.

α	0	10^{o}	20^{o}	30^{o}	40^{o}
$F_{exp.}$ [kN]	392	433	425	381	400
$F_{theo.}$ [kN]	394	386	384	384	384
$F_{theo.}/F_{exp.}$	1.01	0.89	0.90	1.01	0.96
Mean value of $F_{theo.}/F_{exp.}$ = 0.95					

It appears that the predicted failure loads are in very close agreement with the experimental ones in particular when recalling that panels with $\alpha = 10^{o}$ and 20^{o} include vertical reinforcement not considered in the analysis. On the average, the analysis underestimates the failure loads by 5%.

The present section has in particular dealt with different aspects when modelling reinforcement bars that are crossed by cracks. Modelling of the lateral bar stiffness has received special attention and it has been demonstrated that simulation of this stiffness through a suitable shear modulus of the bar material seems not to be a very advantageous method. This conclusion is further supported in section 5.3 where beams failing in shear are treated and it can therefore be concluded that lateral bar stiffness should be treated through its bending stiffness. Except for the purpose of sensitivity studies the value $\kappa = 0$ corresponding to no lateral bar stiffness will therefore be utilized in the program. Using this value, the analysis of different panels has demonstrated that the predic-

ted horizontal displacements grossly overestimate the experimental values. However, the agreement for vertical displacements is fair even though the tension stiffening effect is not considered and the predicted failure loads are in very close agreement with the experimental results.

5.2. Thick-walled closure

This section deals with the analysis of a model of a thick-walled closure for a reactor pressure vessel. The testing of this closure model termed LM-3 (Lid Model-3) is described in detail by the writer and Andersen in (1977a) and some selected results have been presented by them in (1975) and in (1977b). The considered closure is a structure where large triaxial compressive stresses as well as cracking are present. It represents therefore a unique opportunity to evaluate the applicability of the program. The influence on the predicted structural behaviour of different failure criteria and post-failure behaviour is investigated.

The geometry, loading and boundary conditions of the LM-3 closure are shown in fig. 1, where all quantities are in mm. It appears that the closure is loaded by a uniform pressure and that the forces through a heavy steel flange are supported by struts. These 40 struts are loaded uniformly in compression and the inclination to vertical is as an extremely good approximation fixed during loading. A steel liner assures tightness, and

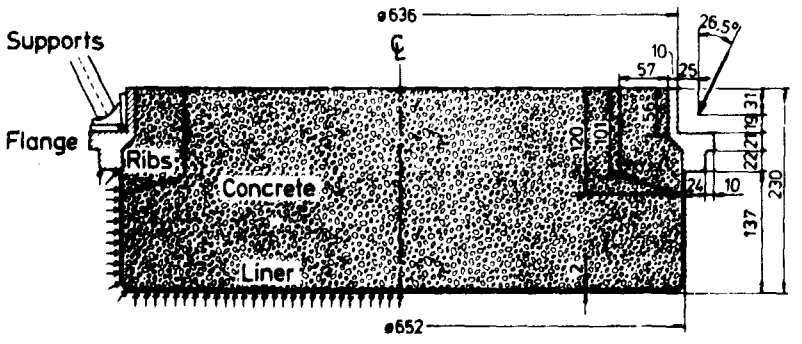

Fig. 5.2-1: Configuration and loading of the LM-3 closure.

40 mild steel ribs with a thickness of 6 mm and uniformly distributed along the periphery stiffen the flange. The ratio of height to diameter is 0.35 indicating a massive structure and even though the model scale is 1 : 11, it is apparent that the model has quite large dimensions (outermost diameter = 720 mm). During testing, the model was pressurized hydraulically by water in a steel pressure vessel. The test duration was around two hours.

The concrete had a w/c - weight ratio equal to 0.68 and the maximum gravel size was 8 mm. Seven standard cylinders (300/150 mm) were cast and cured together with the closure. These cylinders were tested uniaxially in compression simultaneously with the closure model testing that occurred 2 months after concreting. The mean of the experimentally determined stress-strain curve is shown in fig. 2a) together with the approximation employed according to eq. 2.2-3. This approximation utilizes the parameters: σ_c = 45.0 MPa, $\varepsilon_c = 3.06 \cdot 10^{-3}$, $E_i = 2.84 \cdot 10^4$ MPa and D = 0.2.

The concrete parameters necessary for the constitutive model were completely determined by assuming that σ_t/σ_c = 0.08 and ν_i = 0.15. The particular assumption of no-softening in the post-failure region is also shown in fig. 2 a).

The assumed stress-strain curve for the mild steel liner is given in fig. 2b). The ribs and flange were assumed to behave elastically. The values $E = 2.05 \cdot 10^5$ MPa and ν = 0.3 were employed for all steel parts.

Fig. 3 shows the axisymmetric finite element mesh consisting of 298 triangular elements. The liner is simulated as membrane reinforcement. The triangular solid elements that represent the flange appear from the figure. The strut forces are also indicated. The ribs are simulated by RZ-reinforcement bars in the horizontal and vertical direction. In each direction the volume of the bars corresponds to that of the ribs.

The experimentally determined behaviour of the closure is charac-

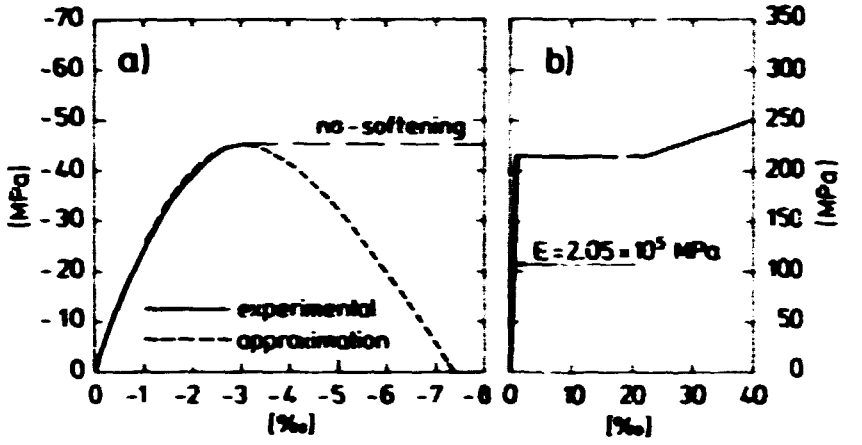

Fig. 5.2-2: Stress-strain curves for the concrete and the liner.

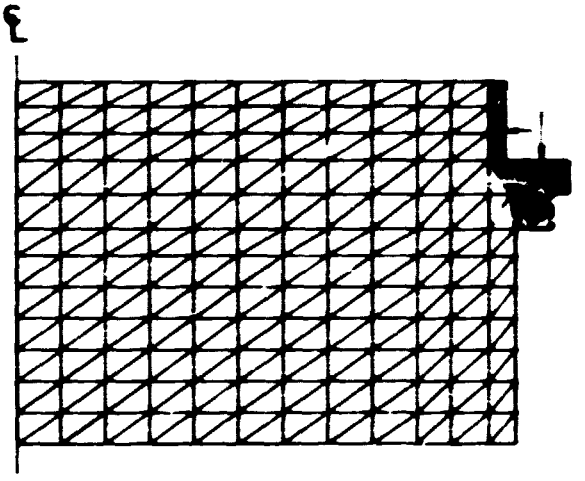

Fig. 5.2-3: Axisymmetric finite element mesh of LM-3.

terized by extensive radial cracking initiating at the centre at a pressure = 3 MPa and extending to the flange when the pressure is around 8.5 MPa. With increasing pressure these radial cracks open considerably and circumferential cracks located approximately half-way between the centre and the flange also are initiated. The maximum pressure obtained was 37.0 MPa where severe cracking was present. This is illustrated in fig. 4 showing the upper surface of the LM-1 closure at maximum pressure. This closure is almost similar to the LM-3 closure. The test terminated dramatically by ejection of the central part of the closure A section through the remaining part of the LM-3 closure is shown in fig. 5

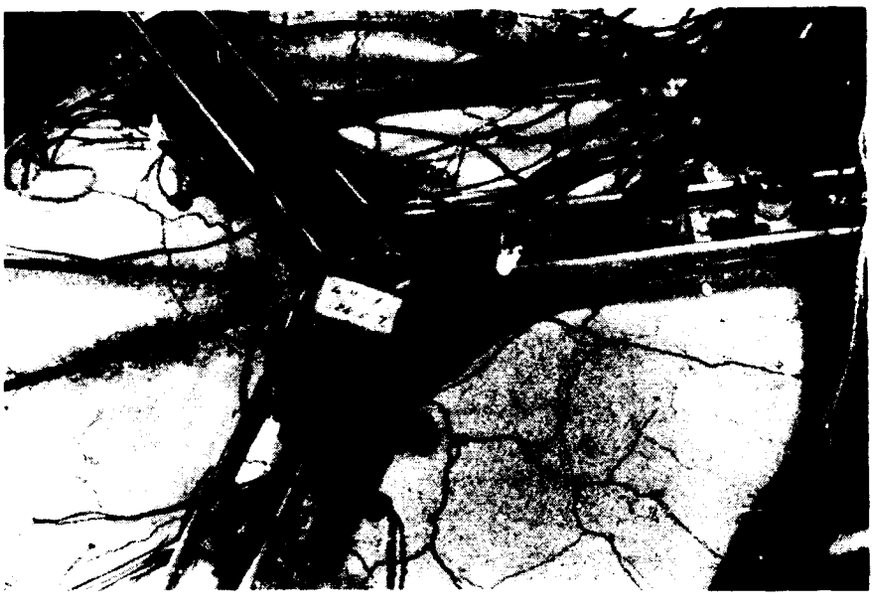

Fig. 5.2-4: Upper surface of the LM-1 closure at maximum pressure.

Fig. 5.2-5: Section through the remaining part of the LM-3 closure after ejection of the central part.

Let us now consider the predicted behaviour using the failure criterion of the writer (1977) and assuming softening of the

concrete in the post-failure region according to fig. 2a).

The predicted crack development is shown in fig. 6 for increasing pressure. Also given on the figure is the ratio of a given loading to the predicted failure load as well as regions where plastic strains exist in the liner. Obviously, when visualizing calculated circumferential cracking as discrete cracks some arbitrariness is necessarily involved. However, in the present report this arbitrariness is minimized by ensuring that for each cracked nodal point one discrete crack will in general be shown.

In accordance with experimental evidence, cracking initiates at the centre when the pressure p = 2.7 MPa and radial cracks develop quickly towards the flange, fig. 6a). At this small pres-

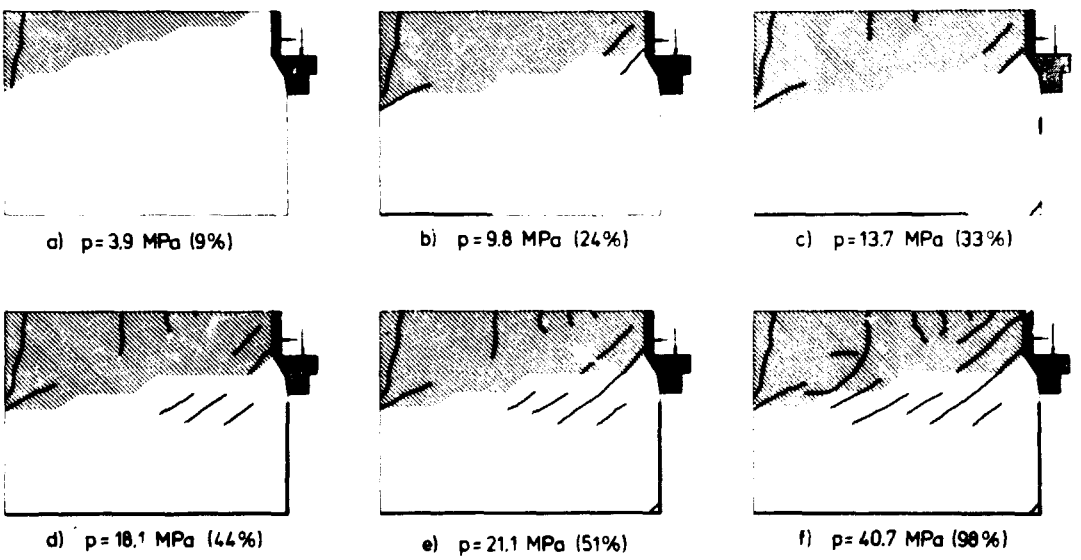

Fig. 5.2-6: Calculated crack development. Regions where plastic strains exist in the liner are also shown.

sure plastic strains in the concrete have already developed at the liner in the central part and at the liner below the flange. Circumferential cracks near the flange initiate at p = 6.9 MPa, cf. fig. 6b) and the radial cracks are already fully developed. Fig. 6b) also shows that the liner becomes plastically deformed in the central region at p = 9.8 MPa and at p = 12.6 MPa the liner yields below the flange, cf. fig. 6c). This latter figure indicates that circumferential cracks half-way between the centre and the flange develop at p = 13.7 MPa. At p = 18.1 MPa in-

clined cracks initiate in the closure, fig. 6d), and at p = 21.1 MPa these cracks join the circumferential cracks near the flange, cf. fig. 6e). The circumferential cracks develop gradually with increasing pressure and the crack pattern just before predicted failure is shown in fig. 6f). Observe that no secondary cracking is present.

To further investigate the structural mechanism of the closure the distribution of the three principal stresses is considered for the loading p = 25.5 MPa (61%) i.e. the cracking is slightly more developed than is indicated in fig. 6e). This stress distribution is shown in fig. 7, where isostress curves are indicated and where the directions of the principal stresses in the RZ-plane are shown in each nodal point. It is apparent that the closure behaves like a dome. Moreover, in accordance with previous remarks it appears that large triaxial compressive concrete stresses exist at the centre near the liner and near the liner below the flange. As an illustration, at failure the largest compressive concrete stress existing at the centre near the liner is 3.2 times the uniaxial compressive strength.

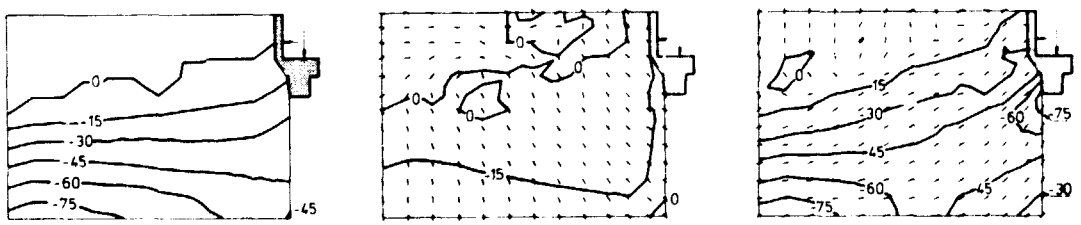

Fig. 5.2-7: Isostress curves of the three principal stresses for p = 25.5 MPa (61%). Quantities are in MPa.

To illustrate the severity of the loading the stress state can be evaluated using the nonlinearity index, cf. section 2.2.1. For this index we have that $0 \leq \beta < 1$, $\beta = 1$, and $\beta > 1$ correspond to stress states located inside, on, and outside the failure surface, respectively. Fig. 8 shows the development of contour lines for the nonlinearity index in per cent with increasing pressure. It appears that the severest loaded region is located

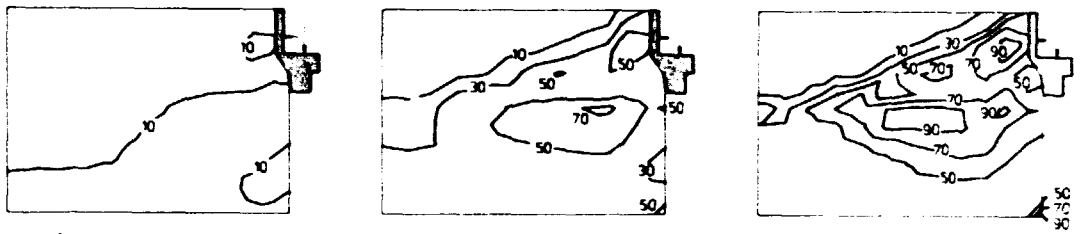

Fig. 5.2-8: Development of contour lines for the nonlinearity index in per cent.

below the ribs where inclined circumferential cracks are present, cf. fig. 6. As supported also by fig. 7 the stress state in this region is close to biaxial compression. The compressive crushing of this region and the far below failure stresses in the central part explain the observed failure mechanism with ejection of the central part of the closure, cf. also fig. 5. Strain softening of the concrete in this severest loaded region initiates when the pressure = 38.7 MPa corresponding to 93% of the predicted failure load.

Let us now consider the experimental and calculated centre deflection of the upper surface as a function of pressure, cf. fig. 9. It appears that with the failure criterion of the writer (1977) the calculations underestimate to some extent the deflections at high pressures. This might be explained as a result of the neglect of plastic strains in the flange. However, the agreement is fair and the predicted failure load is 41.7 MPa which is 13% above the experimental value. The consequence of using the modified Coulomb criterion appears also from the figure and the resulting failure load is 29.4 MPa which is 20% below the experimental value. This underestimate is in accordance with the general conclusions from section 2.1.3. The difference between the two predictions that amounts to about 30% corresponds to initiation of failure in a region where almost biaxial compression exists, cf. fig. 2.1-7.

The extreme assumption of no-softening in the post-failure region has a remarkable effect, cf. fig. 9, where the writer's

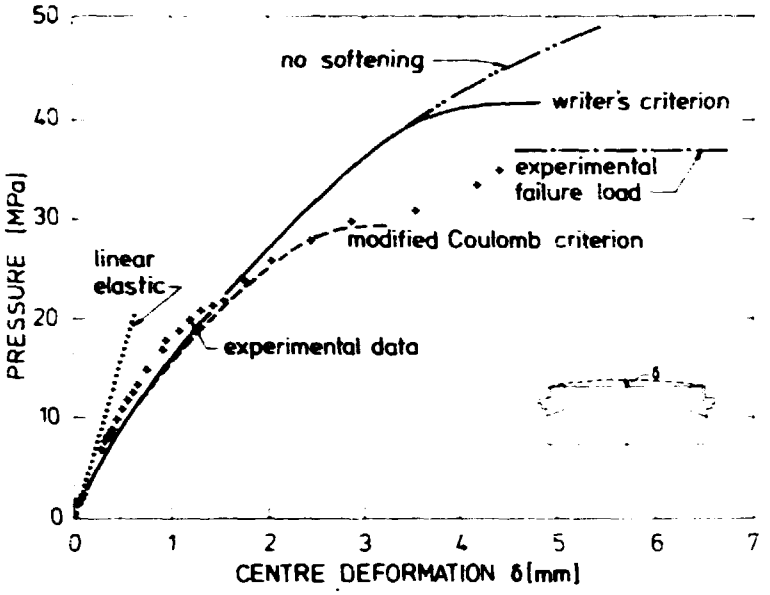

Fig. 5.2-9: Experimental and calculated centre deflections.

criterion (1977) is used again. In fact, the calculations were stopped at p = 49.1 MPa without impending failure and it emphasizes the importance of inclusion of a realistic post-failure behaviour in a constitutive model. This requirement is obviously more pertinent the more inhomogeneously the structure is loaded as stress redistribution then becomes essential. This effect is illustrated in fig. 10, where the contour lines for the nonlinearity index in per cent at p = 49.1 MPa are shown for the case of no-softening. A comparison with fig. 8c) demonstrates clearly the structural mechanism related to the assump-

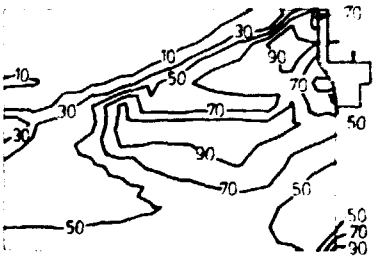

Fig. 5.2-10: Contour lines for the nonlinearity index in per cent. Pressure = 49.1 MPa. No-softening in the post-failure region is assumed.

tion of no-softening, where larger and larger regions contribute significantly to the load-carrying mechanism due to stress redistribution. The importance of realistic post-failure behaviours have been demonstrated earlier by Argyris et al. (1976) analyzing among other structures also the LM-3 closure considered here. In fact, the LM-3 closure has been analyzed extensively by Argyris et al. (1974) as well as by Schimmelpfennig (1975, 1976).

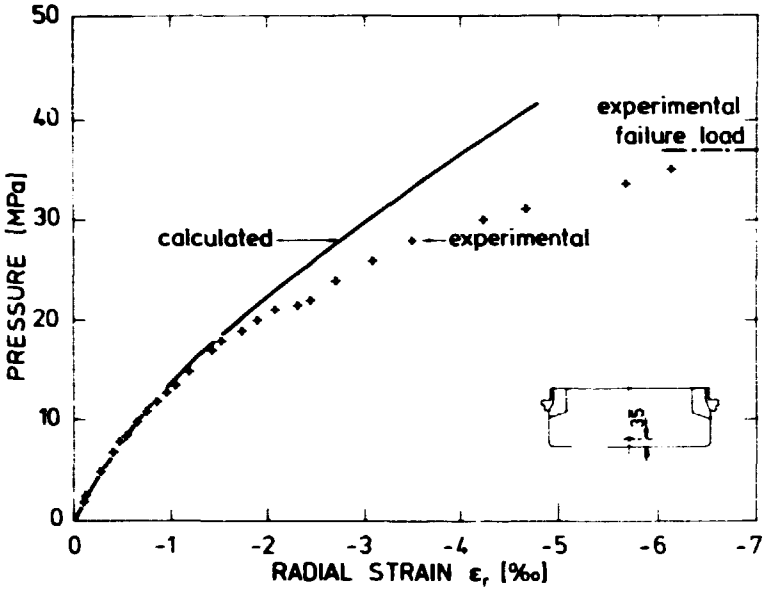

Fig. 5.2-11: Experimental and calculated radial strains at the centre.

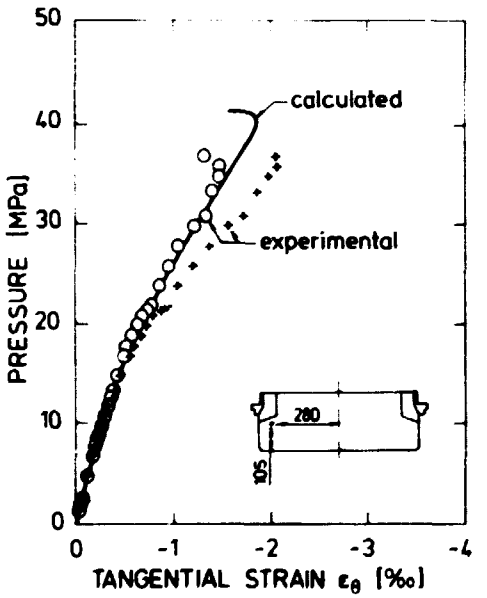

Fig. 5.2-12: Experimental and calculated circumferential strains below the ribs.

Returning to the calculation where the writer's criterion and softening are assumed, figs. 11 and 12 show a further comparison with experimental data. Fair agreement is obtained.

The present section has demonstrated the analysis of a complicated structure where both large triaxial compressive stresses and cracking as well as plastic deformations of the steel parts are involved. It has been shown that suitable analysis of the theoretical data may provide a clear insight in the physical behaviour of a structure. Moreover, the influence of using two different failure criteria has been investigated and the importance of a realistic post-failure behaviour in a constitutive model for concrete has been highlighted. As expected, the use of the writer's failure criterion (1977) and giving consideration to softening effects in the post-failure region result in the closest agreement with experimental data. Deformations and strains are predicted with fair accuracy and the failure load is overestimated by 13%.

5.3. Beams failing in shear

Beams failing in shear represent very delicate problems subject in the past to considerable experimental as well as computational efforts. Despite this, the structural behaviour of shear beams is only partly known and computations are generally of semi-empirical nature. In this section, the calculations will be compared with the classical test results of Bresler and Scordelis (1963); a beam without shear reinforcement as well as an identical beam, but now including shear reinforcement will be considered. The structural behaviour of the beams is illustrated and of special interest is aggregate interlock, secondary cracks, influence of the magnitude of tensile strength and dowel action.

Fig. 1, where all dimensions are in mm, shows the geometry and loading of the beams as well as their reinforcement arrangements. In the tests of Bresler and Scordelis (1963) the beams were labelled OA-2 and A-2 corresponding to no shear reinforcement and shear reinforcement, respectively. The longitudinal tensile reinforcement consists of five #9 bars (nominal area = 645 mm^2)

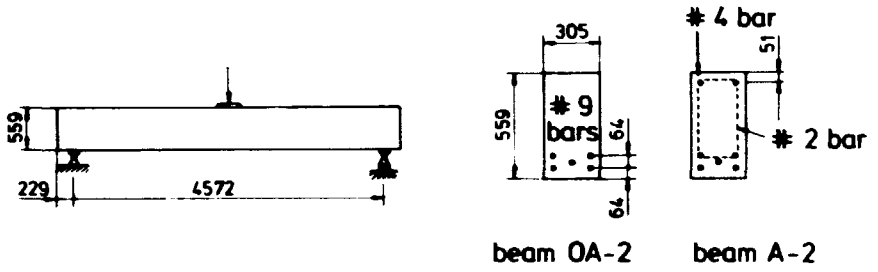

Fig. 5.3-1: Geometry, loading and reinforcement arrangements for the beam without shear reinforcement (OA-2) and the beam with shear reinforcement (A-2).

corresponding to a reinforcement percent = 2.27%, while the compressive steel consists of two #4 bars (nominal area = 126 mm^2) corresponding to a reinforcement percent = 0.18%. Also the stirrup reinforcement consisting of #2 bars (nominal area = 32 mm^2) corresponds to arrangements often found in practice and the same holds for the shear span ratio = 4.94. The trilinear approximations to the stress-strain curves of the bars are shown in fig. 2

Experimentally, it was observed that diagonal cracks developed and splitting occurred at failure in the compressive zone near

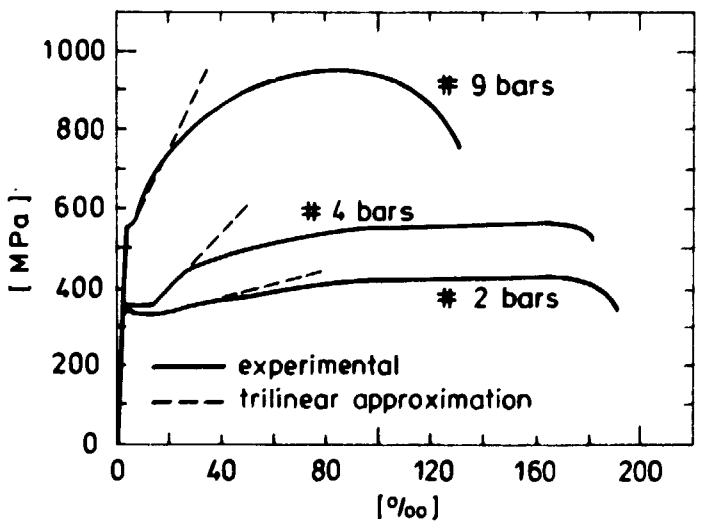

Fig. 5.3-2: Reinforcement stress-strain curves. Tensile, compressive and shear reinforcement consist of #9, #4, and #2 bars, respectively.

the load point for both beams. For the beam without shear reinforcement, horizontal splitting along the tension reinforcement was observed. The failure was characterized as diagonal tension failure for the OA-2 beam and shear-compression failure for the A-2 beam.

The uniaxial compressive strength σ_c and the modulus of rupture $\sigma_{mod.}$ were experimentally determined from concrete specimens cured in the same manner as the beams. The splitting strengths are estimated from these rupture values using the findings of Narrow and Ullberg (1963). The σ_t/σ_c-values given in table 1 are then obtained by approximating splitting strength and uniaxial tensile strength σ_t. The assumptions for the remaining parameters necessary for the constitutive model appear also from this table.

Table 5.3-1: Measured and assumed concrete parameters

	Measured		Assumed				
	σ_c [MPa]	$\sigma_{mod.}$ [MPa]	σ_t/σ_c	E_i [10^4MPa]	ν_i	ε_c [‰]	D
OA-2	23.7	4.3	0.10	3.1	0.2	2	0.1
A-2	24.3	3.7	0.08	3.1	0.2	2	0.1

The finite element mesh consists of 1008 triangular plane stress elements and is shown in fig. 3. Even though no systematic investigations were performed, this detailed element mesh is moti-

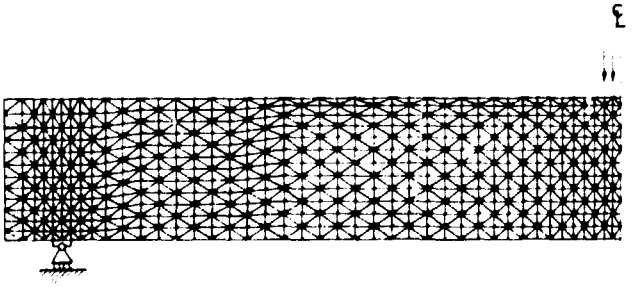

Fig. 5.3-3: Finite element mesh.

vated by two reasons. Firstly, it is well known that the constant strain element utilized requires a detailed mesh to describe bending. Secondly, the stress state in shear beams are two-dimensional with tensile and compressive stresses prevailing in the critical regions of the beams, and accurate description of these small tensile stresses is mandatory for an accurate analysis of the beam. The element mesh is especially detailed near the load point and also at the supports where large gradients exist. Except for the plane stress assumption, the actual locations of the bars are simulated in the finite element modelling.

In the following calculations, the failure criterion of the writer (1977) will be used and softening in the post-failure region as well as the influence of gravity will be considered. In the first place, the program will be used in its standard form, where the shear retention factor is $\eta = 1\%$ and no lateral stiffness of the bars is considered, i.e., $\kappa = 0$. Moreover, the OA-2 beam will be considered first.

To illustrate the stress distribution in the beam, the isostress curves for the principal stresses as well as their directions in the nodal points are shown in fig. 4. The loading is 51% of the predicted failure load. However, no essential difference in the stress distribution exists for other loadings. The arch-action of the beam is quite obvious from the figure and apart from the regions at the support and at the load point where biaxial compressive stresses exist, biaxial tensile-compressive stress states prevail.

The severity of the loading is illustrated in fig. 5 where the development of the contour lines for the nonlinearity index in per cent with increasing loading is shown. The loadings are again expressed in relation to the predicted failure load. It should be recalled that when tensile stresses are present the nonlinearity index is less than unity even when the stress state is located on the failure surface, cf. section 2.2.1. However, it is obvious from fig. 5 that the region adjacent to the load point is severely loaded and strain softening initiates in fact

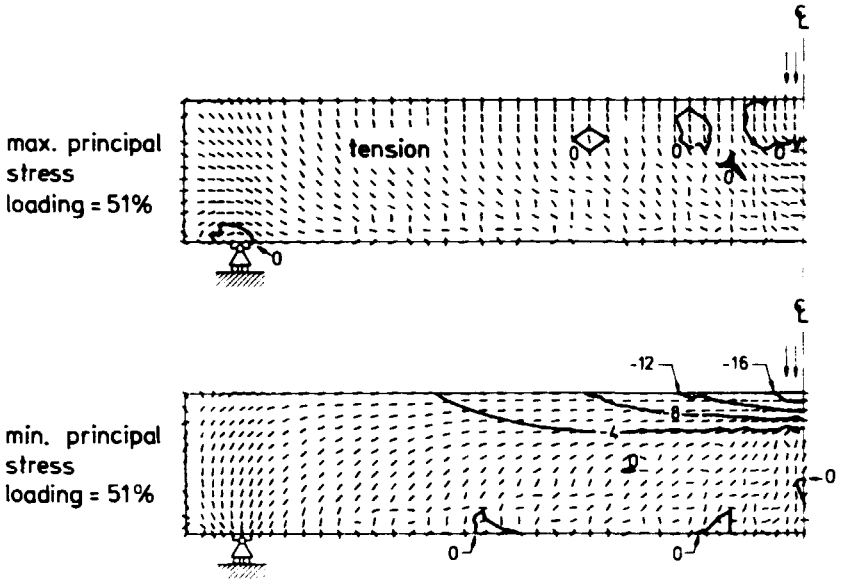

Fig. 5.3-4: Isostress curves and directions of the principal stresses in the OA-2 beam. Loading = 51% of predicted failure load. Quantities are in MPa.

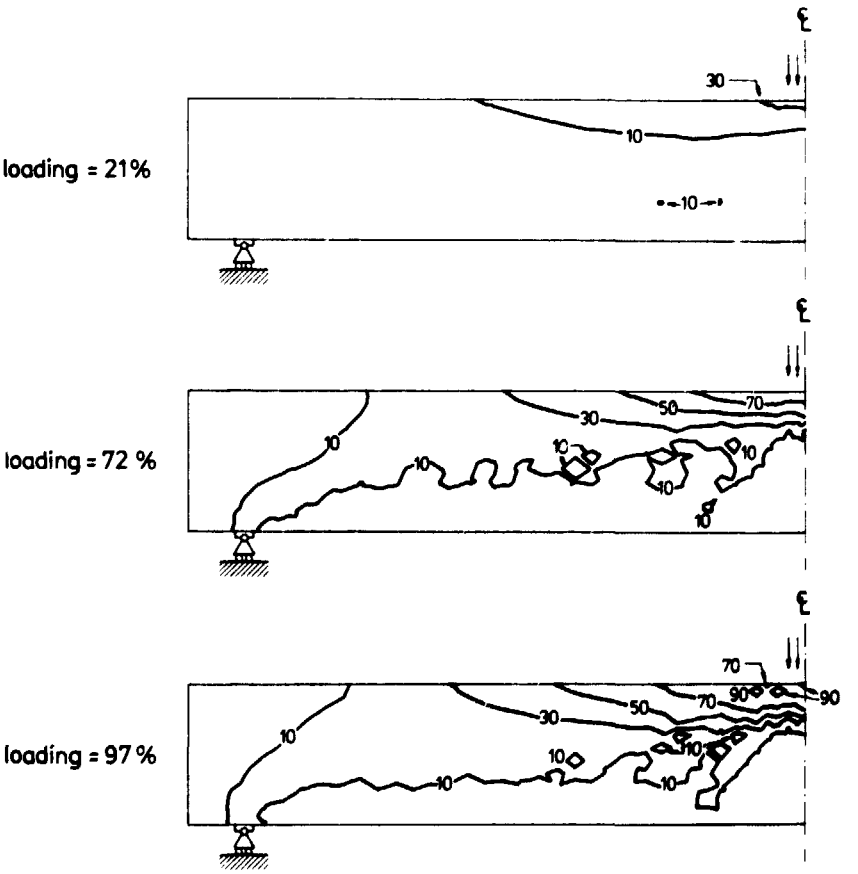

Fig. 5.3.-5: Development in the OA-2 beam of contour lines for the nonlinearity index in per cent. Loadings expressed as per cent of predicted failure load.

here at 82% loading. At the failure load, the region adjacent to the load point is stressed far into the post-failure region and this is considered to be the primary cause of the beam collapse. This underlines the importance of realistic constitutive modelling in the pre- as well as post-failure region for stress states where tensile stresses are present but no cracking occurs. Moreover, the arch-action of the beam is apparent from fig. 5. No plastic deformation of the reinforcement occurs even at failure.

The predicted crack development of the OA-2 beam with increasing loading is shown in fig. 6. Cracking initiates in the middle of the beam as flexural cracks already at 9% loading. Fig. 6a) shows these type of cracks. At increased loading the cracks develop towards the support and a slight inclination of the cracks becomes present, cf. fig. 6b). Secondary cracks where cracks with different inclinations exist at the same location are initiated at 63% loading. The crack pattern just before failure is shown in fig. 6c). The inclination of the cracks as well as the secondary cracks appear from this figure. Fig. 6d) shows the cracking at the failure load at the last iteration before the calculations were terminated. It is of interest to notice the clearly developed diagonal cracks running towards the load point. This is in accordance with the experimentally observed diagonal tension failure. However, it is important to recall that the concrete near the load point is stressed far into the post-failure region and that the primary failure takes place here. This causes a strain localization which in turn results in diagonal cracking. Therefore, the increase of the diagonal cracks is considered more as a consequence of this failure than as its cause.

Fig. 7 shows the experimentally observed cracking after failure of the OA-2 beam. Apart from the horizontal splitting along the reinforcement the predicted cracking is in good agreement with the observed cracking, cf. fig. 6d). However, it is important to note that this horizontal splitting occurs when the beam collapses. Obviously, at failure the concrete has lost its shear capacity and a considerable increase of the dowel forces can therefore be expected resulting in splitting along the rein-

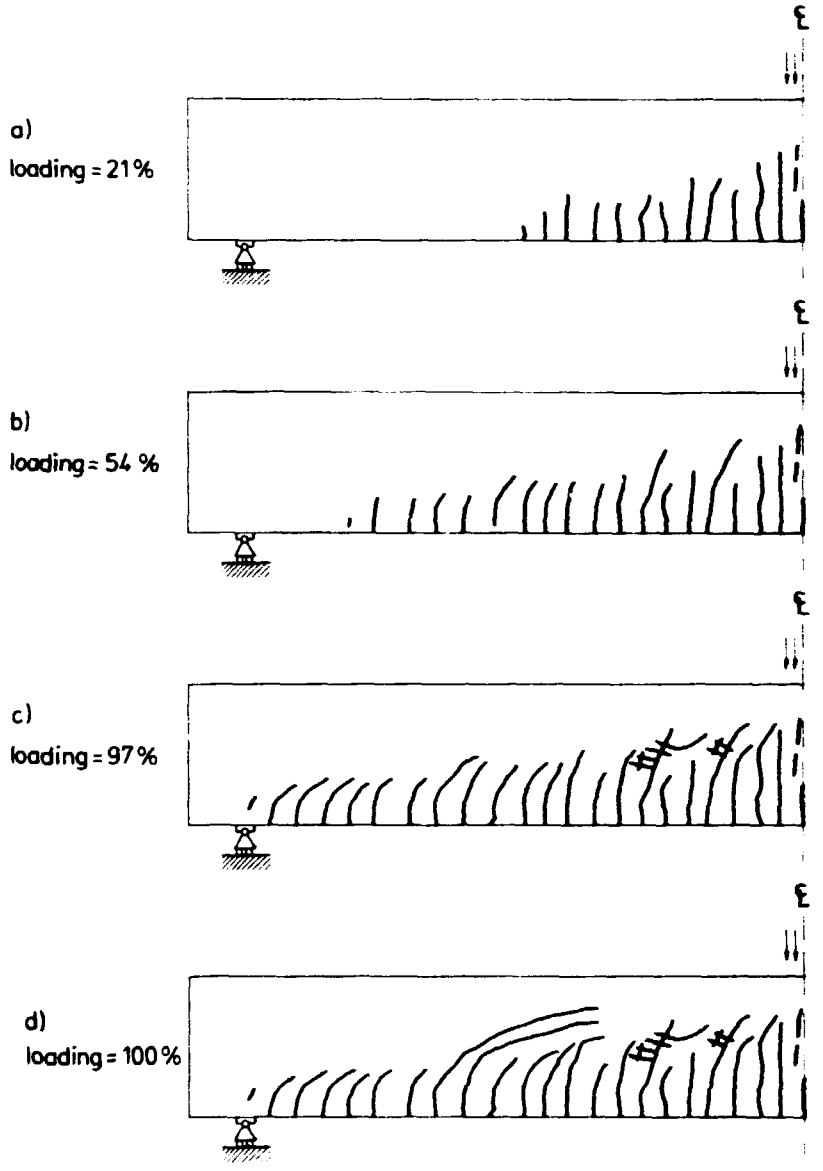

Fig. 5.3-6: Calculated crack development of the OA-2 beam.

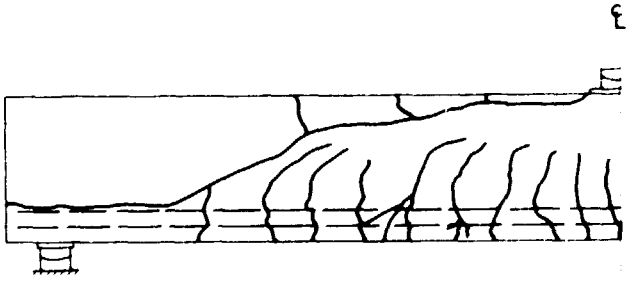

Fig. 5.3-7: Observed cracking after failure of the OA-2 beam.

forcement bars. Thus, splitting is a result of beam collapse and not its cause.

Let us now consider the A-2 beam where shear reinforcement is present and let us illustrate the behaviour of the beam with figures similar to figs. 4-7.

Fig. 8 shows the stress distribution at 63% loading. As previously noted, loadings are expressed in relation to the predicted failure load. Comparison with fig. 4 reveals that no principal difference seems to exist for beams with and without shear reinforcement.

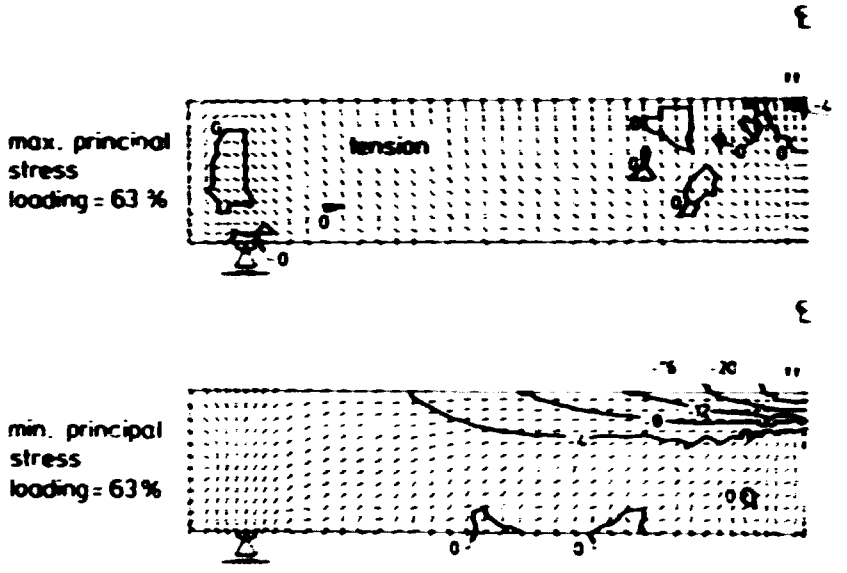

Fig. 5.3-8: Isostress curves and directions of the principal stresses in the A-2 beam. Loading = 63% of predicted failure load. Quantities are in MPa.

Fig. 9 shows the development of the contour lines for the non-linearity index in per cent with increasing loading. A comparison with fig. 5 again reveals no principal difference in the behaviour of the two beams. For the A-2 beam also the region adjacent to the load point is severely loaded; strain softening initiates here a little earlier than for the OA-2 beam namely at 63% loading, i.e. for the stress distribution shown in fig. 8 and on fig. 9. At the failure load, this region is loaded far into the post-failure region and just like the OA-2 beam this situation is considered to be the primary reason for the beam collapse.

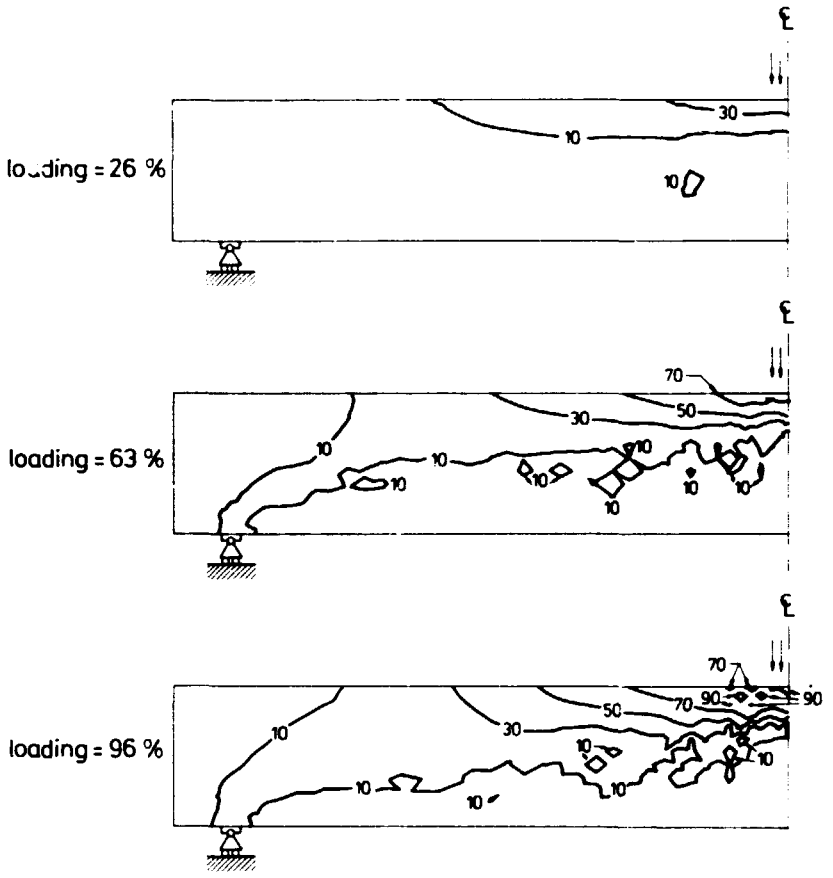

Fig. 5.3-9: Development in the A-2 beam of contour lines for the nonlinearity index in per cent. Loadings expressed as per cent of predicted failure load.

Let us now consider the predicted crack development of the A-2 beam. This is shown in fig. 10. The reinforcement is also shown on this figure by the dotted lines whereas regions where yielding occurs in the bars are indicated by full lines. Note that identical loadings in per cent for the OA-2 and the A-2 beams correspond to a 12% larger absolute load for the A-2 beam. With this in mind figs. 10a) and 10b) correspond quite closely to figs. 6a) and 6b), respectively. However, some changes in the behaviour exist. Secondary cracks initiate now at 51% loading compared to 63% loading for the OA-2 beam. Strain softening adjacent to the load point develops now at 63% loading compared to 82% loading for the OA-2 beam. Yielding of the stirrups follows the location of the inclined cracks. A quite pronounced development of inclined cracks occurs at 81% loading. The crack pattern just before failure, fig. 10c), indicates a somewhat further development of inclined cracks compared to fig. 6c). Yielding at the load point of the compressive steel initiates

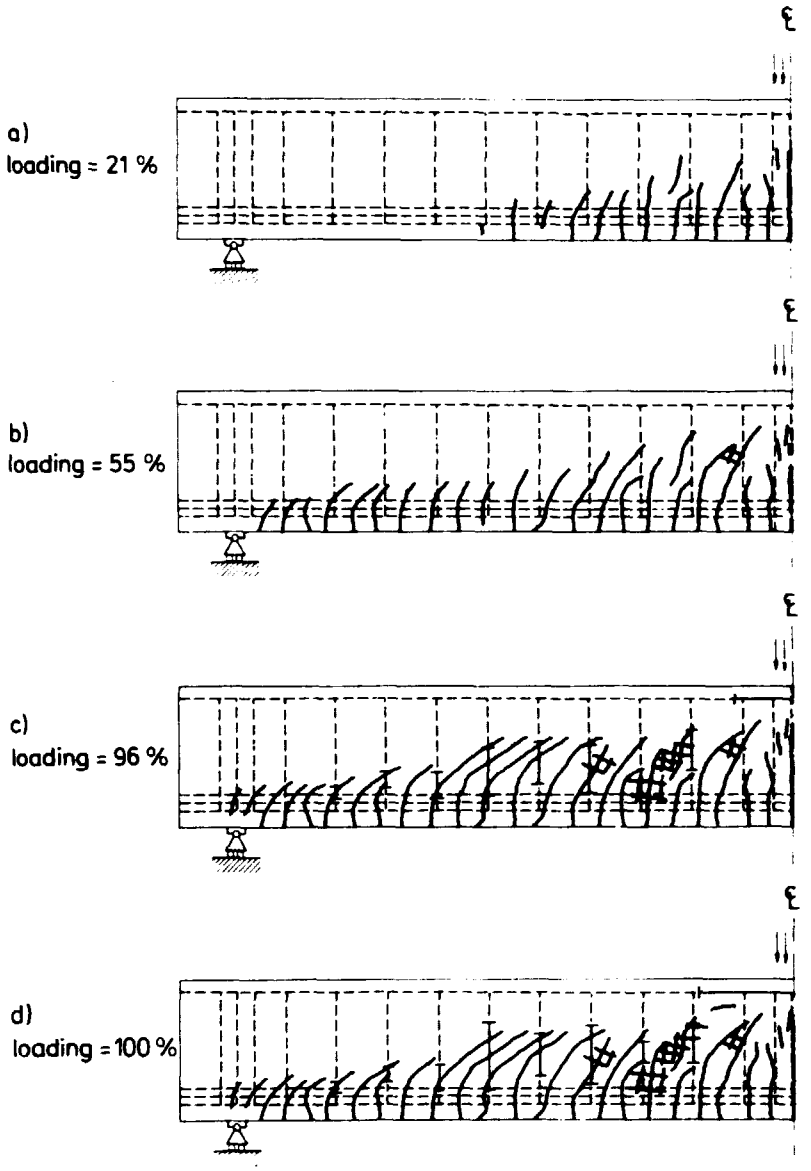

Fig. 5.3-10: Calculated crack development of the A-2 beam.

at 93% loading and appears from fig. 10c). Fig. 10d) shows the situation at the failure load at the last iteration before the calculations were terminated. No yielding occurs of the tensile reinforcement. Note the small, almost horizontal crack adjacent to the load point. However, apart from that, a comparison with fig. 6d) shows that formation of diagonal cracks is postponed. This is in accordance with the calculated failure mechanism that for both beams is caused by strain softening in the region adjacent to the load point where compressive and small tensile stresses exist. A strain localization then follows. For the OA-2 beam without stirrups this primary failure results in a development of diagonal cracks running towards the load point which in turn gives rise to the failure mechanism experimentally charac-

terized as diagonal tension failure. For the A-2 beam the existence of stirrups postpones the development of diagonal cracks in accordance with the experimental failure characterization as a shear-compression failure. Obviously, the stirrups also result in a more ductile failure mode. However, the calculations show that for both beams the primary failures are identical and that failure is caused by strain softening in the region adjacent to the load point.

Fig. 11 shows the experimentally observed cracking after failure of the A-2 beam. A comparison with fig. 10d) shows a close correspondence with the predicted crack pattern. Note in particular the small, almost horizontal crack adjacent to the point load in fig. 10d).

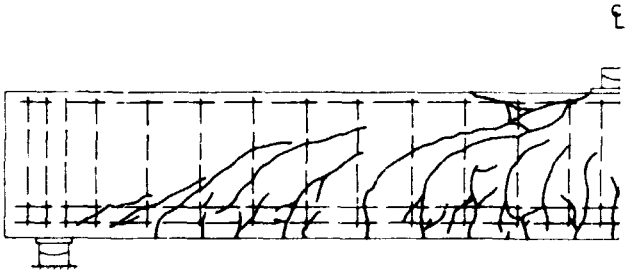

Fig. 5.3-11: Observed cracking after failure of the A-2 beam.

This crack and the neighbouring regions with secondary cracks are in accordance with the experimentally observed cracks running all through the beam. Note also that fig. 11 in contrast to fig. 7 reveals no horizontal splitting along the tensile reinforcement. This is a result of the stirrups preventing a considerable increase of the dowel forces at the failure moment.

Let us now consider deflections as well as failure loads of the two beams. Fig. 12 shows a comparison of the predicted midspan deflections with the observed ones. Experimentally, both the OA-2 beam and the A-2 beam were first loaded to about 30% of the failure load and then the load was removed. After that the load was reapplied until failure occurred and the deflections were recorded only in this final load cycle. In fig. 12 the predicted and observed deflections were therefore made to coincide at

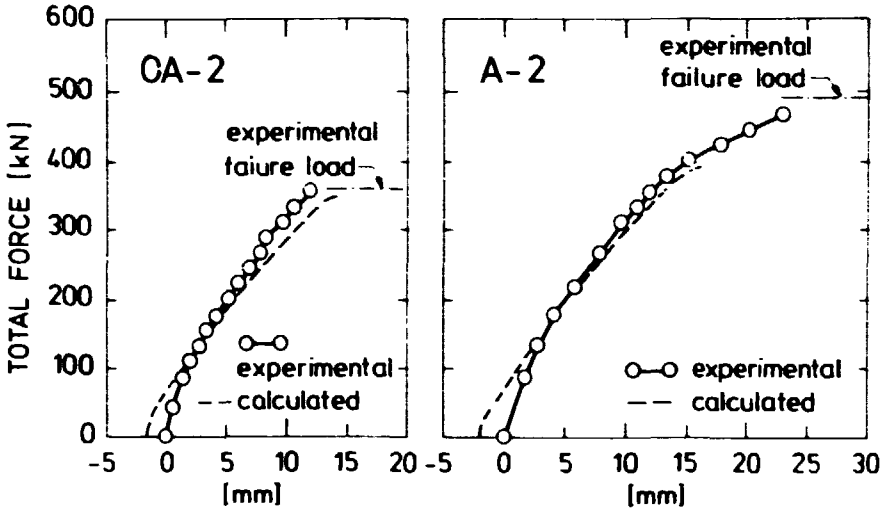

Fig. 5.3-12: Experimental and calculated midspan deflections of the OA-2 and the A-2 beam.

around 30% of the failure load. With this in mind the agreement is quite close except that the finite element models seem to be a little too soft. This may be a consequence of the neglected tension-stiffening effect as discussed in section 5.1. The predicted failure load for the OA-2 beam is only 2% below the actual one whereas the predicted failure load for the A-2 beam underestimates the actual one by 20%. Thus the behaviour of the beam without stirrups was predicted very closely. However, existence of stirrups resulted experimentally in a 38% increase of the failure load whereas the calculations estimate a 12% increase, only. We will return to this aspect later on.

A sequence of calculations was performed to investigate the influence of different parameters on the structural behaviour of the beams. The influence of aggregate interlock as expressed by the shear retention factor η, cf. section 4.2.2, dowel action as modelled by the factor κ, cf. section 4.3, the ratio of uniaxial tensile to compressive strength, σ_t/σ_c, as well as the influence of consideration to secondary cracks were investigated. The results are given in table 2. In this table the term $F_{theo.}/F_{exp.}$ gives the ratio of the theoretical failure load to the experimental one. The ratio σ_t/σ_c is in accordance with table 1 except for case no. 4. Recall that the standard version of the

program utilizes the values $\eta = 0.01$ and $\kappa = 0$ corresponding to case no. 1 and 6 considered until now.

Table 5.3-2: Sensitivity studies on the behaviour of the OA-2 and A-2 beams.

	Case No.	Shear retention factor η	Dowel action κ	σ_t/σ_c	Consideration to secondary cracks	$F_{theo.}/F_{exp.}$	Remarks
Beam OA-2	1	0.01	0	0.10	yes	0.98	standard version of program
	2	0.01	0.25	0.10	yes	1.04	
	3	0.10	0.25	0.10	yes	1.25	
	4	0.01	0.25	0.08	yes	1.01	
	5	0.01	0.25	0.10	no	1.16	failure impending but not occurred
Beam A-2	6	0.01	0	0.08	yes	0.80	standard version of program
	7	0.01	0.25	0.08	yes	0.83	

From table 2 appears that modelling of dowel action by use of a certain shear modulus of the bar material, κG, has only a minor effect on the predicted failure loads. Referring to section 5.1 the value $\kappa = 0.25$ constitutes an upper value, cf. for instance figs. 5.1-3 and 5.1-4. Even so comparison of case no. 2 with no. 1 and case no. 7 with no. 6 reveals that the dowel action dealt with here increases the failure loads only around 5%. Together with the findings in section 5.1 this supports the use of the standard value $\kappa = 0$ in the program. We will return to this subject later on.

The influence of aggregate interlock modelled through the shear retention factor η is investigated by case no. 2 and 3 where the only difference is an increase of η from 0.01 to 0.10. This results in a 20% increase of the failure load. The discussion in section 4.2.2 suggests that the influence of different η-values is largest in structures such as in those considered where shear is dominant. On this background the observed influence is viewed as moderate and supports the acceptance of the use of a fixed η-value. However, the observed influence of the η-factor is in

evident contrast to the finding of Cedolin and Dei Poli (1977) who also investigated beams failing in shear. As here they analysed beams tested by Bresler and Scordelis (1963), but their beams had a shear span ratio = 4 whereas the beams considered here have a shear span ratio = 5. In their important investigation, Cedolin and Dei Poli (1977) found an extreme influence of the η-value as η = 0.25 resulted in a failure load twice as large as that determined when η = 0.025 was utilized. However, the failure loads as determined by Cedolin and Dei Poli (1977) were not clearly related to physical phenomena and large differences between their approach and the present one exist. In particular, the strain softening in the post-failure region was not considered; dilatation and secondary cracking of the concrete was ignored. As here Cedolin and Dei Poli (1977) used constant strain elements, but no diagonal cracking was determined at failure. Cedolin and Dei Poli (1977) suggest this to be a consequence of the smeared crack representation. If true this finding has important consequences, but the present study gives no support to it as diagonal cracking indeed is determined. As previously discussed, diagonal cracking follows as a result of a strain localization in the region adjacent to the load point and this strain localization is a consequence of strain softening. Therefore, modelling of strain softening is considered as decisive.

The behaviour of beams failing in shear is obviously very dependent on the existence of small tensile stresses. However, as demonstrated by case no. 2 and 4 the choice of different realistic tensile strength values has only a minor influence for a 20% decrease of the σ_t-value results in a decrease in failure load of only 3%.

To investigate the importance of modelling of secondary cracks, case no. 5 is compared with case no. 2. In case no. 5 the calculations were terminated before failure was reached. It appears that modelling of secondary cracks is in fact essential. This conclusion is in accordance with the findings of Arnesen et al. (1979) who also analysed beams failing in shear. Considering plane stress states Arnesen et al. (1979) also demonstrated that

no stiffness of the concrete in question should be retained when secondary cracking has occured. This assumption is also utilized here, cf. section 4.2.2.

The sensitivity study of the parameters has focussed on their influence on the failure load. However, some other aspects of beam behaviour are also affected. For instance, use of the value $\kappa = 0.25$ instead of $\kappa = 0$ results in increased secondary cracking along the main reinforcement and it decreases the midspan deflection around 8%. Use of the value $\eta = 0.10$ instead of $\eta = 0.01$ also decreases the midspan deflection around 8%.

The previous analysis using the program in its standard form has demonstrated a close agreement with experimental data. However, one significant disagreement exists. This is shown in fig. 13, where the relative vertical displacements across the beams are depicted. The experimental values indicate that in contrast to the OA-2 beam a considerable thickening occurs for the A-2 beam with stirrups. This phenomenon is not reflected in the calculated values which grossly overestimate the thickening of the beams. This picture is influenced only insignificantly when using the different assumptions given in table 2. One exception is case no. 3 where the shear retention factor is increased, decreasing the thickening values by a factor of approximately 2. Even so, a considerable overestimation results. It is of importance to note that even giving consideration to dowel action through the shear deformation of the reinforcement, cf. case no. 1 with no. 2 and case no. 6 with no. 7, has no significant influence on the results. However, as the reason for the much smaller experimental values in fact is believed to be dowel action of the reinforcement, this is to say that consideration to dowel action must be treated through the bending of the bars and not through their shear deformation. This important conclusion supports the use of the value $\kappa = 0$ in the standard version of the program. However, another important consequence may also be derived from fig. 13. The figure shows that the predicted strains in the stirrups are far too large. Therefore, the predicted influence of stirrups is underestimated and this explains why the existence of stirrups resulted experimentally

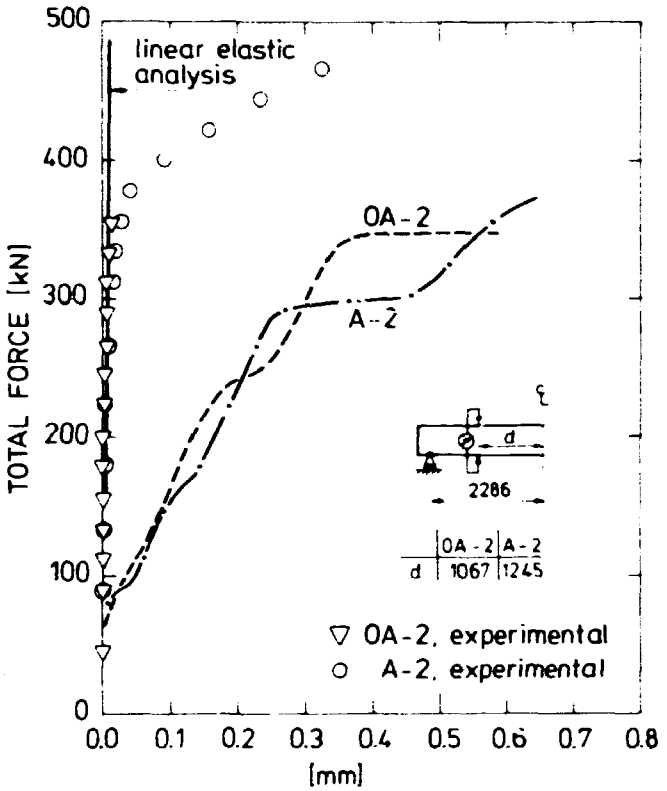

Fig. 5.3-13: Thickening across the beams

in a 38% increase of the failure load whereas the calculations estimate a 12% increase, only. This same trend is also observed in the calculations of Cedolin and Dei Poli (1977) who also did not consider dowel action caused by bending of the reinforcement.

The present section has been devoted to different aspects of the behaviour of beams failing in shear. With the standard version of the program using the writer's failure criterion (1977) and considering strain softening in the post-failure region a close agreement with experimental data has been demonstrated. The predicted failure loads for the OA-2 beam without stirrups and the A-2 beam with stirrups were underestimated by 2% and 20%, respectively. Also the predicted crack patterns including diagonal cracking of the OA-2 beam are in accordance with experimental evidence. Morecver, the analysis has resulted in a clear insight in the structural behaviour of the beams. It has been shown that for both beams the primary cause of failure is strain softening in the region adjacent to the load point. This strain softening causes a strain localization which in turn re-

sults in a tendency to diagonal cracking. For the OA-2 beam without stirrups nothing prevents this tendency and diagonal results in a tendency to diagonal cracking. For the OA-2 beam without stirrups nothing prevents this tendency and diagonal tension failure follows. For the A-2 beam, on the other hand, the stirrups resist the tendency to diagonal cracking and a shear-compression failure results. Obviously, the failure itself is therefore more ductile, but apart from this there is no principal difference in the behaviour of the OA-2 and the A-2 beam. It follows that modelling of strain softening in the post-failure region is decisive in the analysis.

The influence of the shear retention factor has been evaluated and opposed to the finding of Cedolin and Dei Poli (1977), the influence was found to be relatively moderate. Variation of the uniaxial tensile strength within realistic limits influences the results insignificantly. However, in accordance with Arnesen et al. (1979), modelling of secondary cracking was found to be essential. It has also been shown that consideration to dowel action must be treated through the bending of the bars and not through their shear deformation. This conclusion may explain the only observed disagreement with experimental evidence, namely, the overestimation of the thickening of the beam. It also explains why the analysis underestimates the effect of the stirrups.

5.4. Pull-out test (Lok-Test)

A considerable interest is directed towards determination of the in-situ concrete properties and various destructive as well as non-destructive methods are currently applied. Knowledge of the in-situ concrete compressive strength is of particular importance and pull-out tests have been proposed for this purpose. For the pull-out test considered here, the so-called Lok-Test proposed by Kierkegaard-Hansen (1975), a circular steel disc is extracted from the structure using a cylindrical counter-pressure. Experimental data have shown a linear relation between the force required to extract the embedded steel disc and the uniaxial com-

pressive strength.

The present section is devoted to analysis of such Lok-Tests. The influence of the uniaxial compressive strength, the ratio of tensile-to-compressive strength, different failure criteria and post-failure behaviours are investigated. Moreover, as much dispute has been placed on the type of failure actually occurring in the concrete, special attention is given to the structural behaviour and to the failure mode.

As mentioned above, the Lok-Test was proposed by Kierkegaard-Hansen (1975) and several experimental investigations have been carried out. A general status has been given recently by Kierkegaard-Hansen and Bickley (1978). During application, a test bolt, consisting of a stem and a circular steel disc, is mounted inside the form, fig. 1 a). After curing of the concrete, the form is stripped and the stem is unscrewed. At the time of testing, a rod having a slightly smaller diameter than the stem is screwed into the disc and a cylindrical counter-pressure is mounted, fig. 1 b). The rod is loaded by a pull-out force until a small piece of concrete is punched out. As shown in figs. 1 b) and 2, this piece of concrete has the form of a frustrum of a cone. The meridians are almost straight lines that connect the outer periphery of the disc with the inner periphery of the cylindrical counter-pressure.

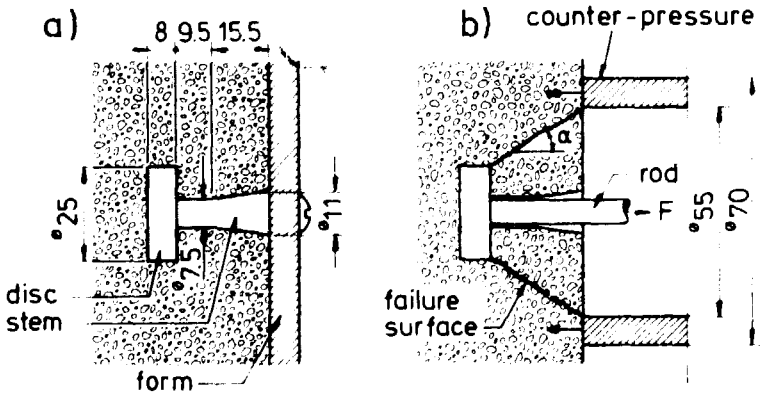

Fig. 5.4-1: Application and configuration of the Lok-Test. All dimensions are in mm.

Fig. 5.4-2: Punched-out piece of concrete. Cracks are made visible using pencil tracting.

Fig. 3 shows the analysed structure as well as the axisymmetric finite element mesh consisting of 441 triangular elements. The elements that represent the steel disc appear from this figure. The pull-out force as well as the boundary conditions at the location of the cylindrical counter-pressure are also indicated.

In the following, we will use the finite element program in its standard form. Strain softening in the post-failure region will be considered and in the first place the failure criterion of the writer (1977) is utilized. To begin with, some important aspects of the structural behaviour of the Lok-Test will be illustrated. After that, the influence of some concrete material data and of different failure criteria will be investigated in detail.

To illustrate the structural behaviour we use concrete material data that can be considered as quite representative and realistic. For this purpose we approximate the behaviour of a specific concrete tested by Kupfer (1973). The constitutive model of this relatively strong concrete is calibrated by the following parameters all in accordance with experimental data: $E_i = 3.24 \cdot 10^4$ MPa, $\nu_i = 0.2$, $\sigma_c = 31.8$ MPa, $\sigma_t/\sigma_c = 0.10$, $\varepsilon_c = 2.17\%$ and $D = 0.2$. Using these data the normalized stress-strain curve is

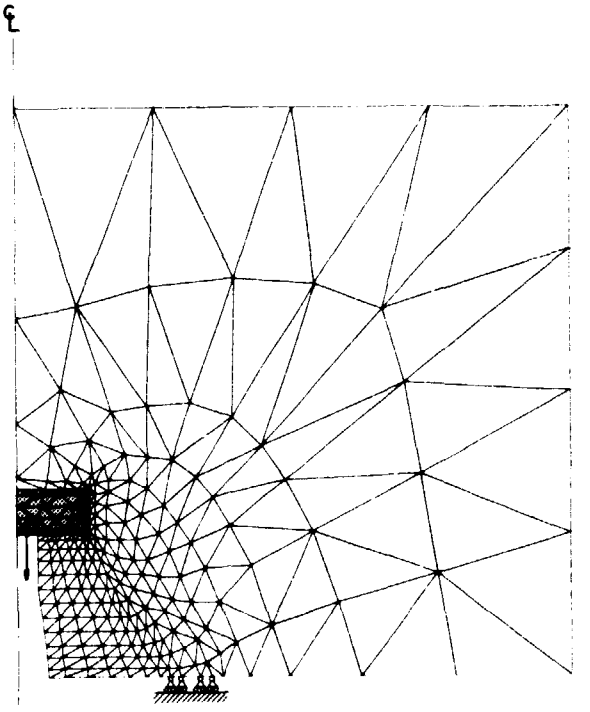

Fig. 5.4-3: Axisymmetric finite element mesh of the Lok-Test.

shown in fig. 4. The values $E = 2.05 \cdot 10^5$ MPa and $\nu = 0.3$ were employed for the steel disc.

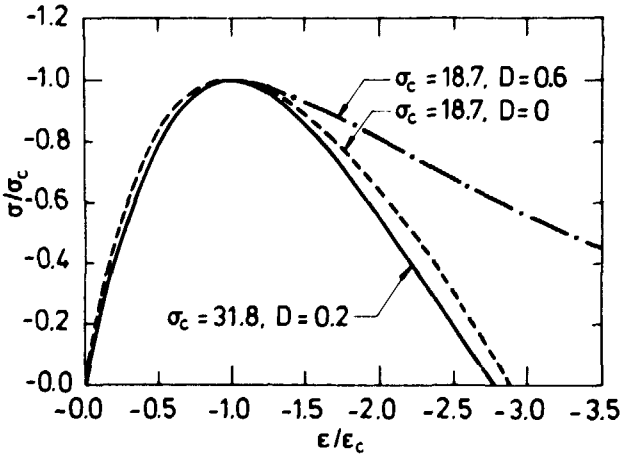

Fig. 5.4-4: Normalized stress-strain curves for the concretes considered here. Strengths are measured in MPa.

Let us now consider the predicted crack development as the loading increases. This is shown in fig. 5, where the loadings are expressed in relation to the predicted failure load. Cracking initiates as circumferential cracks behind the disc at 7% loading. This type of cracking appears from fig. 5 a) and is caused directly by the pull-out force. At 18% loading, radial cracking initiates at the annulus near the outer concrete surface. These cracks are caused by flexure similarly to bending of plates. Such radial cracks appear from fig. 5 b), where the loading is 25% of the predicted failure load. With increased loading the cracks shown in fig. 5 b) develop gradually. However, at 64% loading a considerable development of new circumferential cracks occur. As shown in fig. 5 c), these new circumferential cracks extend from the outer part of the steel disc towards the support. It is of interest to note that even though the concrete is severely cracked, its carrying capacity is far from being exhausted. Therefore, it is obvious that only very little of the pull-out force is carried directly by tension in the concrete. Increased loading in particular causes the radial cracks to develop; the crack pattern just before predicted failure is shown in fig. 5 d).

While the predicted circumferential cracks are supported by experimental evidence, cf. fig. 2, radial cracks have not been observed experimentally prior to the present study. However, whereas the region theoretically exposed to radial cracking is quite large, the corresponding crack widths are estimated to be quite small. If it is conservatively assumed that all tangential deformation is concentrated in only one radial crack, then, just before failure, this crack width is around 0.05 mm that is hardly visible. Moreover, the stresses are unloaded and crack widths reduced after failure thereby supporting the conclusion that no radial cracks are directly visible on the punched-out piece of concrete. However, close inspection of such concrete specimens using a microscope reveals that clear radial cracking is indeed present. Such cracking is visualized on the specimen in fig. 2 using pencil tracing.

To further illustrate the structural behaviour of the Lok-Test,

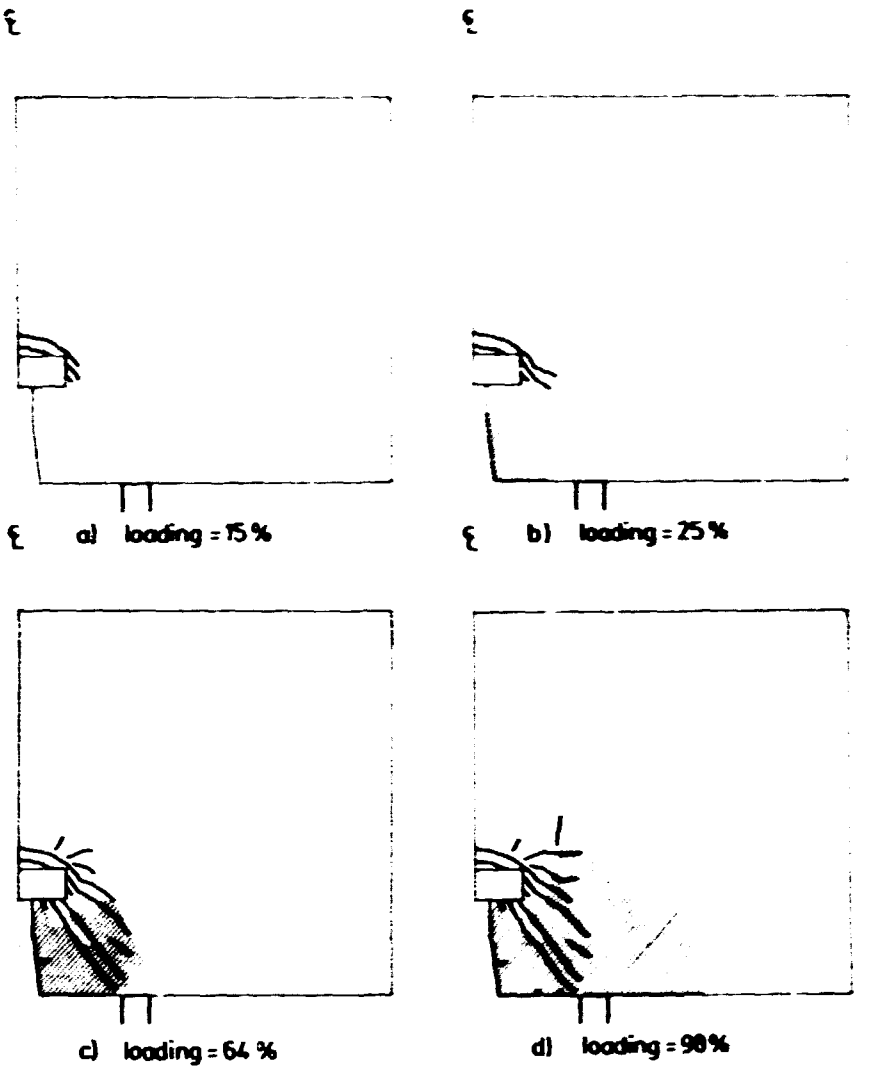

Fig. 5.4-5: Crack development with increasing loading. The loading is expressed in relation to the predicted failure load.

the stress distribution of the three principal stresses is considered at 70% loading, i.e., the cracking is slightly more developed than indicated in fig. 5 c). This stress distribution is shown in fig. 6, where isostress curves are shown and where the directions of the principal stresses in the RZ-plane are given in each nodal point. In accordance with the radial crack development the distribution of the tangential stresses shows large regions where tension exists. Only at the support and notably around the disc do compressive tangential stresses exist. The distribution of the max. principal stress in the RZ-plane indicates also large regions loaded in tension. Only in the vicinity of the disc and notably at the support do small re-

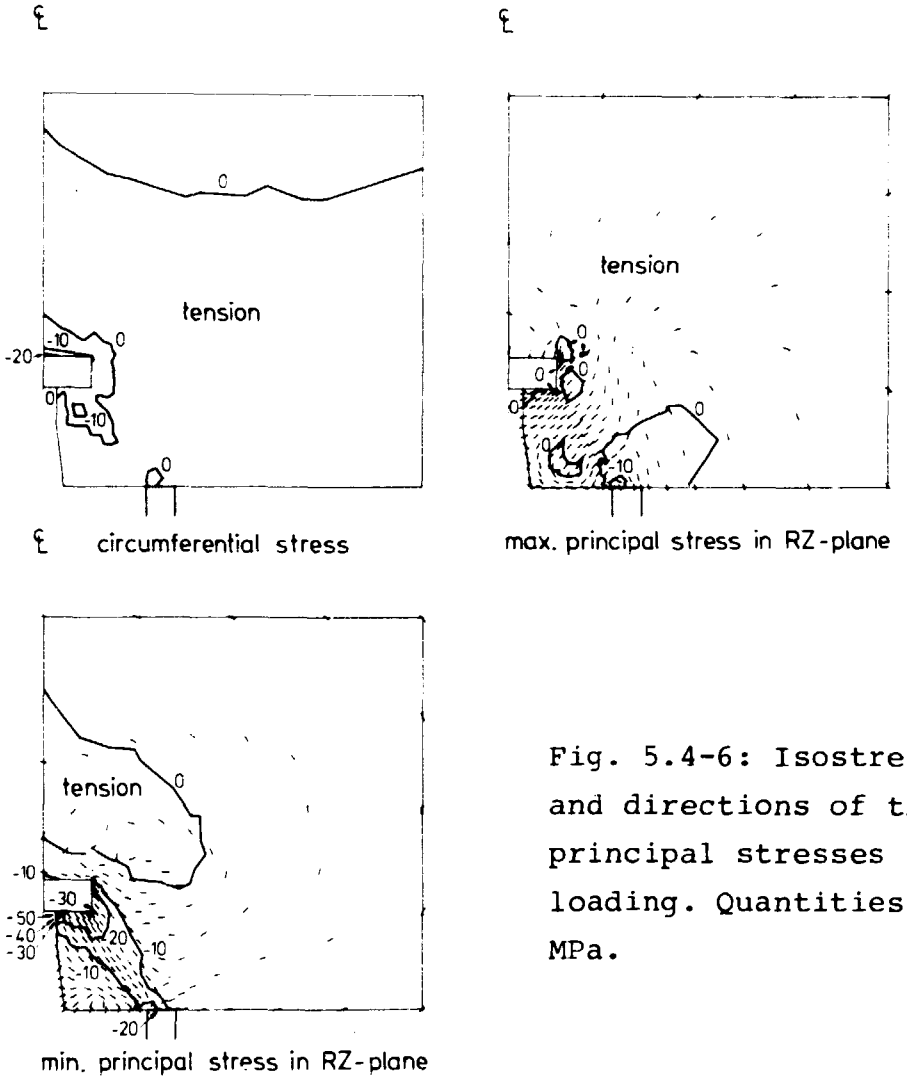

Fig. 5.4-6: Isostress curves and directions of the three principal stresses at 70% loading. Quantities are in MPa.

gions loaded in compression exist. The distribution of the min. principal stress in the RZ-plane is very interesting. Recalling that the uniaxial compressive strength of the concrete is 31.8 MPa and noting that the loading is 70% of the predicted failure load, it appears that large stresses are present at the annulus near the disc. In fact triaxial compression exists here. Moreover, large compressive stresses are found at the outer periphery of the steel disc and comparison with the preceding figures shows that biaxial compression occasionally superposed by a small tensile stress appears in this region. Noting the stress directions it is apparent that large forces run from the disc in a rather narrow band towards the support, where triaxial as well as biaxial compression exist. This carrying mechanism is sup-

ported by the crack pattern, cf. figs. 5 c) and d). It is of interest to note that both the circumferential cracks and the stress directions describe curves that have a slight curvature even though they are almost straight. This small curvature is also observed in practice, cf. fig. 2.

In conclusion, fig. 6 shows that the stress distribution is very inhomogeneous. This suggests strain softening to be of importance. However, large compressive forces run from the disc in a rather narrow band towards the support and this constitutes the load-carrying mechanism. The stress states in this band are primarily biaxial compression occasionally superposed by small tensile stresses.

As in previous sections, the severity of the stress states is conveniently illustrated by means of the nonlinearity index. Fig. 7 shows the development of the contour lines with increasing loading for the nonlinearity index in per cent. The distribution in fig. 7 b) corresponds to the stress distribution given in fig. 6. Fig. 7 supports the preceding observations that the region at the annulus adjacent to the disc is severely loaded and this holds also for the region along the outer periphery of the disc. Moreover, the severely loaded narrow band running from the outer periphery of the disc towards the support is also apparent. It should be recalled that when tensile stresses are present, the nonlinearity index is less than unity even at failure. At 64% loading, strain softening initiates below the steel disc both adjacent to the annulus and at the outer periphery of the disc. At 79% loading, strain softening develops from the outer periphery of the disc towards the support. This development is pronounced at 88% and also at 100% loading; the latter corresponds to the last iteration before the calculations were terminated. At 100% loading, considerable strain softening occurs also at the disc adjacent to the annulus. This can be observed as a decrease in the nonlinearity index, cf. fig. 7c) with 7d). More important, however, is the strain softening occurring in the narrow region adjacent to the outer periphery of the disc and running towards the support. This strain softening appears as a considerable drop of

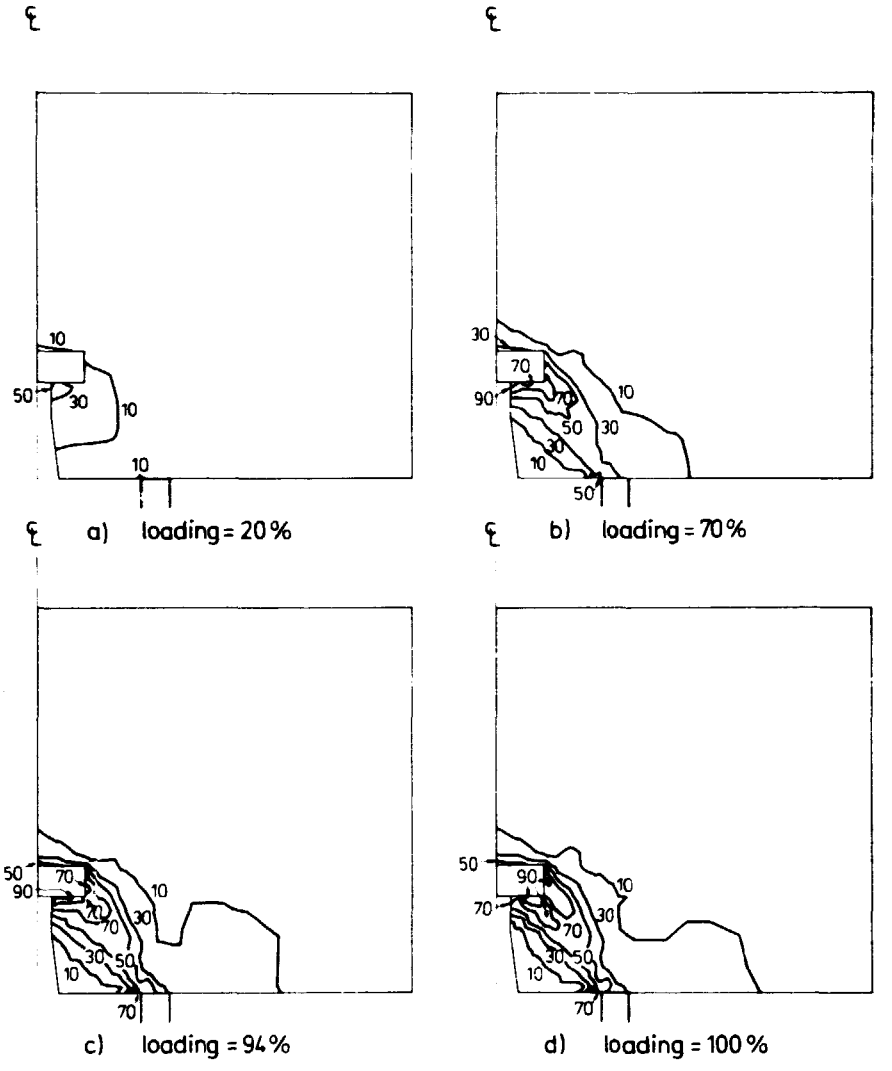

Fig. 5.4-7: Development of contour lines for the nonlinearity index in per cent. Loadings expressed as per cent of predicted failure load.

the nonlinearity index. This effect is very pronounced when comparing fig. 7c) with 7d), but a comparison of fig. 7b) with 7c) already shows this tendency. It is important to realize that this gradual decrease of the nonlinearity index due to strain softening in the post-failure region corresponds to crushing of the concrete. Thus, even though small tensile stresses may exist in addition to the primary biaxial compressive stress states, the failure is caused by crushing of the concrete and not by cracking. Therefore, the force required to extract the embedded disc in a Lok-Test is directly dependent on the com-

pressive strength of the concrete in question. However, the tensile strength may have some indirect influence as discussed later on.

Let us now compare the predicted failure load with experimental data. Based on the results of different test series including a total of 1100 Lok-Tests, Kierkegaard-Hansen and Bickley (1978) suggest the following linear relation between pull-out force F and uniaxial compressive cylinder strength σ_c: $F = 5 + 0.8\ \sigma_c$ where F and σ_c are measured in kN and MPa, respectively. This relation is shown in fig. 8 and is based on concrete mixes, where σ_c ranges from 6-53 MPa. The failure load resulting from the present calculation, where $\sigma_c = 31.8$ MPa, is also indicated. The analysis underestimates the experimental failure load by only 1%.

To investigate the dependence of the σ_c-value a calculation was performed with data from another, weaker concrete. To ensure use of realistic concrete data, test results of Kupfer (1973) were utilized again. In the constitutive model the following parameters are applied: $E_i = 2.89 \cdot 10^4$ MPa, $\nu_i = 0.19$, $\sigma_c = 18.7$ MPa, $\sigma_t/\sigma_c = 0.10$, $\varepsilon_c = 1.87‰$ and D = 0.6. The close agreement

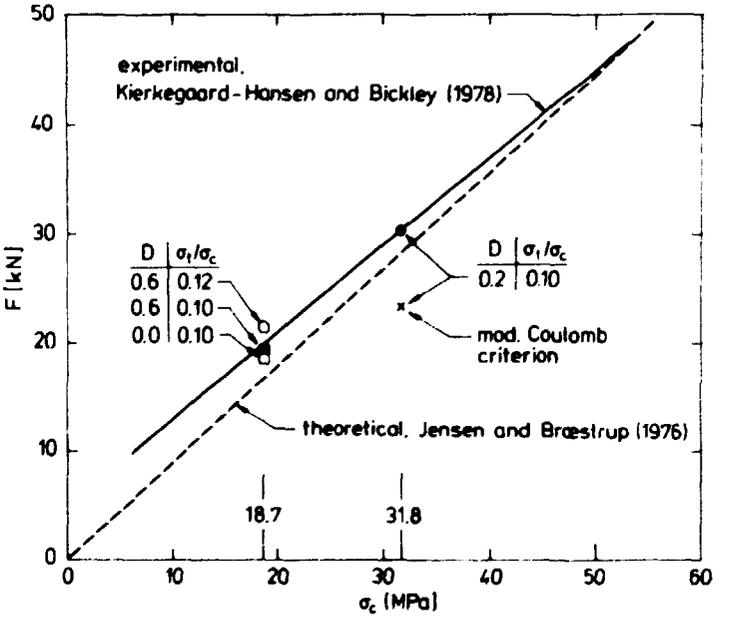

Fig. 5.4.-8: Experimental data compared with theoretical failure values.

of the resulting predictions with the experimental data of Kupfer (1973) has previously been demonstrated, cf. fig. 2.2-6. In this figure, the value D = 0 was used instead of D = 0.6, but this affects the post-failure behaviour, only. In general, the weaker the concrete the more ductile is its post-failure behaviour, cf. for instance, Hognestad et al. (1955). This suggests the use of D = 0.6 instead of D = 0 as is apparent from fig. 4, where the normalized stress-strain curves using these two D-values are shown. The predicted failure load using the above concrete parameters underestimates the actual failure load by only 3%, and is plotted in fig. 8. Therefore, the calculations are in agreement with the experimental evidence showing that within the considered variation of the σ_c-values, a linear relation exists between pull-out force and compressive strength.

It is remarkable that the prolongation of the experimental line in fig. 8 intersects the ordinate axis at some distance from the origin. However, two aspects of concrete behaviour are dependent on compressive strength namely the ductility and the ratio of tensile strength to compressive strength. As has already been touched upon, the post-failure behaviour is more ductile the weaker the concrete. To investigate the influence of minor variations in the post-failure behaviour of the concrete, a calculation was performed using again the concrete having a strength of 18.7 MPa, but now having lesser ductility. Therefore the value D = 0 was used instead of the more realistic one D = 0.6, cf. fig. 4. This in fact decreases the predicted failure load by 5% as shown in fig. 8. That the failure load depends on the particular softening behaviour of the concrete is indeed to be expected considering previous remarks in relation to fig. 7. However, comparison in fig. 4 of the concrete having σ_c = 18.7 MPa and D = 0 with the concrete having σ_c = 31.8 MPa and D = 0.2 shows an almost similar normalized behaviour. Moreover, the σ_t/σ_c-ratios are identical for these concretes. Using dimensional analysis, the failure loads should therefore be almost proportional to the σ_c-value and this is in fact also observed for the two predicted failure loads, cf. fig. 8.

In general, the weaker the concrete the larger is the ratio of tensile strength to compressive strength, cf. for instance, Wastiels (1979a). Let us investigate this effect using the concrete having σ_c = 18.7 MPa and D = 0.6 again, but putting now σ_t/σ_c = 0.12 instead of σ_t/σ_c = 0.10. This increases the predicted failure load by 11% as shown in fig. 8. In reality, Kupfer (1973) determined the σ_t/σ_c-ratio to be 0.105 for the concrete considered and if interpolation is performed between the two calculations having the σ_t/σ_c-ratio equal to 0.10 and 0.12, respectively, the resulting failure load is 0.7% below the actual value. Even though the tensile strength of the concrete certainly has an influence on the failure load of a Lok-Test, it is of importance to realize that this influence is an indirect one. Only very little of the pull-out force is carried directly by tension in the concrete, but the regions where failure take place are primarily in biaxial compression occasionally superposed by a small tensile stress. The failure is caused by crushing, and even a small tensile stress considerably decreases the failure strength, cf. for instance, figs. 2.1-7 and 2.1-9.

The above analysis has demonstrated that the reason that the relation between pull-out force and compressive strength is linear and not proportional is a result of the increasing ductility and the increasing ratio of tensile strength to compressive strength the weaker the concrete.

Let us now investigate the influence of different failure criteria. For this purpose we return to the concrete having σ_c = 31.8 MPa, but now the modified Coulomb criterion is applied. Compared to the previous analysis, this reduces the predicted failure load by 23% as shown in fig. 8. However, at failure the critical regions are loaded primarily in biaxial compression and the modified Coulomb criterion is known to underestimate the failure stresses for such stress states by 25%-30%, cf. fig. 2.1-7. It is of interest to observe that the decrease of failure load, when using the modified Coulomb criterion, is in accordance with the finding that the Lok-Test depends directly on the compressive strength of the concrete and not on its

tensile strength. As demonstrated by figs. 2.1-5 to 2.1-7, the modified Coulomb criterion underestimates the failure stresses, when concrete is loaded in compression, except when extremely large triaxial compressive stress states exist. Moreover, figs. 2.1-7 and 2.1-9 show that this criterion overestimates the failure stresses when tensile stresses are present. Therefore, if the failure in a Lok-Test was caused by tensile cracking then use of the modified Coulomb criterion would result in an increased failure load. However, in accordance with the preceding discussion use of the modified Coulomb criterion decreases the failure load.

Jensen and Bræstrup (1976) have previously determined the failure load for a Lok-Test using rigid-ideal plasticity theory. They also used the modified Coulomb criterion and their result is shown in fig. 8. It appears that close agreement is obtained even though proportionality and not just linearity between the pull-out force and the compressive strength was obtained. However, the failure load determined by Jensen and Bræstrup (1976), when σ_c = 31.8 MPa, is considerably larger than the one determined here when using the modified Coulomb criterion also. This is particularly conspicuous, as Jensen and Bræstrup (1976) in their analysis are forced to use a friction angle equal to the angle as shown in fig. 1b). This results in a friction angle equal to 31° corresponding to the value m = 3.1 in the Coulomb criterion, cf. eq. (2.1-9). Here we use the value m = 4 which, as discussed above, results in some underestimate of the actual failure stresses. Use of the value m = 3.1 would indeed imply a considerably underestimate of actual failure stresses. However, in their analysis, Jensen and Bræstrup (1976) in reality compensate for this, as their analysis is based on rigid-ideal plasticity with no softening effects at all. Consequently, they assume failure all along the plane running from the outer periphery of the disc towards the inner periphery of the support. Previous discussion, cf. for instance, fig. 7, has refuted such an assumption. However, in accordance with findings in the preceding sections, this underlines the importance of including a suitable strain softening behaviour in constitutive modelling of concrete.

In conclusion, the structural behaviour of the Lok-Test has been investigated in detail. Severe cracking occurs and the stress distribution is very inhomogeneous. It has been shown that large compressive forces run from the disc in a rather narrow band towards the support and this constitutes the load-carrying mechanism. Moreover, the failure in a Lok-Test is caused by crushing of the concrete and not by cracking. Therefore, the force required to extract the embedded steel disc in a Lok-Test is directly dependent on the compressive strength of the concrete in question. However, as the stress states, where failure takes place, are primarily biaxial compressive occasionally superposed by small tensile stresses, the tensile strength of the concrete has some indirect influence. The effect of strain softening in the post-failure region is important. In general, weak concrete compared to strong concrete has a relatively larger tensile strength and a higher ductility. This explains why the relation between the failure pull-out force and the compressive strength is linear and not proportional.

The influence of different failure criteria has also been evaluated and it has been shown that use of the writer's failure criterion (1977) coupled with realistic post-failure behaviours gives the closest agreement with experimental data. For the concretes having σ_c = 31.8 MPa, σ_t/σ_c = 0.10, D = 0.2 and σ_c = 18.7 MPa, σ_t/σ_c = 0.10, D = 0.6, the predicted failure loads are 99% and 97%, respectively, of the experimental values.

6. SUMMARY AND CONCLUSIONS

The present study has produced general conclusions within the fields of constitutive modelling of concrete, aspects of finite element modelling and structural behaviour of specific concrete structures. Moreover, a profound documentation of the AXIPLANE-program, applicable for axisymmetric and plane structures, has been given.

Section 2 dealt with failure and nonlinearity of concrete when loaded in the short-term by general stress states. Different failure criteria and their agreement with experimental data were discussed. It was shown that the criterion of the writer (1977) is attractive when considering accuracy, whereas the modified Coulomb criterion possesses an appealing simplicity. Except for very large triaxial compressive stresses, the modified Coulomb criterion in general underestimates the failure stresses for compressive loading. The two criteria mentioned are implemented in the program. A simple failure mode criterion was also compared with experimental data. A constitutive model, proposed by the writer (1979) and implemented in the AXIPLANE-program, was outlined. It is based on nonlinear elasticity, where the secant values of Young's modulus and Poisson's ratio are changed appropriately. This model considers the strain hardening before failure, the failure itself and the strain softening in the post-failure region. Dilatation of concrete as well as the influence of all three stress invariants is considered. Comparison with experimental data shows a close agreement for a wide range of stress states also including tensile stresses. The model is very flexible as different post-failure behaviours and different failure criteria are easily dealt with. Moreover, the calibration of the model to a specific concrete is easily performed as all six parameters in the model are determined by means of standard uniaxial data.

Section 3 has treated the constitutive models for reinforcement and prestressing. These models are quite trivial and interest is focussed only on a formulation that is computational convenient in the AXIPLANE-program.

Section 4 was devoted to the finite element modelling. Some of this section is of interest only for the specific documentation of the AXIPLANE-program. However, using Galerkin's method a general exposition of the fundamental equations in the finite element displacement method was derived. A profound discussion of various aspects of finite element modelling of concrete cracking was also given. The smeared cracking approach was favoured in the present report, as it reflects important aspects

of cracking and as it is easy to incorporate in a finite element program. However, the smeared cracking approach ignores the actual discontinuity in the displacement field, and the shear stiffnesses parallel and normal to the crack plane are, contrary to reality, identical. Special attention was given to the shear retention factor that reflects aggregate interlock. Arguments justifying a fixed value for the shear retention factor were put forward. The standard version of the program uses the shear retention factor $\eta = 0.01$. Concepts of reinforcement simulation were also discussed and the embedded concept was favoured in the present study. This approach infers a perfect bond between concrete and steel. The formulation of reinforcement elements was performed so that dowel action may be considered through the shear deformation of the reinforcement. However, findings in section 5 reveal that such an approach is not preferable and the standard version of the program ignores dowel action. Section 4 closes with general computational aspects.

The main section, section 5, showed applications of the AXIPLANE-program. Different concrete structures were analysed uptil failure and compared with experimental data. This resulted in close insight in the structural behaviour of the considered structures as well as general findings regarding finite element modelling.

The analysis of the panels subjected to tensile forces showed that simulation of lateral bar stiffness through a suitable shear modulus, κG, of the bar material seems to be not an advantageous method. Therefore, the standard version of the program ignores lateral bar stiffness, i.e., the value $\kappa = 0$ is utilized. Consequently, shear displacements of the panels were grossly overestimated. Panel elongations were predicted fairly well even though the tension stiffening effect is ignored; predicted failure loads were in close agreement with experimental data.

The considered thick-walled closure is a structure where large triaxial compressive stresses as well as cracking are present. As a first example in the present study, it was shown that a suitable analysis of the theoretical data may provide a clear

insight into the physical behaviour of a structure. This was demonstrated using figures of crack developments and stress distributions. Figures showing contour lines of the nonlinearity index proved to be very advantageous when evaluating failure regions and failure modes. Using the standard version of the program, the effect of using the two different failure criteria was evaluated and, as expected, use of the writer's criterion resulted in the closest agreement with experimental data. The actual post-failure behaviour of concrete may be expected to have a large influence on those stress redistributions that take place, when the stresses are inhomogeneously distributed. This was indeed confirmed by the finite element analysis, and it was demonstrated that strain softening in the post-failure region must be included in a realistic constitutive model.

Beams failing in shear represent problems of great theoretical and practical importance. With the standard version of the program using the writer's failure criterion and considering strain softening in the post-failure region, a close agreement with experimental data was demonstrated. This holds for the beam without stirrups as well as for the beam with stirrups. For both beams it was shown that the primary cause of failure is strain softening in the region adjacent to the load point. This strain softening causes a strain localization, which in turn results in a tendency to diagonal cracking. For the beam without shear reinforcement nothing prevents this tendency, and diagonal tension failure follows both experimentally and theoretically. For the beam with shear reinforcement, on the other hand, the stirrups resist the tendency to diagonal cracking and a shear-compression failure follows. Apart from the above mentioned, there is no principle difference in the behaviour of the two beams.However, it is important to note that modelling of strain softening seems to be mandatory for the prediction of diagonal cracking. Considering that shear is very dominant in the beams, the influence of different shear retention factors was evaluated to be relatively moderate. Variations, within realistic limits, of the uniaxial tensile strength of the concrete was found to influence the structural behaviour insignificantly. However, the analysis showed that modelling of secondary cracking, where

cracks with different directions exist at the same location, is essential. The only observed disagreement with experimental evidence was a considerable overestimate of the thickening of the beams. Consideration to dowel action through the shear deformation of the bars did not change this finding. In combination with the conclusions from the panel analyses, it implies that dowel action must be treated through the bending of the bars and not by their shear deformation. However, to describe bending of bars by means of the simple elements used here, knowledge of the displacement fields in two subsequent elements is required. The resulting increase of the bandwidth of the equation system makes such an approach prohibitive. This problem may be overcomed using more complicated elements, where the displacement fields in itself can describe bar bending.

The Lok-Test was the last structural problem that was analysed and compared with experimental data. This pull-out test is used to determine the in-situ compressive strength of the concrete. In accordance with the experimental evidence, it was shown that the failure load of the pull-out force is linearly related to the compressive strength of the concrete. It was demonstrated that the reason that this relation is linear and not proportional is a result of the increasing ductility and the increasing ratio of tensile strength to compressive strength the weaker the concrete. The analysis showed that the failure is caused by crushing of the concrete and not by cracking. Moreover, use of the modified Coulomb criterion resulted in some underestimate of the failure load. Finally, consideration to a realistic strain-softening behaviour in the post-failure region was again found to be of extreme importance.

Regarding general aspects of constitutive modelling of concrete, the present study has shown that inclusion of an accurate failure criterion is very essential. Moreover, the consideration of strain softening in the post-failure region turns out to be of extreme importance.

The ultimate load capacity of structures has been the quantity of primary concern here. To give an impression of the accuracy

obtained using the AXIPLANE-program, table 1 shows a comparison between predicted and experimental failure loads. The predicted values were obtained using the standard version of the program, where the shear retention factor is $\eta = 0.01$ and lateral bar stiffness is ignored, i.e., $\kappa = 0$. In all cases, the failure criterion of the writer was utilized, and realistic strain softening in the post-failure region was considered. Moreover, all material parameters in the program were calibrated using uniaxial data, only. In this table, the term $F_{theo.}/F_{exp.}$ gives the ratio of the theoretical failure load to the experimental value. As widely different structures with delicate structural behaviours were considered, this table clearly demonstrates the benefits of the AXIPLANE-program. Within its axisymmetric and plane applications, the potential of the AXIPLANE-program seems to be quite attractive.

Table 6-1: Predicted and experimental failure loads of the considered structures.

Structure	$F_{theo.}/F_{exp.}$
Panels (mean value)	0.95
Thick-walled closure	1.13
Beam without stirrups	0.98
Beam with stirrups	0.80
Lok-Test (σ_c = 18.7 MPa)	0.97
Lok-Test (σ_c = 31.8 MPa)	0.99

REFERENCES

ANDERSEN, P.S. (1968a). The Finite Element Method Employed for the Calculation of Stationary and Nonstationary Temperature Fields. Risø National Laboratory, Denmark. Risø-M-2012 (Internal Report) 22 p.

ANDERSEN, P.S. (1968b). A Computer Programme for the Solution of $\frac{\partial}{\partial x}\left(k_x \frac{\partial \phi}{\partial x}\right) + \frac{\partial}{\partial y}\left(k_y \frac{\partial \phi}{\partial y}\right) + q''' - \frac{\partial \phi}{\partial t} = 0$ by the Finite Element Method. Risø National Laboratory, Denmark. Risø-M-2013 (Internal Report) 23 p.

ARGYRIS, J.H., FAUST, G., SZIMMAT, J., WARNKE, E.P., and WILLAM, K.J. (1974). Recent Developments in the Finite Element Analysis of Prestressed Concrete Reactor Vessels. Nucl. Eng. Des. 28, 42-75.

ARGYRIS, J.H., FAUST, G. and WILLAM, K.J. (1976). Limit Load Analysis of Thick-Walled Concrete Structures - A Finite Element Approach to Fracture. Comput. Methods Appl. Mech. Eng. 8, 215-243.

ARNESEN, A., SØRENSEN, S.I. and BERGAN, P.G. (1979). Nonlinear Analysis of Reinforced Concrete. Paper presented at the International Conference on Engineering Application of the Finite Element Method. Oslo, Norway. May 9-11, 1979.

BALMER, G.G. (1949). Shearing strength of concrete under high triaxial stress - computation of Mohrs envelope as a curve. United States Department of the Interior. Bureau of Reclamation. Structural Research Laboratory. Report No. SP-23, 13 p.

BATHE, K-J. and RAMASWAMY, S. (1979). On Three-Dimensional Nonlinear Analysis of Concrete Structures. Nucl. Eng. Des. 52, 385-409.

BAŽANT, Z.P. and BHAT, P.D. (1976). Endochronic Theory of Inelasticity and Failure of Concrete. J. Eng. Mech. Div., ASCE, 102, 701-722.

BAŽANT, Z.P. and SHIEH, C.-L. (1978). Endochronic Model for Nonlinear Triaxial Behaviour of Concrete. Nucl. Eng. Des. 47, 305-315.

BAŽANT, Z.P. and GAMBAROVA, P. (1979a). Rough Cracks in Reinforced Concrete. Paper presented at ASCE Spring Convention, Session on Finite Element Analysis of Reinforced Concrete. Boston. April 1979.

BAŽANT, Z.P. and GAMBAROVA, P. (1979b). Ductility and failure of netreinforced concrete shell walls. In: Transactions of the 5th International Conference on Structural Mechanics in Reactor Technology, Berlin, 13-17 August 1979. Edited by Thomas A. Jaeger and Bruno A. Boley. Vol. J (North-Holland, Amsterdam), paper J4/9.

BRESLER, B. and SCORDELIS, A.C. (1963). Shear Strength of Reinforced Concrete Beams. Proc. Am. Concr. Inst. 60, 51-74.

BROWNE, R.D. and BLUNDELL, R. (1972). The Behaviour of Concrete in Prestressed Concrete Pressure Vessels. Nucl. Eng. Des. 20, 429-475.

CEDERBERG, H. and DAVIS, M. (1969). Computation of Creep Effects in Prestressed Concrete Pressure Vessels using Dynamic Relaxation. Nucl. Eng. Des. 9, 439-448.

CEDOLIN, L. and DEI POLI, S. (1977). Finite Element Studies of Shear-Critical R/C Beams. J. Eng. Mech. Div., ASCE 103, 395-410.

CEDOLIN, L., CRUTZEN, Y.R.J. and DEI POLI, S. (1977). Triaxial Stress-Strain Relationship for Concrete. J. Eng. Mech. Div., ASCE, 103, 423-439.

CERVENKA, V. and GERSTLE, K.H. (1971). Inelastic Analysis of Reinforced Concrete Panels: Theory. International Association for Bridge and Structural Engineering. Publications. Zürich. Switzerland. 31-II, 31-45.

CHEN, A.C.T. and CHEN, W.F. (1975). Constitutive Relations for Concrete. J. Eng. Mech. Div., ASCE, 101, 465-481.

CHINN, J. and ZIMMERMAN, R.M. (1965). Behaviour of Plain Concrete under Various High Triaxial Compression Conditions. Air Force Weapons Laboratory. New Mexico. Technical Report No. WL 64-163 (AD468460). 134 p.

COON, M.D. and EVANS, R.J. (1972). Incremental Constitutive Laws and Their Associated Failure Criteria with Applications to Plain Concrete. Int. J. Solids Struct. 8, 1169-1183.

COWAN, H.J. (1953). The Strength of Plain, Reinforced and Prestressed Concrete under Action of Combined Stresses, with Particular Reference to the Combined Bending and Torsion of Rectangular Sections. Mag. Concr. Res. 5, 75-86.

DARWIN, D. and PECKNOLD, D.A. (1977). Analysis of Cyclic Loading of Plane R/C Structures. Comput. Struct. 7, 137-147.

DESAYI, P. and KRISHNAN, S. (1964). Equation for the Stress-Strain Curve of Concrete. Proc. Am. Concr. Inst. 61, 345-350.

DOUGILL, J.W. (1976). On Stable Progressively Fracturing Solids. J. Appl. Math. Phys. (ZAMP), 27, 423-437.

DRUCKER, D.C. (1952). A More Fundamental Approach to Plastic Stress-Strain Relations. In: Proceedings of the First U.S. National Congress of Applied Mechanics, Chicago, June 11-16, 1951 (ASME, New York) 487-491.

DRUCKER, D.C. and PRAGER, W. (1952). Soil Mechanics and Plastic Analysis or Limit Design. Q. Appl. Math. 10, 157-165.

FERRARA, G., ROSSI, P., ROSSI, P.P., and RUGGERI, L. (1976). Dispositivi di prova per l'analisi sperimentale del comportamento di comglomerati cementizi sottoposi a stati tensionali di sollecitazione. Presented at the 4th Associazione Italiana Analisi Sollecitazione Congress. Rome, Italy. Oct. 1976.

GERSTLE, K.H., LINSE, D.L., BERTACCHI, P., KOTSOVOS, M.D., KO, H-Y., NEWMAN, J.B., ROSSI, P., SCHICKERT, G., TAYLOR, M.A., TRAINA, L.A., ZIMMERMAN, R.M., and BERLOTTI, R. (1978). Strength of concrete under multiaxial stress states. In: Douglas McHenry International Symposium on Concrete and Concrete Structures, held in Mexico City, October 1976 (American Concrete Institute, Detroit) (ACI Publication, SP-55) paper SP 55-5, 103-131.

GREEN, S.J. and SWANSON, S.R. (1973). Static Constitutive Relations for Concrete. Air Force Weapons Laboratory. New Mexico. Technical Report No. AFWL-TR-72-244 (AD761820). 136 p.

GROOTENBOER, H.J. (1979). Finite element analysis of two-dimensional reinforced concrete structures, taking account of non-linear physical behaviour and the development of discrete cracks. Dissertation (dr.ir.) Technical University of Delft, Holland, 102 p.

HAND, F.R., PECKNOLD, D.A. and SCHNOBRICH, W.C. (1973). Non-linear Layered Analysis of RC Plates and Shells. J. Struct. Div., ASCE, 99, 1491-1505.

HANNANT, D.J. (1969). Creep and Creep Recovery of Concrete Sujected to Multiaxial Compressive Stresses. Proc. Am. Concr. Inst. 66, 391-394.

HANNANT, D.J. (1974). Nomograms for the failure of plain concrete subjected to short-term multiaxial stresses. Struct. Eng. 52, 151-165.

HERRMANN, B. (1975). M.Sc. thesis, unpublished.

HERRMANN, B. (1978). Konstitutive Ligninger for Beton ved Fler-aksede Spændingstilstande. Risø National Laboratory, Denmark. Risø-M-2121 (Ph.D. Thesis). 131 p.

HERRMANN, B. (1979). A kinematic and isotropic hardening plasicity model for plain concrete under general triaxial stress conditions. In: IABSE Colloquim: Plasticity in Reinforced Concrete, Copenhagen, Denmark, May 21-23, 1979 (International Association for Bridge and Structural Engineering, Zürich) (Reports of the Working Commissions, vol. 29) 11-18.

HOBBS, D.W. (1970). Strength and Deformation Properties of Plain Concrete Subject to Combined Stress. Part 1. Cement and Concrete Association, London, Technical Report 42.451, 12 p.

HOBBS, D.W. (1974). Strength and Deformation Properties of Plain Concrete Subject to Combined Stress. Part 3. Cement and Concrete Association, London, Technical Report 43.497, 20 p.

HOBBS, D.W., POMEROY, C.D. and NEWMAN, J.B. (1977). Design stresses for concrete structures subject to multiaxial stresses. Struct. Eng. 55, 151-164.

HOGNESTAD, E. (1951). A Study of Combined Bending and Axial Load in Reinforced Concrete Members. University of Illinois, Engineering Experiment Station, Bulletin Series No. 399, 128 p.

HOGNESTAD, E., HANSON, N.W. and McHENRY, D. (1955). Concrete Stress Distribution in Ultimate Strength Design. Proc. Am. Concr. Inst. 52, 455-479.

HUANG, Y.H. (1969). Finite Element Analysis of Nonlinear Soil Media. In: Proceedings of the Symposium on: Application of Finite Element Methods in Civil Engineering, Nashville, Tennessee, 13-14 November, 1969. Edited by W.H. Rowan and R.M. Hackett (ASCE, New York) 663-690.

JANDA, L. (1974). A method of analysis of reinforced or prestressed concrete structures under triaxial stress. In: Seminar on Concrete Structures Subjected to Triaxial Stresses, Bergamo, Italy, May 17-19, 1974 (International Association for Bridge and Structural Engineering, Zürich) (Reports of the Working Commissions, Vol. 19) paper 3/7.

JENSEN, B.C. and BRÆSTRUP, M.W. (1976). Lok-Tests determine the compressive strength of concrete. Nord. Betong No. 2, 9-11.

JOHANSEN, K.W. (1958). Brudbetingelser for sten og beton. Bygningsstatiske Meddelelser 29, 25-44.

JOHANSEN, J.W. (1959). Discussion of: Strength of Concrete under Combined Stresses. Proc. Am. Concr. Inst. 56, 1043-1045.

KARSAN, I.D. and JIRSA, J.O. (1969). Behaviour of Concrete under Compressive Loadings. J. Struct. Div., ASCE, 95, 2543-2563.

KIERKEGAARD-HANSEN, P. (1975). Lok-Strength. Nord. Betong No. 3, 19-28.

KIERKEGAARD-HANSEN, P. and BICKLEY, J.A. (1978). In-Situ Strength Evaluation of Concrete by the Lok-Test System. Paper presented at the 1978 Fall Convention, American Concrete Institute, Houston, Texas. Oct. 29 - Nov. 3, 1978.

KOTSOVOS, M.D. and NEWMAN, J.B. (1977). Behaviour of Concrete under Multiaxial Stress, Proc. Am. Concr. Inst. 74, 443-446.

KOTSOVOS, M.D. and NEWMAN, J.P. (1978). Generalized Stress-Strain Relations for Concrete. J. Eng. Mech. Div., ASCE, 104, 845-856.

KUPFER, H., HILSDORF, H.K. and RÜSCH, H. (1969). Behaviour of Concrete under Biaxial Stresses. Proc. Am. Concr. Inst. 66, 656-666.

KUPFER, H. (1973). Das Verhalten des Betons under Mehrachsigen Kurzzeitbelastung under besonderer Berücksichtigung der Zweiachsigen Beanspruchung. Deutscher Ausschuss für Stahlbeton. Heft 229, 105 p.

KUPFER, H. and GERSTLE, K. (1973). Behaviour of Concrete under Biaxial Stress. J. Eng. Mech. Div., ASCE, 99, 852-866.

LAUNAY, P., GACHON, H. and POITEVIN, P. (1970). Déformation et résistence ultime du béton sons étreinte triaxiale. Ann. Inst. Tech. Batiment Trav. Publ. 23, No. 269, 21-48.

LAUNAY, P. and GACHON, H. (1971). Strain and Ultimate Strength of Concrete under Triaxial Stress. In: Proceedings of the First International Conference on Structural Mechanics in Reactor Technology, Berlin, September 20-24, 1971. Vol. 3 (Commission of the European Communities, Brussels) (EUR-4820) paper H1/3, p. 23-40.

LAUNAY, P. and GACHON, H. (1972). Strain and Ultimate Strength of Concrete under Triaxial Stress. In: ACI Publication SP-34 (American Concrete Institute, Detroit) paper 13, 269-282.

LEKHNITSKII, S.G. (1963). Theory of elasticity of an anisotropic elastic body. (Holden-Day, San Francisco, California) 404 p.

LIN, C.-S. and SCORDELIS, A.C. (1975). Nonlinear Analysis of RC Shells of General Form. J. Struct. Div., ASCE, 101, 523-538.

LINK, J., SCHÄFER, H. and MELHORN, G. (1974). Eine Formulierung des Zweiachsigen Bruch- und Verformungsverhaltens von Beton. Beton- und Stahlbetonbau, 9, 206-214.

LINK, J. (1975). Numerical Analysis Oriented Biaxial Stress-Strain Relation and Failure Criterion of Plain Concrete. In: Transactions of the Third International Conference on Structural Mechanics in Reactor Technology, London, Septemper 1-5, 1975. Vol. 3 (Commission of the European Communities, Luxemburg) paper H1/2.

LIU, T.C.Y., NILSON, A.H. and SLATE, F.O. (1972). Biaxial Stress-Strain Relations for Concrete. J. Struct. Div., ASCE, 98, 1025-1034.

MARCHERTAS, A.H., FISTEDIS, S.H., BAŽANT, Z.P., and BELYTSCHKO, T.B. (1978). Analysis and Application of Prestressed Concrete Reactor Vessels for LMFBR. Nucl. Eng. Des. 49, 155-173.

MENDELSON, A. (1968). Plasticity: Theory and Application (The Mac Millan Comp., New York) 353 p.

MILLS, L.L. and ZIMMERMAN, R.M. (1970). Compressive Strength of Plain Concrete under Multiaxial Loading Conditions. Proc. Am. Concr. Inst. 67, 802-807.

MOHRAZ, B. and SCHNOBRICH, W.C. (1970). Crack Development in a Prestressed Concrete Reactor Vessel as determined by a Lumped Parameter Method. Nucl. Eng. Des. 11, 286-294.

MROZ, Z. (1972). Mathematical Models of Inelastic Concrete Behaviour. In: Inelasticity and Non-Linearity in Structural Concrete. Edited by M.Z. Cohn (University of Waterloo Press, Waterloo, Ontario, Canada) SM Study No. 8. 47-72.

NARROW, I. and ULLBERG, E. (1963). Correlation between Tensile Splitting Strength and Flexural Strength of Concrete. Proc. Am. Concr. Inst. 60, 27-38.

NEWMAN, K. and NEWMAN, J.B. (1971). Failure Theories and Design Criteria for Plain Concrete. In: Structure, Solid Mechanics and Engineering Design: the Proceedings of the Southhampton 1969 Civil Engineering Materials Conference, Southhampton, April 1969. Edited by M. Te'eni (Wiley-Interscience, London) 963-995.

NEWMAN, J.B. and NEWMAN, K. (1973). The Cracking and Failure of Concrete under Combined Stresses and its Implications for Structural Design. In: International Symposium on the Deformation and Rupture of Solids Subjected to Multiaxial Stresses, held at Cannes, France, October 4-6, 1972. Vol. 1 (Eyrolles, Paris) 149-168.

NGO, D. and SCORDELIS, A.C. (1967). Finite Element Analysis of Reinforced Concrete Beams. Proc. Am. Concr. Inst. 64, 152-163.

NIELSEN, M.P., HANSEN, L.P. and RATHKJEN, A. (1977). Mekanik 2.2. Del 2. 2. udg., Technical University of Denmark, Afd. for Bærende Konstruktioner, Lyngby, Denmark. 696 p.

NILSON, A.H. (1968). Nonlinear Analysis of Reinforced Concrete by the Finite Element Method. Proc. Am. Concr. Inst. 65, 757-766.

OTTOSEN, N.S. (1975). Failure and Elasticity of Concrete. Risø National Laboratory, Denmark. Risø-M-1801. 67 p.

OTTOSEN, N.S. and ANDERSEN, S.I. (1975). Theoretical and Experimental Studies for Optimization of PCRV Top Closures. In: Transactions of the Third International Conference on Structural Mechanics in Reactor Technology, London, September 1-5, 1975. Vol. 3. (Commission of the European Communities, Luxemburg) paper H3/6.

OTTOSEN, N.S. and ANDERSEN, S.I. (1977a). Overload Behaviour of Top-Closure Models LM-C to LM-7. Final Report. Risø National Laboratory. Engineering Department. Denmark. BT-3-D-068, 144 p.

OTTOSEN, N.S. and ANDERSEN, S.I. (1977b). Structural Failure of Thick-Walled Concrete Elements. In: Transactions of the 4th International Conference on Structural Mechanics in Reactor Technology, San Francisco, California, 15-19 August 1977. Edited by Thomas A. Jaeger and Bruno A. Boley. Vol. H. (Commission of the European Communities, Luxembourg) paper H4/3.

OTTOSEN, N.S. (1977). A Failure Criterion for Concrete. J. Eng. Mech. Div., ASCE, 103, 527-535.

OTTOSEN, N.S. (1978). A Constitutive Model for Rock Salt. Risø National Laboratory, Denmark. Risø Report No. 383, 20 p.

OTTOSEN, N.S. (1979). Constitutive Model for Short-Time Loading of Concrete. J. Eng. Mech. Div., ASCE, 105, 127-141.

OTTOSEN, N.S. and KRENK, S. (1979). Nonlinear Analysis of Cavities in Rock Salt. Int. J. Rock. Mech. Min. Sci. & Geomech. Abstr. 16, 245-252.

OTTOSEN, N.S. (1980). Manual for the Finite Element Program, AXIPLANE, Applicable for Nonlinear Analysis of Concrete and Rock Salt Structures. Risø National Laboratory, Denmark. Risø-R-412 (to be published).

PALANISWAMY, R. and SHAH, S.P. (1974). Fracture and Stress-Strain Relation of Concrete under Triaxial Compression. J. Struct. Div., ASCE, 100, 901-916.

PAUL, B. (1961). A Modification of the Coulomb-Mohr Theory of Fracture. J. Appl. Mech. 28, 259-268.

PETER, J. (1964). Zur Bewehrung von Scheiben und Schalen für Hauptspannungen Schiefwinklig zur Bewehrungsrichtung. Dissertation (Dr.-Ing.). Tech. University of Stuttgart, Germany 213 p.

PHILLIPS, D.V. and ZIENKIEWICZ, O.C. (1976). Finite Element Nonlinear Analysis of Concrete Structures. Proc., Inst. Civ. Eng. 61, Part 2, 59-88.

RASHID, Y.R. (1968). Ultimate Strength Analysis of Prestressed Concrete Pressure Vessels. Nucl. Eng. Des. 7, 334-344.

REIMANN, H. (1965). Kritische Spannungszustände der Betons bei mehrachsiger, ruhender Kurzzeitbelastung. Deutscher Ausschuss für Stahlbeton. Heft 175, 36-63.

RICCIONI, R., ROBUTTI, G., DAL BO, C., and SCOTTO, F.L. (1977). Finite Element and Physical Model Analysis of a Removable Lid of a PCRV for BWR. In: Transactions of the 4th International Conference on Structural Mechanics in Reactor Technology, San Francisco, California, 15-19 August 1977. Edited by Thomas A. Jaeger and Bruno A. Boley. Vol. H (Commission of the European Communities, Luxembourg) paper H6/5.

RICHART, F.E., BRAENDTZAEG, A., and BROWN, R.L. (1928). A Study of the Failure of Concrete under Combined Compressive Stress. University of Illinois. Engineering Experimental Station. Bulletin No. 185, 103 p.

ROBUTTI, G., RONZONI, E., and OTTOSEN, N.S. (1979). Failure Strength and Elastic Limit for Concrete: A Comparative Study. In: Transactions of the 5th International Conference on Structural Mechanics in Reactor Technology, Berlin 13-17 August 1979. Edited by Thomas A. Jaeger and Bruno A. Boley. Vol. H (North-Holland, Amsterdam) paper H2/5.

ROMSTAD, K.M., TAYLOR, M.A. and HERRMANN, L.R. (1974). Numerical Biaxial Characterization for Concrete. J. Eng. Mech. Div., ASCE, 100, 935-948.

RÜSCH, H. (1960). Researches toward a general flexural theory for structural concrete. Proc. Am. Concr. Inst. 57, 1-28.

SAENZ, L.P. (1964). Discussion of: Equation for the Stress-Strain Curve of Concrete. Proc. Am. Concr. Inst. 61, 1229-1235.

SANDLER, I.S. (1978). On the Uniqueness and Stability of Endochronic Theories of Material Behaviour. J. Appl. Mech. 45, 263-266.

SARGIN, M. (1971). Stress-Strain Relationships for Concrete and the Analysis of Structural Concrete Sections. In: University of Waterloo, Canada, Solid Mechanics Division, SM Study No. 4, 23-46.

SAUGY, B. (1969). Contribution a l'étude théorique du comportement nonlinéare des structures massive en béton armé sons charge rapides. Bulletin Technique de la Suisse Romande 95, 1-18.

SCHIMMELPFENNIG, K. (1971). Die Festigkeit des Betons bei Mehraxialer Belastung. Ruhr-Universität. Institut für Konstruktiven Ingenieurbau. Forschungsgruppe Reaktordruckbehälter, Bochum, Germany. Bericht Nr. 5, 2 ergänzte Auflage, 85 p.

SCHIMMELPFENNIG, K. (1975). Ultimate Load Analysis of Prestressed Concrete Reactor Vessels Considering a General Material Law. In: Transactions of the Third International Conference on Structural Mechanics in Reactor Technology, London, September 1-5, 1975. Vol. 3 (Commission of the European Communities, Luxemburg) paper H4/6.

SCHIMMELPFENNIG, K. (1976). Brucksicherheitsberechnung von Spannbeton-Druckbehältern. Deutscher Ausschuss für Stahlbeton. Heft 257, 48 p.

SUIDAN, M. and SCHNOBRICH, W.C. (1973). Finite Element Analysis of Reinforced Concrete. J. Struct. Div., ASCE, 99, 2109-2122.

SØRENSEN, K.G. (1968). Løsning af et lineært ligningssystem, hvor matricen er en symmetrisk båndmatrix. ALGOL procedure BANDSYMEQ og FORTRAN subroutine BANDSY. Risø National Laboratory. Computing Center. Denmark. SF/SA-105. (Internal Report) 6 p.

TIMOSHENKO, S. and GOODIER, J.N. (1951). Theory of Elasticity. 2ed. (McGraw-Hill, New York) 506 p.

TINGLEFF, O. (1969). P-479 Stresses in PCRV. Nyeste Ændringer i Programmet. Risø National Laboratory. Engineering Department, Denmark. TPM-70/6 (Internal Report) 10 p.

TINGLEFF, O. (1973). A Method for Simulating Concentrated Forces and Local Reinforcements in Stress Computation. In: The Mathematics of Finite Elements and Applications. Edited by J.P. Whiteman (Academic Press, New York) 463-470.

UEDA, M., KAWAHARA, M., YOSHIOKA, Y., and KIKUCHE, M. (1974). Nonlinear Visco-Elastic and Elasto-Plastic Finite Elements for Concrete Structures. In: Proceedings of the International Symposium on Discrete Methods in Engineering, 19-20 September 1974, Milano (ETAS Libri, Milano) 391-403.

WASTIELS, J. (1979a). Behaviour of Concrete under Multiaxial Stresses - A Review. Cem. Concr. Res. 9, 35-44.

WASTIELS, J. (1979b). Failure Criteria for Concrete under Multiaxial Stress States. In: IABSE Colloquium: Plasticity

in Reinforced Concrete, Copenhagen, Denmark, May 21-23, 1979 (International Association for Bridge and Structural Engineering, Zürich) (Reports of the Working Commissions, Vol. 29) 3-10.

WILLAM, K.J. and WARNKE, E.P. (1974). Constitutive Model for the Triaxial Behavior of Concrete. In: Seminar on Concrete Structures subjected to Triaxial Stresses, Bergamo, Italy, May 17-19, 1974 (International Association for Bridge and Structural Engineering, Zürich) (Reports of the Working Commissions, Vol. 19) paper 3/1.

WÄSTLUND, G. (1937). Nye rön angående betongens grundläggende hållfasthetsegenskaber. Betong 3, Stockholm, Sweden, 189-206.

YUZUGULLU, O. and SCHNOBRICH, W.C. (1973). A Numerical Procedure for the Determination of the Behavior of a Shear Wall Frame System. Proc. Am. Concr. Inst. 70, 474-479.

ZIENKIEWICZ, O.C. and CHEUNG, Y.K. (1967). The Finite Element Method in Structural and Continuum Mechanics (McGraw-Hill, London) 274 p.

ZIENKIEWICZ, O.C., VALLIAPPAN, S. and KING, I.P. (1969). Elasto-Plastic Solutions of Engineering Problems. Initial-Stress. Finite Element Approach. Int. J. Numer. Methods 1, 75-100.

ZIENKIEWICZ, O.C., OWEN, D.R.J., PHILLIPS, D.V., and NAYAK, G.C. (1972). Finite Element Methods in the Analysis of Reactor Vessels. Nucl. Eng. Des. 20, 507-541.

ZIENKIEWICZ, O.C., PHILLIPS, D.V. and OWEN, D.R.J. (1974). Finite Element Analysis of some Concrete Non-Linearities. Theory and Examples. In: Seminar on Concrete Structures subjected to Triaxial Stresses, Bergamo, Italy, May 17-19, 1974 (International Association for Bridge and Structural Engineering, Zürich) (Reports of the Working Commission, vol. 19) paper 3/2.

ZIENKIWICZ, O.C. (1977). The Finite Element Method. 3ed. (McGraw-Hill, London) 787 p.

LIST OF SYMBOLS

Unless otherwise stated, the following symbols are used in the present report:

A = parameter in failure criterion, eq. (2.1-5);

$A = E_i/E_c$ = parameter in stress-strain equation (2.2-3);

B = parameter in failure criterion, eq. (2.1-5);

$B_{ij\alpha}$ = tensor relating strains and nodal displacements, eq. (4.1-11);

$\bar{\bar{B}}$ = matrix relating strains and nodal displacements, eqs. (4.2-6) and (4.2-7);

$\bar{\bar{B}}'_b$ = matrix in a local coordinate system relating reinforcement strains with reinforcement nodal displacements, eqs. (4.3-4) and (4.3-5);

D = strain softening parameter in stress-strain equation (2.2-3);

D_{ijkl} = elasticity tensor, eq. (4.1-3);

$\bar{\bar{D}}$ = constitutive or material matrix, eq. (4.2-10);

$\bar{\bar{D}}_C$ = material matrix when circumferential cracks exist, eq. (4.2-21);

$\bar{\bar{D}}_{CR}$ = material matrix when circumferential and radial cracks exist, eq. (4.2-25);

$\bar{\bar{D}}_{CCR}$ = material matrix when secondary circumferential cracks exist together with radial cracks, eq. (4.2-28);

$\bar{\bar{D}}_R$ = material matrix when radial cracks exist, eq. (4.2-23);

$\bar{\bar{D}}'_b$ = material matrix in a local coordinate system for a reinforcement element, eqs. (4.3-6) to (4.3-9);

E = Young's modulus;

E_A = Young's modulus, see fig. 2.2-4 and eq. (2.2-6);

$E_c = \sigma_c/\varepsilon_c$ = secant value of Young's modulus at uniaxial compressive failure;

$E_{eff.}$ = effective E-modulus, eq. (2.3-3);

E_f = secant value of Young's modulus at triaxial compressive failure, eq. (2.2-5);

E_i = initial Young's modulus;

E_M = Young's modulus, see fig. 2.2-4 and eq. (2.2-6);

E_{MN} = Young's modulus, see fig. 2.2-4 and eq. (2.2-6);

E_S = secant value of Young's modulus, eq. (2.2-4);

F = force;

F_α^{be} = body force vector, eqs. (4.1-19) and (4.1-21);

F_α^{Pe} = discrete point force vector, eqs. (4.1-19) and (4.1-22);

F_α^{te} = traction force vector, eqs. (4.1-19) and (4.1-23);

$F_\alpha^{\varepsilon_o e}$ = force vector due to initial strain, eqs. (4.1-19) and (4.1-24);

$F_\alpha^{\sigma_o e}$ = force vector due to initial stress, eqs. (4.1-19) and (4.1-25);

$\bar{F}$ = total force vector, eq. (4.6-8);

$\bar{F}_b$ = body force vector, section 4.2.1;

$\bar{F}_P$ = discrete force vector, section 4.2.1;

$\bar{F}_t$ = traction force vector, section 4.2.1;

$\bar{F}_{\varepsilon_o}$ = force vector due to initial strains, section 4.2.1;

$\bar{F}_{\varepsilon_o b}$ = force vector for a bar element due to initial strains, eqs. (4.3-16);

$\bar{F}_{\varepsilon_o r}$ = force vector due to initial strains in reinforcement. This vector relates to the nodal points of the triangular element in question, see eqs. (4.3-19) and (4.2-22);

$\bar{F}_{\sigma_o}$ = force vector due to initial stresses, eq. (4.3-25);

$\bar{F}_{\sigma_o r}$ = force vector due to initial stresses in reinforcement. This vector relates to the nodal points of the triangular element in question, see eq. (4.3-30);

$\bar{F}'_{\varepsilon_o b}$ = force vector for a bar element due to initial strains. Local coordinates are use, see eqs. (4.3-10) and (4.3-12);

$\bar{F}'_{\sigma_o b}$ = force vector for a bar element due to initial stresses. Local coordinates are used, eq. (4.3-26);

G = shear modulus;

$I_1 = \sigma_{ii}$ = first invariant of the stress tensor;

$J = \cos 3\theta$ = invariant of the stress tensor;

$J_2 = \frac{1}{2} s_{ij} s_{ij}$ = second invariant of the stress deviator tensor, eq. (2.1-2);

$J_3 = \frac{1}{3} s_{ij} s_{jk} s_{ki}$ = third invariant of the stress deviator tensor;

K = parameter, eq. (4.2-22);

$K^e_{\alpha\beta}$ = stiffness tensor of the element, eqs. (4.1-19) and (4.1-20);

$\bar{\bar{K}}$ = stiffness matrix of the element, eq. (4.2-12);

$\bar{\bar{K}}$ = total stiffness matrix, eq. (4.6-1);

$\bar{\bar{K}}'_b$ = stiffness matrix in local coordinates of a bar element, see eqs. (4.3-10) and (4.3-11);

$\bar{\bar{K}}_r$ = stiffness contribution due to reinforcement. This contribution relates to the nodal points of the triangular element in question, see eq. (4.3-2);

K_1 = parameter in failure criterion, eq. (2.1-8);

K_2 = parameter in failure criterion, eq. (2.1-8);

$\bar{\bar{L}}$ = transformation matrix relating local and global coordinates, eqs. (4.3-13) and (4.3-14);

M = parameter, eq. (4.2-26);

$N_{i\alpha}$ = tensor relating displacements and nodal displacements, eq. (4.1-10);

$N^{e}_{i\alpha}$ = tensor relating displacements and nodal displacements for a specific element, eq. (4.1-16);

$\bar{\bar{N}}$ = matrix relating element displacements and nodal displacements, eq. (4.2-3);

P_i = point forces, eqs. (4.1-21) and (4.1-22);

$\bar{P}$ = point force vector, eq. (4.2-13);

R = parameter, eq. (3-10);

S = parameter, eq. (3-10);

S = surface;

T = temperature in ^{o}C, see eqs. (2.3-4) and (2.3-5);

$\bar{\bar{T}}$ = transformation matrix relating strains in local and global coordinates, eqs. (4.2-14) and (4.2-15); and

V = volume;

a_α = nodal displacements, eq. (4.1-10);

a^{*}_{α} = chosen nodal displacements, eq. (4.1-13);

a^{e}_{α} = nodal displacements for an element, eq. (4.1-16);

$\bar{a}$ = nodal displacement vector for triangular element, eq. (4.2-2);

$\bar{a}$ = total nodal displacement vector, eq. (4.6-1);

$\bar{a}_b$ = nodal displacement vector for a bar element, eq. (4.3-13);

$\bar{a}'_b$ = nodal displacement vector for a bar element. This vector relates to local coordinates, eq. (4.3-1);

$\tilde{b}_i$ = prescribed body forces, eq. (4.1-1);

$\bar{b}$ = body forces, section 4.2-1;

e_{ij} = deviatoric strain tensor, $e_{ij} = \varepsilon_{ij} - \frac{1}{3}\delta_{ij}\varepsilon_{kk}$, section 3;

e^e_{ij} = deviatoric elastic strain tensor, $e^e_{ij} = \varepsilon^e_{ij} - \frac{1}{3}\delta_{ij}\varepsilon^e_{kk}$, section 3;

e_{et} = equivalent total strain, eq. (3-18);

d = distance, see fig. 4.3-2;

m = parameter in Coulomb's criterion, eq. (2.1-9);

n_i = outward unit vector normal the boundary, eq. (4.1-4);

p = pressure;

r = radius;

r_m = mean radius of the triangular element, section 4.2.1;

r' = abscisse in local coordinate system, fig. 4.3-2;

r* = mean radius of a reinforcement element;

s_{ij} = deviatoric stress tensor, $s_{ij} = \sigma_{ij} - \frac{1}{3}\delta_{ij}\sigma_{kk}$;

s_1, s_2, s_3 = principal stress deviators;

t = time, eq. (2.3-4);

t = thickness of reinforcement element;

$\tilde{t}$ = prescribed tractions, eq. (4.1-4);

t^r_i = tractions corresponding to unknown reaction forces, eq. (4.1-8);

$\bar{t}$ = traction force vector, section 4.2.1;

u = displacement in radial direction, eq. (4.2-1);

u' = displacement in the R'-direction, fig. 4.3-2;

u_i, u_j, u_m = radial nodal displacements of a triangular element, eq. (4.2-2);

u_i = displacements, eq. (4.1-2);

$\tilde{u}_i$ = prescribed displacements, eq. (4.1-5);

u^*_i = chosen displacements, eqs. (4.1-6) and (4.1-13);

$\bar{u}$ = displacement vector, eq. (4.2-1);

$\bar{u}'$ = displacement vector in loacl coordinates, section 4.3.1;

v = displacement in vertical direction, eq. (4.2-1);

v' = displacement in the Z'-direction, fig. 4.3-2;

$x = \left(\frac{\sqrt{J}_2}{\sigma_c}\right)_f - \frac{1}{\sqrt{3}}$ = stress invariant, see eq. (2.2-5);

Z = ordinate; and

Z' = ordinate in local coordinate system, fig. 4.3-2;

α = angle

α = coefficient of thermal expansion, see eqs. (4.2-11) and (4.3-7) to (4.3-9);

β = nonlinearity index, see eqs. (2.2-1) and (2.2-2);

γ_{RZ} = engineering shearing strain, eq. (4.2-5);

γ'_{RZ} = engineering shearing strain in local coordinates, eq. (4.3-3);

Δ = area of a triangular element, section 4.2.1;

ΔT = temperature rise, eqs. (4.2-11) and (4.3-7) to (4.3-9);

δ_{ij} = Kroneckers delta;

ε = strain, elongation is positive;

$\varepsilon_1, \varepsilon_2, \varepsilon_3$ = principal strains;

ε_c = strain at uniaxial sompressive failure ($\varepsilon_c > o$) eq. (2.2-3);

ε_o = initial strain;

ε_R = radial strain, eq. (4.2-5);

ε_Z = vertical strain, eq. (4.2-5);

ε_θ = circumferential strain, eq. (4.2-5);

ε^c = creep strain, see eq. (2.3-1);

ε^e = elastic strain, section 2.3;

ε^P = equivalent plastic strain, see eqs. (3-2) and (3-6);

ε'_R = strain in the R'-direction, see fig. 4.3-2 and eq. (4.3-3);

ε'_θ = circumferential strain, eq. (4.3-3);

ε_{ij} = strain tensor, eq. (4.1-2);

ε^{sp} = specific creep strain, eq. (2.3-1);

ε^e_{ij} = elastic strain tensor, eq. (3-7);

ε^e_{ij} = strain tensor in an element, eq. (4.1-27);

ε^o_{ij} = initial strain tensor, eq. (4.1-3);

ε^p_{ij} = plastic strain tensor, eq. (3-7);

ε^{oe}_{ij} = initial strain tensor in an element, eq. (4.1-28);

$\bar{\varepsilon}$ = strain vector, eq. (4.2-5);

$\bar{\varepsilon}'$ = strain vector in the local coordinate system, fig. 4.2-3;

$\bar{\varepsilon}_o$ = initial strain vector, eqs. (4.2-9) and (4.2-11);

$\bar{\varepsilon}'_b$ = strain vector for a bar element. This vector is related to local coordinates, eq. (4.3-3);

$\bar{\varepsilon}'_{ob}$ = initial strain vector for a bar element. This vector is related to local coordinates, eqs. (4.3-6) to (4.3-9);

η = shear retention factor, eq. (4.2-20);

θ = angle in deviatoric plane, see fig. 2.1-1 b) and eq. (2.1-3);

κ = factor describing the shear stiffness of the reinforcement, cf. section 4.3 and eq. (4.3-8);

λ = function in the failure criterion, eqs. (2.1-5) and (2.1-8);

λ = positive function in the flow rule, see eq. (3-3);

ν = Poisson's ratio;

ν_i = initial Poisson's ratio, eq. (2.2-7);

ν_f = secant value of Poisson's ratio at failure, eqs. (2.2-7) and (2.2-8);

ν_s = secant value of Poisson's ratio, eq. (2.2-7);

$\xi = \frac{I_1}{\sqrt{3}}$ = stress invariant, see fig. 2.1-1a);

$\rho = \sqrt{2J_2}$ = stress invariant, see fig. 2.1-1;

σ = stress, tensile is positive;

$\sigma_1, \sigma_2, \sigma_3$ = principal stresses, $\sigma_1 \geq \sigma_2 \geq \sigma_3$;

σ_c = uniaxial compressive strength ($\sigma_c > o$);

σ_e = equivalent stress, eq. (3-1);

σ_R = radial stress, eq. (4.2-8);

σ_t = uniaxial tensile strength ($\sigma_t > o$);

σ_Z = vertical stress, eq. (4.2-8);

σ_o = initial stress, eq. (3-19);

σ_θ = tangential stress, eq. (4.2-8);

σ'_R = stress in the R'-direction, see fig. 4.3-2;

σ'_θ = circumferential stress, section 4.3.1;

σ_{cb} = biaxial compressive strength ($\sigma_{cb} > o$);

σ_{ij} = stress tensor;

σ_{01} = initial principal stress, eq. (3-11);

σ_{02} = initial principal stress, eq. (3-11);

σ^e_{ij} = stress tensor in an element, eq. (4.1-28);

σ^o_{ij} = initial stress tensor, eq. (4.1-3);

σ^{oe}_{ij} = initial stress tensor in an element, eq. (4.1-28);

$\bar{\sigma}$ = stress vector, eq. (4.2-8);

$\bar{\sigma}_o$ = initial stress vector, eq. (4.3-24);

$\bar{\sigma}'$ = stress vector in the local coordinate system, fig. 4.2-3;

$\bar{\sigma}'_b$ = stress vector for a bar element. This vector is related to local coordinates, eq. (4.3-6);

$\bar{\sigma}'_{ob}$ = initial stress vector for a bar element. This vector is related to local coordinates, eqs. (4.3-27) to (4.3-29);

τ_{RZ} = shear stress, eq. (4.2-8); and

τ'_{RZ} = shear stress in local coordinates, section 4.3.1.

Subscripts

b = bar;

c = compressive;

f = failure value;

i = initial value;

o = initial stress or strain;

r = reinforcement;

s = secant value; and

t = tensile.

Supercripts

~ = prescribed;

- = vector;

= = matrix;

' = local coordinate system;

c = creep;

e = elastic or element; and

p = plastic.

APPENDIX A

The λ-Function in the Failure Criterion

In section 2.1.3 it was indicated by means of eq. (2.1-6) that when the function $r = 1/\lambda(\cos 3\theta)$ in the polar coordinates (r,θ) describes a smooth convex curve varying between an equilateral triangle and a circle, the same holds for the trace of the failure surface in the deviatoric plane.

To determine the λ-function, a membrane subjected to uniform tension S per unit length and supported along the edges of an equivalent triangle, fig. 1, is loaded by a uniform lateral

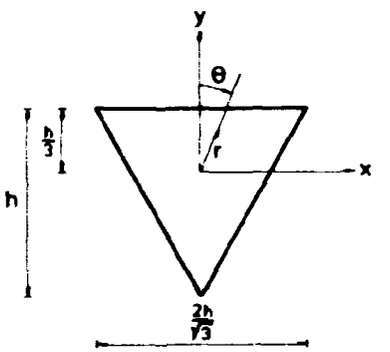

Fig. A-1: Equilateral triangle.

pressure p. Referring for instance to Timoshenko and Goodier (1951) pp. 268-269 the lateral deflection w of the membrane satisfies the Poisson equation

$$\frac{\partial^2 w}{\partial x^2} + \frac{\partial^2 w}{\partial y^2} = -\frac{p}{s}$$

Following the above reference p. 266, this equation and its boundary conditions are satisfied by

$$w = \frac{p}{4hs}\left(\frac{h}{3} - y\right)\left[\left(y + \frac{2h}{3}\right)^2 - 3x^2\right]$$

A transformation to polar coordinates r and θ, fig. 1, is performed by the substitutions $x = r\sin\theta$ and $y = r\cos\theta$, and using the identify $\cos 3\theta = 4\cos^3\theta - 3\cos\theta$ we derive

$$w = \frac{p}{4hS}\left(\frac{4}{27}h^3 - hr^2 - r^3\cos 3\theta\right) \qquad (A\text{-}1)$$

The contour lines of the deflected membrane in the polar coordinates r and θ are determined by this equation treating w as a constant. It is obvious that these contour lines are smooth and convex and varying between the equilateral triangle and a circle. To determine these contour lines we note that the maximum deflection $w_{max} = ph^2/27S$ occurs at $r = 0$ and disregarding in the following the point $r = 0$, the positive constant D is defined by

$$D = \sqrt{3\left(\frac{4h^2}{27} - \frac{4Sw}{p}\right)}$$

Introducing this constant in eq. (1) and rearranging this equation we obtain

$$\frac{1}{r^3} - \frac{3}{D^2}\frac{1}{r} - \frac{3\cos 3\theta}{hD^2} = 0$$

Solving this cubic equation by standard methods it appears that the roots of interest are only

$$\lambda = \frac{1}{r} = K_1 \cos\left[\frac{1}{3}\operatorname{Arccos}(K_2\cos 3\theta)\right]; \qquad \cos 3\theta \geq 0$$

$$\lambda = \frac{1}{r} = K_1 \cos\left[\frac{\pi}{3} - \frac{1}{3}\operatorname{Arccos}(-K_2\cos 3\theta)\right]; \qquad \cos 3\theta \leq 0$$

where $K_1 = 2/D$ and $K_2 = 3D/2h$. These two equations determine explicitly the contour lines and the λ-function in terms of two positive constants K_1 and K_2. It appears that the first coefficient is a size factor, while the second is a shape factor varying between zero and unity. This terminology for K_2 is convenient as the contour line approaches the equilateral triangle and a circle when K_2 approaches unity and zero, respectively.

APPENDIX B

Skewed Kinematic Constraints

The finite element modelling results in the equation system given by eq. (4.6-1). This equation system refers to the RZ-coordinate system; when nodal displacements are prescribed in the R- and Z-direction a modification of the equation system in accordance with eq. (4.6-2) is performed. However, if nodal displacements are prescribed in other directions than the R- or Z-axis, i.e., if skewed kinematic constraints are present, then eq. (4.6-1) has to be transformed to the R'Z'-coordinate system shown in fig. 1. After that a modification of the equation system corresponding to eq. (4.6-2) is performed and

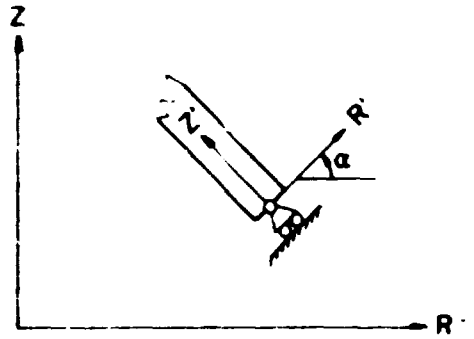

Fig. B-1: Skewed kinematic constraint.

a retransformation back to the original RZ-coordinate system is then carried out. Using a transformation matrix similar to eq. (4.3-14) and noting the transformation formula of eq. (4.3-15), after trivial matrix multiplications the above procedure results in the following:

If the displacement in the R'-direction at nodal point i is prescribed to be γ then the following contributions should be added to elements in the matrix $\bar{\bar{K}}$ in eq. (4.6-1)

$K_1(10^{10}-1)\cos^2\alpha$ is added to element $K_{2i-1,2i-1}$

$K_1(10^{10}-1)\cos\alpha\sin\alpha$ is added to element $K_{2i-1,2i}$

$K_1(10^{10}-1)\sin^2\alpha$ is added to element $K_{2i,2i}$

where

$$K_1 = K_{2i-1,2i-1}\cos^2\alpha + 2K_{2i-1,2i}\cos\alpha\sin\alpha + K_{2i,2i}\sin^2\alpha \qquad (B-1)$$

The modified stiffness matrix continues to be symmetric. Correspondingly, the following contributions should be added to elements in the vector $\bar{F}$ in eq. (4.6-1)

$P_1\cos\alpha$ is added to element F_{2i-1}

$P_1\sin\alpha$ is added to element F_{2i}

where

$$P_1 = K_1\, 10^{10}\,\gamma - (F_{2i-1}\cos\alpha + F_{2i}\sin\alpha)$$

and K_1 is given by eq. (1).

Similarly, if the displacement in Z'-direction at nodal point i is prescribed to be γ then the following modifications of matrix $\bar{\bar{K}}$ and vector $\bar{F}$ in eq. (4.6-1) are carried out

$K_2(10^{10}-1)\sin^2\alpha$ is added to element $K_{2i-1,2i-1}$

$-K_2(10^{10}-1)\sin\alpha\cos\alpha$ is added to element $K_{2i-1,2i}$

$K_2(10^{10}-1)\cos^2\alpha$ is added to element $K_{2i,2i}$

where

$$K_2 = K_{2i-1,2i-1} \sin^2\alpha - 2K_{2i-1,2i} \sin\alpha\cos\alpha + K_{2i,2i} \cos^2\alpha \qquad \text{(B-2)}$$

Moreover

- $P_2 \sin\alpha$ is added to element F_{2i-1}

  $P_2 \cos\alpha$ is added to element F_{2i}

where

$$P_2 = K_2 \, 10^{10} \gamma - (- F_{2i-1} \sin\alpha + F_{2i} \cos\alpha)$$

and K_2 is given by eq. (2).

Sales distributors:
Jul. Gjellerup, Sølvgade 87,
DK-1307 Copenhagen K, Denmark

Available on exchange from:
Risø Library, Risø National Laboratory,
P. O. Box 49, DK-4000 Roskilde, Denmark

ISBN 87-550-0649-3
ISSN 0106-2840